Yang, L., Serada, S., Fujimoto, M. et al. (2012). Periostin facilitates skin sclerosis via PI3K/Akt dependent mechanism in a mouse model of scleroderma. PLoS ONE *7*, e41994.
Zeisberg, M., Maeshima, Y., Mosterman, B., and Kalluri, R. (2002). Renal fibrosis. Extracellular matrix microenvironment regulates migratory behavior of activated tubular epithelial cells. Am. J. Pathol. *160*, 2001–2008.

Supporting information

Additional Supporting Information may be found in the online version of this article:

Table S1. List of all proteins identified by iTraq.
Data S1. Methods.

INTERNATIONAL JOURNAL OF ONCOLOGY 44: 1461-1469, 2014

The translation elongation factor eEF2 is a novel tumor-associated antigen overexpressed in various types of cancers

YUSUKE OJI[1], NAOYA TATSUMI[1], MARI FUKUDA[2], SHIN-ICHI NAKATSUKA[12], SAYAKA AOYAGI[2], ERIKA HIRATA[2], ISAMU NANCHI[2], FUMIHIRO FUJIKI[3], HIROKO NAKAJIMA[3], YUMIKO YAMAMOTO[2], SYOHEI SHIBATA[2], MICHIYO NAKAMURA[2], KANA HASEGAWA[1], SAYAKA TAKAGI[2], IKUYO FUKUDA[2], TOMOKO HOSHIKAWA[2], YUI MURAKAMI[2], MASAHIDE MORI[13], MASAYOSHI INOUE[4], TETSUJI NAKA[5], TAKESHI TOMONAGA[15], YOSHIFUMI SHIMIZU[16], MASASHI NAKAGAWA[17], JUNICHI HASEGAWA[18], RIICHIRO NEZU[18], HIDENORI INOHARA[6], SHUICHI IZUMOTO[7], NORIO NONOMURA[8], TOSHIKI YOSHIMINE[7], MEINOSHIN OKUMURA[4], EIICHI MORII[9], HAJIME MAEDA[14], SUMIYUKI NISHIDA[10], NAOKI HOSEN[11], AKIHIRO TSUBOI[10], YOSHIHIRO OKA[5] and HARUO SUGIYAMA[2]

Departments of [1]Cancer Stem Cell Biology, [2]Functional Diagnostic Science, [3]Cancer Immunology, [4]Surgery, [5]Respiratory Medicine and Allergy, Rheumatic Diseases, [6]Otolaryngology and Sensory Organ Surgery, [7]Neurosurgery, [8]Urology, [9]Pathology, [10]Cancer Immunotherapy, and [11]Biomedical Informatics, Osaka University Graduate School of Medicine, Osaka; [12]Department of Pathology, Kansai Rosai Hospital, Hyogo; Departments of [13]Thoracic Oncology, and [14]General Thoracic Surgery, Toneyama National Hospital; [15]Laboratory of Proteome Research, National Institute of Biomedical Innovation, Osaka; [16]Department of Internal Medicine, Takarazuka City Hospital, Hyogo; [17]Department of Internal Medicine, Nissay Hospital; [18]Department of Surgery, Osaka Rosai Hospital, Osaka, Japan

Received December 2, 2013; Accepted December 30, 2013

DOI: 10.3892/ijo.2014.2318

Abstract. Recent studies have shown that cancer immunotherapy could be a promising therapeutic approach for the treatment of cancer. In the present study, to identify novel tumor-associated antigens (TAAs), the proteins expressed in a panel of cancer cells were serologically screened by immunoblot analysis and the eukaryotic elongation factor 2 (eEF2) was identified as an antigen that was recognized by IgG autoantibody in sera from a group of patients with head and neck squamous cell carcinoma (HNSCC) or colon cancer. Enzyme-linked immunosorbent assay showed that serum eEF2 IgG Ab levels were significantly higher in colorectal and gastric cancer patients compared to healthy individuals. Immunohistochemistry experiments showed that the eEF2 protein was overexpressed in the majority of lung, esophageal, pancreatic, breast and prostate cancers, HNSCC, glioblastoma multiforme and non-Hodgkin's lymphoma (NHL). Knockdown of eEF2 by short hairpin RNA (shRNA) significantly inhibited the growth in four eEF2-expressing cell lines, PC14 lung cancer, PCI6 pancreatic cancer, HT1080 fibrosarcoma and A172 glioblastoma cells, but not in eEF2-undetectable MCF7 cells. Furthermore, eEF2-derived 9-mer peptides, EF786 (eEF2 786-794 aa) and EF292 (eEF2 292-300 aa), elicited cytotoxic T lymphocyte (CTL) responses in peripheral blood mononuclear cells (PBMCs) from an HLA-A*24:02- and an HLA-A*02:01-positive healthy donor, respectively, in an HLA-A-restricted manner. These results indicated that the *eEF2* gene is overexpressed in the majority of several types of cancers and plays an oncogenic role in cancer cell growth. Moreover, the *eEF2* gene product is immunogenic and a promising target molecule of cancer immunotherapy for several types of cancers.

Correspondence to: Professor Yusuke Oji, Department of Cancer Stem Cell Biology, Osaka University Graduate School of Medicine, 1-7 Yamada-oka Suita, Osaka 565-0871, Japan
E-mail: oji@sahs.med.osaka-u.ac.jp

Key words: eukaryotic elongation factor 2, tumor associated antigen, cytotoxic T lymphocyte, autoantibody, cancer immunotherapy

Introduction

Cancer immunotherapy consists of therapeutic approaches to elicit effective antitumor immunity through active or passive immunization. Recent studies have shown that cancer immunotherapy have potential to provide anticancer activity as a single agent or in combination with conventional surgery, radiation and chemotherapy as reviewed (1-4). These findings indicate that cancer immunotherapy should be a promising therapeutic option for the cancer treatment.

Strategies of cancer immunotherapy include antitumor monoclonal antibodies, cancer vaccines, adoptive transfer

of *ex vivo* activated T and natural killer cells, and administration of antibodies or recombinant proteins that either costimulate immune cells or block immune inhibitory pathways (5). Among these strategies, cancer vaccines are approaches to specifically activate host T cells against tumor antigens. The target antigens of cancer vaccine should be: i) highly immunogenic; ii) expressed in a significant proportion of cancer patients; iii) not expressed (or expressed in limited populations) in normal tissues; and iv) required for cancer cell growth and/or survival. Although large number of tumor-associated antigens (TAAs) have been identified using recently developed new technologies such as SEREX and protein microarrays (6,7), there are limited number of antigens that fit all of these criteria in current cancer vaccines.

High level protein biosynthesis is one of the characteristics of cancer cell metabolism (8). Translation is regulated at the initiation and elongation step and deregulated in cancer through a variety of mechanisms (9). Eukaryotic elongation factor 2 (*eEF2*) is a gene that plays an essential role in the polypeptide chain elongation step. Cells control translation levels at elongation step through regulation of eEF2 activity under multiple biological conditions such as cell cycle progression (10) and genotoxic stress (11,12), or in response to endogenous carbon monoxide that exerts antiproliferative effects (13). Previously, we showed that eEF2 was overexpressed in the majority of gastric and colorectal cancers and promoted progression of G_2/M of the cell cycle in association with activation of Akt and a G_2/M regulator, cdc2 proteins, resulting in the enhancement of *in vitro* and *in vivo* cancer cell growth (14). However, the role for eEF2 in the tumorigenesis remains largely unknown and it is undetermined whether eEF2 can be a target molecule of molecule-targeted cancer therapy.

In the present study, we identified eEF2 as an antigen eliciting humoral immune responses in a group of patients with HNSCC or colorectal cancer by immunoblot analysis and showed that eEF2 was overexpressed in the majority of various types of cancers such as lung, esophageal, pancreatic, breast and prostate cancers, HNSCC, glioblastoma multiforme and NHL. Knockdown of eEF2 by shRNA significantly inhibited growth of cancer cells. Furthermore, eEF2-derived 9-mer peptides, EF786 (eEF2 786-794 aa) and EF292 (eEF2 292-300 aa), elicited cytotoxic T lymphocyte (CTL) responses in PBMCs from an HLA-A*24:02- and an HLA-A*02:01-positive healthy donors, respectively, in an HLA-A-restricted manner.

Materials and methods

Cell lines. Lung cancer cell lines PC14 and LU99B, pancreatic cancer cell line PCI6, glioblastoma cell line A172, fibrosarcoma cell line HT1080, gastric cancer cell lines MKN28 and AZ-521, and breast cancer cell line MCF7 were cultured in Dulbecco's modified essential medium supplemented with 10% fetal bovine serum (FBS). Leukemia cell line K562, colon cancer cell line SW480, parent T2 and T2 cells with forced expression of either HLA-A24:02 (T2-2402) (15) or HLA-A02:01 (T2-0201) (16) were cultured in RPMI-1640 medium supplemented with 10% FBS. Leukemia cell line TF-1 was cultured in RPMI-1640 medium supplemented with 10% FBS containing 2 ng/ml human recombinant GM-CSF (Peprotech, Rocky Hill, NJ, USA).

Sera samples. Sera were obtained from 79 colorectal and 80 gastric cancer patients, 10 patients with head and neck squamous cell carcinoma (HNSCC) and 40 healthy individuals with informed consent at Osaka University Hospital and Osaka Rosai Hospital and stored at -80°C until use.

Tissue samples. Tumor tissues were obtained from 31 lung adenocarcinoma, 20 small-cell lung cancer, 15 esophageal squamous cell carcinoma, 21 HNSCC, 28 pancreatic cancer, 8 breast cancer, 16 glioblastoma, 4 prostate cancer and 50 NHL (40 diffuse large B-cell lymphoma and 10 follicular lymphoma) patients. All samples were obtained with informed consent at Osaka University Hospital, Toneyama National Hospital, NHO Osaka Minami Medical Center, and Higashiosaka City General Hospital.

Western blot analysis. Proteins were separated by SDS-PAGE and transferred to Immobilon polyvinylidene difluoride membrane. After blocking of non-specific binding, the membranes were incubated with the first antibodies, followed by incubation with the corresponding secondary antibodies conjugated with alkaline phosphatase, and visualized using BCIP/NBT kit (Nacalai Tesque, Kyoto, Japan). Polyclonal anti-EF2 (Santa Cruz Biotechnology, Santa Cruz, CA, USA) and anti-GAPDH (Chemicon International, Temecula, CA, USA) were used as the first antibodies.

Density gradient isoelectric focusing. Density gradient isoelectric focusing was performed by the method reported previously (17) with minor modifications. In brief, K562 cells ($5x10^7$ cells) were lysed in 2 ml of 0.1% Triton X-100/PBS. After centrifugation, the supernatant was collected as cytoplasmic fraction. Proteins of the cytoplasmic fraction were precipitated with acetone and the pellet was solved in 1 ml of dH_2O containing 4% CHAPS and 7 M urea. Isoelectric focusing was carried out using an LKB column (NA-1720, Nihon-Eido Co., Tokyo, Japan) according to the manufacturer's instructions. On completion of the run, effluent fractions (3 ml each) were collected and twice dialyzed to 200 volume of de-ionized water for 18 h, and then the proteins were precipitated with acetone and stored at -80°C until use.

MALDI-TOF mass spectrometry. The bands on the silver stained gels were excised with surgical blazor. After dehydration with acetonitrile, the gel slice was dried with Speed Vac. The dried gels were digested with Trypsin (Promega, Madison, WI, USA) at 37°C for 24 h and the tryptic peptides were analyzed. All peptide mass fingerprinting (PMF) spectra were obtained by Matrix-assisted laser desorption/ionization time-of-flight (MALDI-TOF) mass spectrometry using an ultraflex spectrometer (Bruker Daltonics, Bremen, Germany). PMF data were then searched with MS-FIT software against NCBInr database.

Immunohistochemistry. Formalin-fixed tissue sections were cut from each paraffin-block. After dewaxing and rehydration, the sections were antigen retrieved using Pascal (Dako Cytometry, Glostrup, Denmark) and reacted with the first antibody at 4°C overnight and then reacted with Dako Envision kit/HRP (Dako Cytometry) at room temperature for 30 min. After treatment with 3% H_2O_2 solution to reduce endogenous peroxidase activity, immunoreactive eEF2 protein was visualized using diaminobenzidine (DAB). The sections were then counterstained with hematoxylin. The intensity of stain in tumor cells was scored as positive (increased staining in carcinoma cells compared to that in normal cells) or negative (less or negative staining in carcinoma cells) by a pathologist. eEF2-H118 antibody (Santa Cruz Biotechnology) that recognized 741-858aa of eEF2 protein and Sigma-Aldrich #SAB4500695 antibody that recognized the N terminus of eEF2 protein were used as first antibodies. Non-immune rabbit immunoglobulin (Dako Cytometry) was used as negative control for non-specific staining.

Sequencing. The *eEF2* gene overexpressed in tumors was RT-PCR amplified and directly sequenced in both directions by the method previously described (14).

Transient expression of shRNA targeting eEF2. Two different shRNA vectors targeting eEF2 mRNA (shEF-1918 and shEF-2804 targeting 1918-1947 and 2804-2833 nt of eEF2 sequence, respectively) were prepared as described previously (14). shRNA targeting luciferase (shLuc) was used as a control. shRNA vectors were transiently expressed as described previously (14).

Enzyme-linked immunosorbent assay (ELISA). ELISA was established to measure serum eEF2 IgG Ab levels by a method previously reported (18) with modifications. ELISA 96-well plates were coated with recombinant GST-tagged eEF2 fragmented protein (Ref Seq NM_001961, 411-858 aa) (2 μg/well). Plates were blocked with TBS containing 0.05% Tween-20 and 1% gelatin. Sera were diluted at 1:100 in TBS containing 0.05% Tween-20 (0.05% TBST) and pre-absorbed by immobilized GST protein at 4°C overnight. Then, 100 μl of the diluted sera was added to each well for overnight incubation at 4°C. After washing, captured eEF2 IgG Ab was detected using ALP-conjugated goat anti-human IgG Ab (Santa Cruz Biotechnology) and BCIP/NBT kit. Then, absorbance at 550 nm was measured using a microplate reader. All sera were examined in duplicate. The titers of eEF2 IgG Ab were calculated by interpolation from the standard line which was constructed for each assay from the results of simultaneous measurements of serial dilutions of rabbit polyclonal eEF2 H-118 Ab using the corresponding second Ab (data not shown). eEF2 Ab titer that produces the absorbance at 550 nm equal to that produced by 1.0 μg/ml of eEF2 H-118 Ab in the ELISA system was defined as 1.0 EF2-reacting-unit (ERU).

Synthetic peptides. The primary amino acid sequence of human eEF2 was analyzed for consensus motifs for 9-mer peptides capable of binding to HLA-A*24:02 or 02:01 using ProPred-I computer algorithm (Table I). Then, the top 4 candidate peptides for HLA-A*02:01 and 24:02 each were synthesized at immunological grade (Sigma Genosys, Hokkaido, Japan). Synthesized peptide was solved in dH_2O (2 mg/ml) and stored at -20°C until use.

MHC stabilization assay. Binding of the synthetic peptides to HLA-A*24:02 or 02:01 molecules was evaluated by MHC stabilization assay using antigen processing mutant T2-2402 or T2-0201 cells as described previously (19). Expression of HLA-A24 or HLA-A02 molecules was measured with a FACSort flow cytometer (BD Biosciences, San Jose, CA, USA) and the mean fluorescence intensity (MFI) was recorded.

In vitro generation of eEF2 peptide-specific $CD8^+$ T cells. PBMCs were obtained from an HLA-A*24:02-positive and an HLA-A*02:01-positive healthy donors by density gradient centrifugation. $CD4^+CD25^+$ Treg cells were depleted from PBMCs by using CD25 MicroBeads (Miltenyi Biotech, Auburn, CA, USA). For generation of autologous dendritic cells (DCs), $CD14^+$ monocytes were isolated from the donor PBMCs using BD IMag CD14 isolation kit (BD Bioscience) and cultured in X-VIVO15 (Bio Whittaker, Walkersville, MD, USA) supplemented with 1% human AB serum (Nabi, Miami, FL, USA) containing IL-4 (1,000 U/ml) and GM-CSF (800 U/ml). After 24 h, IL-1β (10 ng/ml), IL-6 (1,000 U/ml), TNF-α (10 ng/ml), and PGE-2 (1 μg/ml) were added to the culture for DC maturation and the cells were cultured for 48 h. DCs were pulsed with EF2 peptide at the concentration of 10 μg/ml in X-VIVO15 supplemented with 1% human AB serum at 37°C for 2 h, irradiated at 30 Gy, and washed 3 times with RPMI-1640 medium. Then, Treg-depleted PBMCs ($2x10^6$ cells) were stimulated by co-culture with the EF2 peptide-pulsed DCs at the DC: PBMC ratio of 1:10 in X-VIVO15 supplemented with 5% human AB serum. After 24 h of co-culture, IL-2 (20 U/ml) was added to the culture. The cultured cells were repeatedly stimulated with the EF2 peptide-pulsed, irradiated autologous PBMCs at 10-day intervals. After several times of re-stimulation, the cultured cells were maintained as the established T cell lines in X-VIVO15 supplemented with 5% human AB serum, IL-7 (10 IU/ml) and IL-15 (10 IU/ml) and used for cytotoxic assays.

^{51}Cr release cytotoxicity assay. Effector cells were prepared from the established T cell lines using Human CD8 T Lymphocyte Enrichment Set-DM (BD Bioscience). Target cells (listed in Table III) were labeled with 100 μCi of ^{51}Cr (Perkin-Elmer, Waltham, MA, USA) at 37°C for 1.5 h and the target cells ($1x10^4$ cells) were added to wells containing varying numbers of effector cells in 96-well plates. After 4 h of incubation at 37°C, 100 μl of supernatants were collected from each well and measured for radioactivity. The percentage of specific lysis was calculated as follows: percentage of specific lysis = (cpm of experimental release - cpm of spontaneous release)x100/(cpm of maximal release - cpm of spontaneous release). Radioactivity of the supernatant of the target cells that were cultured without effector cells and the radioactivity of target cells that were completely lysed by the treatment with 1% Triton X-100 was used for spontaneous and maximal release, respectively. The characteristics of target cells in cytotoxicity assay are listed in Table III.

Statistics. The statistical significance in a difference between arithmetical means of test groups was assessed by unpaired t-test or Kruskal-Wallis test. After Kruskal-Wallis test, Scheffe's F-test was used as a post hoc test.

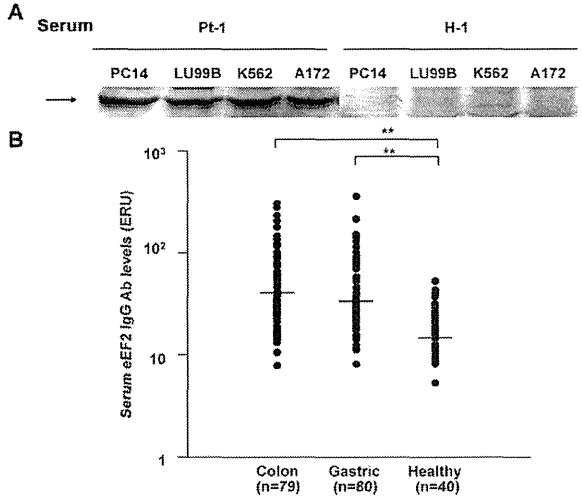

Figure 1. Elevation of serum eEF2 IgG autoantibody levels in cancer patients. (A) Cytoplasmic proteins from PC14, LU99B, K562 and A172 cells were subjected to immunoblot analysis using sera as the first antibodies. Representative results with sera from an HNSCC patient (Pt-1) and a healthy control individual (H-1) are shown. Arrows indicate the protein that is recognized by IgG autoantibody in the sera from the HNSCC patient. (B) Elevation of serum eEF2 IgG autoantibody levels in cancer patients. Assays were performed in duplicate. Colon, colorectal cancer; gastric, gastric cancer; and healthy, healthy individuals. Standard bar represents median value. **p<0.01. eEF2 Ab levels that produces the absorbance at 450 nm equal to that produced by 1 μg/ml of anti-eEF2 H-118 Ab in the ELISA system were defined as 1.0 eEF2-reacting-unit (ERU).

Results

Production of IgG autoantibody against eukaryotic elongation factor 2 (eEF2) in cancer patients. To identify novel tumor-associated antigens (TAAs) with high molecular weight (more than 100 kDa), which were difficult to isolate by standard two dimensional electrophoresis methods because they could not be absorbed into a strip gel, proteins from tumor lysates were first separated by SDS-PAGE, transferred to PVDF membrane, and then probed with sera from tumor-bearing patients. As shown in Fig. 1A, an approximately 100 kDa protein was recognized by sera from 4 of 10 HNSCC and 2 of 3 colon cancer patients in cytoplasmic proteins from two lung cell lines (PC14 and LU99B), one leukemic cell line (K562) and one glioblastoma cell line (A172), whereas it was not recognized by the sera from 5 healthy individuals. To identify this protein, cytoplasmic proteins of K562 cells were fractionated by density gradient isoelectric focusing, separated by SDS-PAGE, and subjected to immunoblot analysis using sera from an HNSCC patient as the first antibody. Since immunoblot analysis detected this protein in fractions of pH 6.62 and pH 6.75, the silver-stained band corresponding to this protein was excised from the SDS-PAGE gel and the protein was analyzed by MALDI-TOF Mass Spectrometry. The search for NCBInr database by MS-Fit software identified the protein as human eukaryotic elongation factor 2 (eEF2) that had M.W. of 95.3-kDa and calculated pI of 6.4.

Elevation of serum eEF2 IgG antibody levels in cancer patients. Serum eEF2 IgG Ab levels were examined by ELISA in 79 colorectal and 80 gastric cancer patients and 40 healthy individuals and detected in all the samples examined (Fig. 1B). eEF2 IgG Ab levels ranged from 7.8 to 301.7 (median 41.1), from 8.1 to 353.9 (median 33.6) and from 5.2 to 53.0 (median 20.6) ERU in colorectal and gastric cancer patients and healthy individuals, respectively. eEF2 IgG Ab levels were significantly ($p<0.01$) higher in both colorectal and gastric cancer patients than healthy individuals.

Overexpression of eEF2 in various types of human cancers. eEF2 protein was immunohistochemically examined in 51 lung cancers, 15 esophageal squamous cell carcinomas, 21 HNSCCs, 28 pancreatic cancers, 8 breast cancers, 16 glioblastoma multiformes, 4 prostate cancers and 50 NHLs. Immunohistochemical analysis with two different anti-EF2 antibodies recognizing different regions of eEF2 protein showed similar results. Overexpression of eEF2 protein was detected in 71.0% (22 of 31) of lung adenocarcinoma, 95.0% (19 of 20) of small-cell lung cancer, 73.3% (11 of 15) of esophageal cancer, 60.7% (17 of 28) of pancreatic cancer, 50.0% (4 of 8) of breast cancer, 75.0% (3 of 4) of prostate cancer, 52.4% (11 of 21) of HNSCC, 75.0% (12 of 16) of glioblastoma multiformes, and 94.0% (47 of 50) of NHL. Results are summarized in Table I. Representative results are shown in Fig. 2.

Table I. Overexpression of eEF2 in human cancers.

Cancer	Overexpression of eEF2 (%)
Lung cancer	80.4 (41/51)
Lung adenocarcinoma	71.0 (22/31)
Small cell lung cancer	95.0 (19/20)
Esophageal squamous cell carcinoma	73.3 (11/15)
Head and neck squamous cell carcinoma	52.4 (11/21)
Pancreatic cancer	60.7 (17/28)
Breast cancer	50.0 (4/8)
Glioblastoma	75.0 (12/16)
Prostate cancer	75.0 (3/4)
Non-Hodgkin's lymphoma	94.0 (47/50)
Diffuse large B cell lymphoma	92.5 (37/40)
Follicular lymphoma	100 (10/10)

Expression of eEF2 protein in human cancers was examined by immunohistochemistry. Immunostaining was evaluated as positive when cancer cells were stained brown in >10% of the cells.

Overexpressed eEF2 gene is a non-mutated, wild-type. To examine whether or not the overexpressed *eEF2* gene was non-mutated, wild-type, the 5' (84-1334 nt) and the 3' (1314-2660 nt) sequences of eEF2 mRNA (coding sequence: 84-2660 nt) from five lung adenocarcinomas and five HNSCCs were amplified by RT-PCR and direct sequencing. No mutation was found in the *eEF2* gene in the 10 cancers examined (data not shown).

Knockdown of eEF2 inhibits cancer cell growth. To examine the role of eEF2 in cancer cell growth, either of two different shRNAs targeting eEF2 (shEF-1918 and shEF-2804) or a control shRNA targeting luciferase (shLuc) was transfected into four eEF2-expressing cells, lung cancer PC14, pancreatic cancer PCI6, fibrosarcoma HT-1080, and glioblastoma A172 and eEF2-undetectable breast cancer MCF7 cells. After culture for 72 h, both of the two shRNAs targeting eEF2 (shEF-1918 and shEF-2804) reduced eEF2 protein expression levels (Fig. 3A) and significantly inhibited cell growth in all the four eEF2-expressing cells examined (Fig. 3B). However, neither of the two shRNAs targeting eEF2 inhibited growth of eEF2-undetectable MCF7 cells.

*Identification of eEF2 peptides that bind to HLA-A*24:02 or HLA-A*02:01 molecules.* Epitope candidates of eEF2 that bound to HLA-A*24:02 or HLA-A*02:01 molecules were first analysed using ProPred-I computer algorithm (Table II).

As candidate epitope peptides that bound to HLA-A*24:02 molecules, EF78, EF786, EF701 and EF412 peptides were selected and analyzed for binding affinity to HLA-A*24:02 molecules by the MHC stabilization assay. These peptides were pulsed to T2-2402 cells and the expression of HLA-A*24:02 molecules on the cell surface was analyzed by flow cytometry. As shown in Table II, all the four peptides increased the expression of HLA-A24:02 molecules on T2-2402 cells as a result of the stabilization of HLA-A24:02 molecules. Among the four peptides, EF786 peptide showed binding affinity higher than $CMVpp65_{328-336}$, which was an exogenous cytomegalovirus antigen epitope, to the HLA-A*24:02 molecules. As candidate peptides that bound to HLA-A*02:01 molecules, EF292, EF739, EF519 and EF671 peptides were selected and analyzed for binding affinity to HLA-A*02:01 molecules by the MHC stabilization assay. As shown in Table II, all the four peptides increased the expression of HLA-A02:01 molecules on T2-0201 cells and EF292 peptide showed the highest binding affinity to HLA-A*02:01 molecules among the four HLA-A*02:01-binding peptides examined.

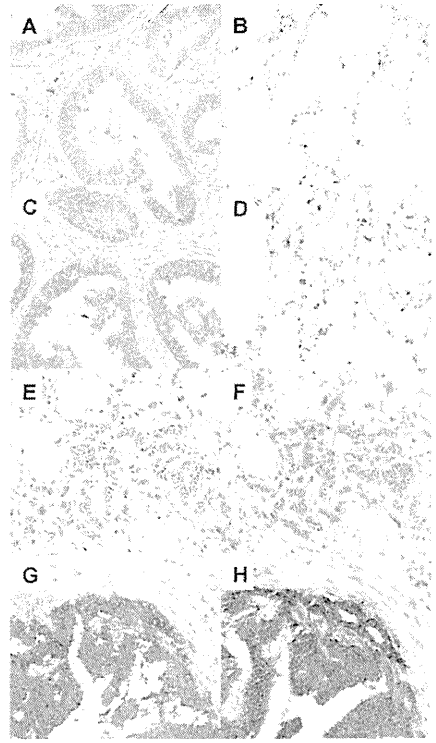

Figure 2. Overexpression of eEF2 in various types of cancers. Representative results of immunohistochemical analysis for eEF2 protein expression in (A and C) lung adenocarcinoma, (B and D) normal lung cells, (E and F) breast cancer, and (G and H) prostate cancer. eEF2 was stained with (A, B, E and G) eEF2-H118 antibody or (C, D, F and H) #SAB4500695 antibody. eEF2 protein was stained brown. Macrophages are non-specifically stained in normal lung tissues.

*Generation of EF2-specific CTLs from HLA-A*24:02- or HLA-A*02:01-positive donors.* Treg-depleted PBMCs from

Table II. Characteristics of EF2-derived peptides and results of the MHC stabilization assay.

Peptide	Position (aa)	Sequence	Score	%MFI increase
HLA-A*24:02-binding peptides				
EF78	78-86	FYELSENDL	360	40.5
EF786	786-794	AYLPVNESF	252	1552.1
EF701	701-709	RFDVHDVTL	40	297.3
EF412	412-420	AFGRVFSGL	33.6	47.9
CMVpp65 328-336		QYDPVAALF		1344.1
HLA-A*02:01-binding peptides				
EF292	292-300	LILDPIFKV	3290	183.3
EF739	739-747	RLMEPIYLV	2426	141.1
EF519	519-527	KLVEGLKRL	705	58.9
EF671	671-679	YLNEIKDSV	642	89.6

The primary amino acid sequences of human eEF2 were analyzed for consensus motifs for 9-mer peptides capable of binding to HLA-A*24:02 or 02:01 molecules using ProPred-I software. Percentage MFI increase in MHC stabilization assay was calculated as follows: percentage MFI increase = (MFI with the given peptide - MFI without peptide)/(MFI without peptide) x 100.

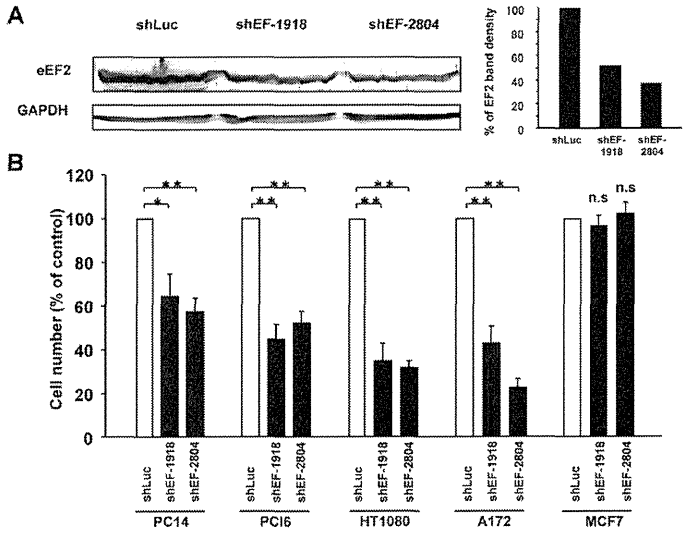

Figure 3. Knockdown of eEF2 inhibits cancer cell growth. Two shRNA vectors targeting different sequences of eEF2 (shEF-1918 and shEF-2804 targeting 1918-1947 and 2804-2833 nt of eEF2 sequence, respectively) or control shRNA targeting luciferase (shLuc) was transfected into PC14, PCI6, HT1080, A172 and MCF7 cells. (A) Reduction in eEF2 protein expression levels in HT1080 cells. Results of western blot analysis are shown. (B) After 72 h of transfection, the cell numbers were examined. *p<0.05; **p<0.01. Experiments were independently performed three times.

HLA-A*24:02- or HLA-A*02:01-positive healthy donors were repeatedly stimulated with EF2 peptides (EF786 and EF292 peptides for HLA-A*24:02- and HLA-A*02:01-positive healthy donors, respectively) and pulsed irradiated autologous DCs and EF2 peptide-specific CTLs were established.

To examine whether EF2 peptides are capable of eliciting CTL responses, CTL activities of established CTLs were examined. As shown in Fig. 4A, EF786-specific, HLA-A*24:02-restricted CTLs lysed EF786 peptide-pulsed T2-2402 cells but not unpulsed ones. The EF786-specific

Table III. Characteristics of target cells in the killing assay.

Target cells	HLA-A*24:02 expression	HLA-A*02:01 expression	eEF2 expression
T2	-	-	Undetectable
T2-2402	+	-	Undetectable
T2-0201	-	+	Undetectable
SW480	+		+
AZ-521	-		+
MKN28	-		+
TF-1		+	+
K562	-	-	+
MCF7		+	Undetectable

Cell surface protein expression of HLA-A molecules was confirmed by flow cytometry. Expression of eEF2 protein was analyzed by western blot analysis.

CTLs lysed HLA-A*24:02-positive, eEF2-expressing SW480 cells, but not HLA-A*24:02-negative, eEF2-expressing AZ-521 and MKN28 cells. As shown in a Fig. 4B, EF292 peptide-specific, HLA-A*02:01-restricted CTLs lysed EF292 peptide-pulsed T2-0201 cells but not unpulsed ones. Moreover, the EF292-specific CTLs lysed HLA-A*02:01-positive, eEF2-expressing TF-1 cells, but not HLA-A*02:01-negative, eEF2-expressing K562 cells and HLA-A*02:01-positive, eEF2-undetectable MCF7 cells (Fig. 4B).

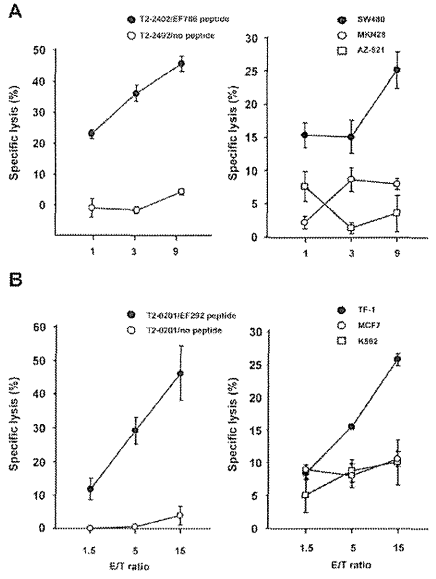

Figure 4. Generation of eEF2-specific CTLs. (A, left panel) Specific lysis of EF786 peptide-pulsed T2-2402 cells by EF786-specific, HLA-A*24:02-restricted CTLs. (A, right panel) Specific lysis of eEF2-expressing, HLA-A*24:02-positive SW480 by EF786-specific, HLA-A*24:02-restricted CTLs. AZ-521 and MKN28 are eEF2-expressing, but HLA-A*24:02-negative. (B, left panel) Specific lysis of EF292 peptide-pulsed T2-0201 cells by EF292-specific, HLA-A*02:01-restricted CTLs. (B, right panel) Specific lysis of eEF2-expressing, HLA-A*02:01-positive TF-1 cells by EF292-specific, HLA-A*02:01-restricted CTLs. K562 is eEF2-expressing and HLA-A*02:01-negative, and MCF7 is eEF2-undetectable and HLA-A*02:01-positive. E/T, effector/target ratio. CTL cytotoxic assays were performed in triplicate.

Discussion

We showed that eEF2 was overexpressed in the majority of various types of tumors such as lung, esophageal, pancreatic, and breast cancer and promoted growth of various types of cancer cells. Moreover, *eEF2* gene product elicited both humoral and cellular eEF2-specific immune responses. The production of eEF2 IgG autoantibody was enhanced in patients with colorectal and gastric cancer and 9-mer eEF2 peptides elicited EF2-specific CTLs from healthy donors. These results indicated that overexpressed eEF2 played an oncogenic role and served as a TAA in these tumors.

It is considered that production of autoantibody indicates the potential of its antigen as a target of cancer immunotherapy (20). In the present study, we showed the elevation of serum EF2 IgG levels in colorectal and gastric cancer patients, indicating that eEF2 overexpressed in cancer cells was recognized by the host immune system and induced eEF2-specific immune responses. Since production of IgG autoantibody needed help from $CD4^+$ helper T cells (Th cells) for class switch from IgM to IgG, elevation of EF2 IgG Ab levels indicated the activation of EF2-specific Th cells. It is well established that Th cells play an important role in the immune responses against cancer (21). $CD4^+$ Th cells are required for activation and maintenance of $CD8^+$ CTLs, but they could also exert cytotoxic function against cancer in the absence of $CD8^+$ CTLs recognizing antigenic peptides presented by MHC class II molecules (22,23). These results indicated that EF2 protein was an immunogenic molecule that is capable of eliciting not only humoral but also cellular immune responses. In fact, eEF2-derived EF786 peptide showed the binding affinity higher than CMVpp65328-336, an exogenous viral antigen epitope, and elicited *in vitro* EF786-specific CTLs from PBMCs of HLA-A*24:02-positive healthy donors. Taken together, eEF2 protein is highly immunogenic and a promising target molecule for cancer immunotherapy.

Expression of target molecules in tumor cells is the first requisite for TAA-targeting cancer immunotherapy. Survivin is a member of the family of the inhibitor of apoptosis proteins and functions as a key regulator of mitosis and programmed cell death (24). Survivin is overexpressed in various types of tumors with the frequency of 34.5% in gastric cancers (25), 50-60% in colorectal cancers (25,26), 64% in malignant gliomas (27), 53-72% in lung cancers (28,29), and 70.7% in breast cancers (30). Cancer vaccines to induce an antigen-specific immune responses against survivin-expressing tumor cells have been developed with

promising results (31,32). Thus, survivin appears to be a promising TAA. However, survivin-targeted immunotherapy may be applicable to a limited population of patients because of its low expression rates in several tumors. In addition, the frequency of survivin-positive tumor cells may vary in individual tumors (25). Thus, the existence of tumor cells lacking survivin could result in tumor evasion from CTL responses against survivin induced by vaccination. NY-ESO-1 is a member of cancer testis antigens and is expressed in a variety of common cancers. Clinical trials that evaluate therapeutic responses against NY-ESO-1 are underway in various cancers (33). However, NY-ESO-1 protein was expressed in only 20 to 30% of lung (34), bladder and ovarian cancers (35) and melanoma and was undetectable in colon and renal cancers (36). Thus, therapeutic strategy against NY-ESO-1 is applicable to a minor population of cancer patients. Compared to these TAAs, eEF2 is more attractive as a target molecule of cancer immunotherapy because of its high frequency of overexpression in various types of cancers. The frequency of eEF2 overexpression exceeded 70% in lung, esophageal, breast and prostate cancers, and 90% in gastric and colorectal cancers and NHL, as shown in the present and previous (14) studies. These results indicated that eEF2-targeted immunotherapy should be a therapeutic strategy that would be applicable to the majority of cancer patients. WT1 is also a promising target molecule of immunotherapy and was ranked as top of TAAs (37). WT1 is overexpressed in the majority of leukemia (38) and various types of tumors such as lung (39), colorectal (40) and pancreatic cancer (41), and glioblastoma multiforme (42). However, WT1 might be less expressed in malignant lymphoma. In diffuse large B-cell lymphoma the most common type of NHL, WT1 protein was detected in only 33% of the cases examined (43). Thus, eEF2-targeted immunotherapy may have a priority for NHL.

One mechanism for escape from immune surveillance is the loss of expression of target molecules in cancer cells (44). Therefore, it is important to know whether or not loss of eEF2 expression affects tumor growth in consideration of the potential of eEF2 as a target molecule for cancer immmunotherapy. As shown in the present study, knockdown of eEF2 by shRNA significantly inhibited cancer cell growth. Also, we have demonstrated that eEF2 was overexpressed in the majority of gastric and colorectal cancers and promoted progression of G_2/M in the cell cycle, resulting in the enhancement of *in vitro* and *in vivo* cancer cell growth (14). Based on these findings showing the involvement of eEF2 in cancer cell growth, it is unlikely that antigenic loss of eEF2 could become a mechanism of tumor escape from eEF2-specific immune responses.

A primary goal of cancer immunotherapy is generation of effective CTL responses through the expansion of robust pre-existing, naturally occurring $CD8^+$ CTL precursors and the establishment of long-lasting memory $CD8^+$ T cells. This critically depends on the activation of pre-existing antigen-specific CTL precursors as the initial step to induce immune responses. In the present study, eEF2-specific CTL clones were established from HLA-A*24:02- or HLA-A*02:01-positive healthy donors. In addition, eEF2 IgG autoantibody is detected at low levels in healthy individuals examined. Since these results indicated the existence of not only eEF2-specific CTL precursors but also eEF2-specific B and Th cells even in healthy donors without cancer, the host immune system of cancer patients should have a potential to make robust immune responses against eEF2-expressing cancers by vaccination with EF2 protein or peptide.

In conclusion, eEF2 that is overexpressed in a wide variety of cancers is a promising cancer antigen that can elicit both humoral and cellular immune responses and shows promise as a target molecule of cancer immunotherapy.

Acknowledgements

We thank Shigemi Norioka (Osaka University) and Mamoru Sato (Chiba University) for their technical support on isoelectric focusing. We also thank Kaori Miyazaki and Atsushi Okumura (Osaka University) for their experimental assistance. This study was supported in part by a Grant-in-Aid from the Ministry of Education, Science, Sports, Culture and Technology, Japan, the Ministry of Health, Labour and Welfare, Japan and Fukui Satoshi Medical Research Foundation.

References

1. Lesterhuis WJ, Haanen JB and Punt CJ: Cancer immunotherapy - revisited. Nat Rev Drug Discov 10: 591-600, 2011.
2. Wright SE: Immunotherapy of breast cancer. Expert Opin Biol Ther 12: 479-490, 2012.
3. Slingluff CL Jr: The present and future of peptide vaccines for cancer: single or multiple, long or short, alone or in combination? Cancer J 17: 343-350, 2011.
4. Murala S, Alli V, Kreisel D, Gelman AE and Krupnick AS: Current status of immunotherapy for the treatment of lung cancer. J Thorac Dis 2: 237-244, 2010.
5. Topalian SL, Weiner GJ and Pardoll DM: Cancer immunotherapy comes of age. J Clin Oncol 29: 4828-4836, 2011.
6. Desmetz C, Mange A, Maudelonde T and Solassol J: Autoantibody signatures: progress and perspectives for early cancer detection. J Cell Mol Med 15: 2013-2024, 2011.
7. Murphy MA, O'Leary JJ and Cahill DJ: Assessment of the humoral immune response to cancer. J Proteomics 75: 4573-4579, 2012.
8. Grzmil M and Hemmings BA: Translation regulation as a therapeutic target in cancer. Cancer Res 72: 3891-3900, 2012.
9. Bilanges B and Stokoe D: Mechanism of translational deregulation in human tumors and therapeutic intervention strategies. Oncogene 26: 5973-5990, 2007.
10. Hizli AA, Chi Y, Swanger J, Carter JH, Liao Y, Welcker M, Ryazanov AG and Clurman BE: Phosphorylation of eukaryotic elongation factor 2 (eEF2) by cyclin A-cyclin-dependent kinase 2 regulates its inhibition by eEF2 kinase. Mol Cell Biol 33: 596-604, 2013.
11. White SJ, Kasman LM, Kelly MM, Lu P, Spruill L, McDermott PJ and Voelkel-Johnson C: Doxorubicin generates a proapoptotic phenotype by phosphorylation of EF-2. Free Radic Biol Med 43: 1313-1321, 2007.
12. Kruiswijk F, Yuniati L, Magliozzi R, Low TY, Lim R, Bolder R, Mohammed S, Proud CG, Heck AJ, Pagano M and Guardavaccaro D: Coupled activation and degradation of eEF2K regulates protein synthesis in response to genotoxic stress. Sci Signal 5: ra40, 2012.
13. Schwer CI, Stoll P, Rospert S, Fitzke E, Schallner N, Burkle H, Schmidt R and Humar M: Carbon monoxide releasing molecule-2 CORM-2 represses global protein synthesis by inhibition of eukaryotic elongation factor eEF2. Int J Biochem Cell Biol 45: 201-212, 2013.
14. Nakamura J, Aoyagi S, Nanchi I, Nakatsuka S, Hirata E, Shibata S, Fukuda M, Yamamoto Y, Fukuda I, Tatsumi N, Ueda T, Fujiki F, Nomura M, Nishida S, Shirakata T, Hosen N, Tsuboi A, Oka Y, Nezu R, Mori M, Doki Y, Aozasa K, Sugiyama H and Oji Y: Overexpression of eukaryotic elongation factor eEF2 in gastrointestinal cancers and its involvement in G_2/M progression in the cell cycle. Int J Oncol 34: 1181-1189, 2009.

15. Kuzushima K, Hayashi N, Kimura H and Tsurumi T: Efficient identification of HLA-A*2402-restricted cytomegalovirus-specific CD8(+) T-cell epitopes by a computer algorithm and an enzyme-linked immunospot assay. Blood 98: 1872-1881, 2001.
16. Oka Y, Elisseeva OA, Tsuboi A, Ogawa H, Tamaki H, Li H, Oji Y, Kim EH, Soma T, Asada M, Ueda K, Maruya E, Saji H, Kishimoto T, Udaka K and Sugiyama H: Human cytotoxic T lymphocyte responses specific for peptides of wild-type Wilms' tumor gene WT1 product. Immunogenetics 51: 99-107, 2000.
17. Masuda T, Ide N and Kitabatake N: Effects of chemical modification of lysine residues on the sweetness of lysozyme. Chem Senses 30: 253-264, 2005.
18. Oji Y, Kitamura Y, Kamino E, Kitano A, Sawabata N, Inoue M, Mori M, Nakatsuka S, Sakaguchi N, Miyazaki K, Nakamura M, Fukuda I, Nakamura J, Tatsumi N, Takakuwa T, Nishida S, Shirakata T, Hosen N, Tsuboi A, Nezu R, Maeda H, Oka Y, Kawase I, Aozasa K, Okumura M, Miyoshi S and Sugiyama H: WT1 IgG antibody for early detection of nonsmall cell lung cancer and as its prognostic factor. Int J Cancer 125: 381-387, 2009.
19. Morishima S, Akatsuka Y, Nawa A, Kondo E, Kiyono T, Torikai H, Nakanishi T, Ito Y, Tsujimura K, Iwata K, Ito K, Kodera Y, Morishima Y, Kuzushima K and Takahashi T: Identification of an HLA-A24- restricted cytotoxic T lymphocyte epitope from human papillomavirus type-16 E6: the combined effects of bortezomib and interferon-gamma on the presentation of a cryptic epitope. Int J Cancer 120: 594-604, 2007.
20. Chiriva-Internati M, Yu Y, Mirandola L, D'Cunha N, Hardwicke F, Cannon MJ, Cobos E and Kast WM: Identification of AKAP-4 as a new cancer/testis antigen for detection and immunotherapy of prostate cancer. Prostate 72: 12-23, 2012.
21. Qin Z and Blankenstein T: $CD4^+$ T cell-mediated tumor rejection involves inhibition of angiogenesis that is dependent on IFNγ receptor expression by nonhematopoietic cells. Immunity 12: 677-686, 2000.
22. Bogen B, Munthe L, Sollien A, Hofgaard P, Omholt H, Dagnaes F, Dembic Z and Lauritzsen GF: Naive $CD4^+$ T cells confer idiotype-specific tumor resistance in the absence of antibodies. Eur J Immunol 25: 3079-3086, 1995.
23. Lin Y, Fujiki F, Katsuhara A, Oka Y, Tsuboi A, Aoyama N, Tanii S, Nakajima H, Tatsumi N, Morimoto S, Tamanaka T, Tachino S, Hosen N, Nishida S, Oji Y, Kumanogoh A and Sugiyama H: HLA-DPB1*05:01-restricted WT1 332-specific TCR-transduced $CD4^+$ T lymphocytes display a helper activity for WT1-specific CTL induction and a cytotoxicity against leukemia cells. J Immunother 36: 159-170, 2013.
24. Mita AC, Mita MM, Nawrocki ST and Giles FJ: Survivin: key regulator of mitosis and apoptosis and novel target for cancer therapeutics. Clin Cancer Res 14: 5000-5005, 2008.
25. Lu CD, Altieri DC and Tanigawa N: Expression of a novel anti-apoptosis gene, survivin, correlated with tumor cell apoptosis and p53 accumulation in gastric carcinomas. Cancer Res 58: 1808-1812, 1998.
26. Kawasaki H, Altieri DC, Lu CD, Toyoda M, Tenjo T and Tanigawa N: Inhibition of apoptosis by survivin predicts shorter survival rates in colorectal cancer. Cancer Res 58: 5071-5074, 1998.
27. Chakravarti A, Noll E, Black PM, Finkelstein DF, Finkelstein DM, Dyson NJ and Loeffler JS: Quantitatively determined survivin expression levels are of prognostic value in human gliomas. J Clin Oncol 20: 1063-1068, 2002.
28. Wang M, Liu BG, Yang ZY, Hong X and Chen GY: Significance of survivin expression: Prognostic value and survival in stage III non-small cell lung cancer. Exp Ther Med 3: 983-988, 2012.
29. Bria E, Visca P, Novelli F, Casini B, Diodoro MG, Perrone-Donnorso R, Botti C, Sperduti I, Facciolo F, Milella M, Cecere FL, Cognetti F and Mottolese M: Nuclear and cytoplasmic cellular distribution of survivin as survival predictor in resected non-small-cell lung cancer. Eur J Surg Oncol 34: 593-598, 2008.
30. Tanaka K, Iwamoto S, Gon G, Nohara T, Iwamoto M and Tanigawa N: Expression of survivin and its relationship to loss of apoptosis in breast carcinomas. Clin Cancer Res 6: 127-134, 2000.
31. Idenoue S, Hirohashi Y, Torigoe T, Sato Y, Tamura Y, Hariu H, Yamamoto M, Kurotaki T, Tsuruma T, Asanuma H, Kanaseki T, Ikeda H, Kashiwagi K, Okazaki M, Sasaki K, Sato T, Ohmura T, Hata F, Yamaguchi K, Hirata K and Sato N: A potent immunogenic general cancer vaccine that targets survivin, an inhibitor of apoptosis proteins. Clin Cancer Res 11: 1474-1482, 2005.
32. Kameshima H, Tsuruma T, Torigoe T, Takahashi A, Hirohashi Y, Tamura Y, Tsukahara T, Ichimiya S, Kanaseki T, Iwayama Y, Sato N and Hirata K: Immunogenic enhancement and clinical effect by type-I interferon of anti-apoptotic protein, survivin-derived peptide vaccine, in advanced colorectal cancer patients. Cancer Sci 102: 1181-1187, 2011.
33. Cebon J, Knights A, Ebert L, Jackson H and Chen W: Evaluation of cellular immune responses in cancer vaccine recipients: lessons from NY-ESO-1. Expert Rev Vaccines 9: 617-629, 2010.
34. Kim SH, Lee S, Lee CH, Lee MK, Kim YD, Shin DH, Choi KU, Kim JY, Park do Y and Sol MY: Expression of cancer-testis antigens MAGE-A3/6 and NY-ESO-1 in non-small-cell lung carcinomas and their relationship with immune cell infiltration. Lung 187: 401-411, 2009.
35. Yakirevich E, Sabo E, Lavie O, Mazareb S, Spagnoli GC and Resnick MB: Expression of the MAGE-A4 and NY-ESO-1 cancer-testis antigens in serous ovarian neoplasms. Clin Cancer Res 9: 6453-6460, 2003.
36. Jungbluth AA, Chen YT, Stockert E, Busam KJ, Kolb D, Iversen K, Coplan K, Williamson B, Altorki N and Old LJ: Immunohistochemical analysis of NY-ESO-1 antigen expression in normal and malignant human tissues. Int J Cancer 92: 856-860, 2001.
37. Cheever MA, Allison JP, Ferris AS, Finn OJ, Hastings BM, Hecht TT, Mellman I, Prindiville SA, Viner JL, Weiner LM and Matrisian LM: The prioritization of cancer antigens: a national cancer institute pilot project for the acceleration of translational research. Clin Cancer Res 15: 5323-5337, 2009.
38. Inoue K, Sugiyama H, Ogawa H, Nakagawa M, Yamagami T, Miwa H, Kita K, Hiraoka A, Masaoka T, Nasu K, Kyo T, Dohy H, Nakauchi H, Ishidate T, Akiyama T and Kishimoto T: WT1 as a new prognostic factor and a new marker for the detection of minimal residual disease in acute leukemia. Blood 84: 3071-3079, 1994.
39. Oji Y, Miyoshi S, Maeda H, Hayashi S, Tamaki H, Nakatsuka S, Yao M, Takahashi E, Nakano Y, Hirabayashi H, Shintani Y, Oka Y, Tsuboi A, Hosen N, Asada M, Fujioka T, Murakami M, Kanato K, Motomura M, Kim EH, Kawakami M, Ikegame K, Ogawa H, Aozasa K, Kawase I and Sugiyama H: Overexpression of the Wilms' tumor gene WT1 in de novo lung cancers. Int J Cancer 100: 297-303, 2002.
40. Oji Y, Yamamoto H, Nomura M, Nakano Y, Ikeba A, Nakatsuka S, Abeno S, Kiyotoh E, Jomgeow T, Sekimoto M, Nezu R, Yoshikawa Y, Inoue Y, Hosen N, Kawakami M, Tsuboi A, Oka Y, Ogawa H, Souda S, Aozasa K, Monden M and Sugiyama H: Overexpression of the Wilms' tumor gene WT1 in colorectal adenocarcinoma. Cancer Sci 94: 712-717, 2003.
41. Oji Y, Nakamori S, Fujikawa M, Nakatsuka S, Yokota A, Tatsumi N, Abeno S, Ikeba A, Takashima S, Tsujie M, Yamamoto H, Sakon M, Nezu R, Kawano K, Nishida S, Ikegame K, Kawakami M, Tsuboi A, Oka Y, Yoshikawa K, Aozasa K, Monden M and Sugiyama H: Overexpression of the Wilms' tumor gene WT1 in pancreatic ductal adenocarcinoma. Cancer Sci 95: 583-587, 2004.
42. Oji Y, Suzuki T, Nakano Y, Maruno M, Nakatsuka S, Jomgeow T, Abeno S, Tatsumi N, Yokota A, Aoyagi S, Nakazawa T, Ito K, Kanato K, Shirakata T, Nishida S, Hosen N, Kawakami M, Tsuboi A, Oka Y, Aozasa K, Yoshimine T and Sugiyama H: Overexpression of the Wilms' tumor gene WT1 in primary astrocytic tumors. Cancer Sci 95: 822-827, 2004.
43. Drakos E, Rassidakis GZ, Tsioli P, Lai R, Jones D and Medeiros LJ: Differential expression of WT1 gene product in non-Hodgkin lymphomas. Appl Immunohistochem Mol Morphol 13: 132-137, 2005.
44. Schreiber RD, Old LJ and Smyth MJ: Cancer immunoediting: integrating immunity's roles in cancer suppression and promotion. Science 331: 1565-1570, 2011.

Histamine Contributes to Tissue Remodeling via Periostin Expression

Lingli Yang[1], Hiroyuki Murota[1], Satoshi Serada[2], Minoru Fujimoto[2], Akira Kudo[3], Tetsuji Naka[2] and Ichiro Katayama[1]

Histamine is thought to have a critical role in the synthesis of extracellular matrix in skin and may be involved in tissue remodeling of allergic diseases. Recent studies revealed that periostin, a matricelluar protein, contributed to tissue remodeling; however, a link between periostin and histamine remains unproven. We investigated whether periostin was involved in histamine-induced collagen production. Cultured dermal fibroblasts derived from wild-type (WT) or periostin knockout ($PN^{-/-}$) mice were stimulated with histamine, and then collagen and periostin production was evaluated. Histamine induced collagen gene expression in WT fibroblasts in the late phase but not in the early phase, whereas no effect on collagen expression was observed in histamine-stimulated $PN^{-/-}$ fibroblasts. In WT fibroblasts, histamine directly induced periostin expression in a dose-dependent manner, and an H1 receptor antagonist blocked both periostin and collagen expression. Histamine activated extracellular signal-regulated kinase 1/2 (ERK1/2) through the H1 receptor. Periostin induction was inhibited by either H1 antagonist or ERK1/2 inhibitor treatment *in vitro* and was attenuated in $H1R^{-/-}$ mice. Elevated expression of periostin was found in lesional skin from atopic dermatitis patients. These results suggest that histamine mediates periostin induction and collagen production through activation of the H1 receptor–mediated ERK1/2 pathway; furthermore, histamine may accelerate the chronicity of atopic dermatitis.

Journal of Investigative Dermatology advance online publication, 3 April 2014; doi:10.1038/jid.2014.120

INTRODUCTION

Tissue remodeling is both a cause and a consequence of allergic inflammation and is considered a target for therapeutic intervention.

Understanding the underlying mechanisms that cause tissue remodeling is progressing gradually, and certain factors that are correlated with allergic inflammation have been found to be involved in tissue remodeling. Among them, histamine has been found to induce *de novo* synthesis of collagen from fibroblasts in both *in vivo* and *in vitro* experiments (Sandberg, 1962, 1964; Cohen *et al.*, 1972; Murota *et al.*, 2008). Furthermore, it is well known that antihistamine drugs used for the treatment of allergic disorders improve hypertrophic scars (Murakami *et al.*, 1998). These results indicate that histamine may be involved in the mechanism of tissue remodeling in allergic diseases; however, it remains unknown how histamine contributes to tissue remodeling.

Recent studies showed that expression of periostin, a matricellular protein with profibrogenic function, increased in sera and lesional tissue from patients with allergic diseases, such as allergic rhinitis, asthma, and atopic dermatitis (AD), and that this expression was associated with airway or other tissue remodeling (Takayama *et al.*, 2006; Hur *et al.*, 2012; Masuoka *et al.*, 2012). Furthermore, periostin has also emerged as a key regulator in the development of wound healing and scleroderma (Ontsuka *et al.*, 2012; Yang *et al.*, 2012). To the best of our knowledge, the impact of histamine on the expression level of periostin is unknown. Therefore, in this study, we investigated the correlation between histamine and the fibrotic factor periostin in primary cultured dermal fibroblasts.

[1]Department of Dermatology, Osaka University Graduate School of Medicine, Osaka, Japan; [2]Laboratory for Immune Signal, National Institute of Biomedical Innovation, Osaka, Japan and [3]Department of Biological Information, Tokyo Institute of Technology, Yokohama, Japan

Correspondence: Hiroyuki Murota, Department of Dermatology, Osaka University Graduate School of Medicine, 2-2 Yamadaoka, Suita 565-0871, Osaka, Japan. E-mail: h-murota@derma.med.osaka-u.ac.jp

Abbreviations: AD, atopic dermatitis; CREB, cAMP response element-binding protein; ERK1/2, extracellular signal-regulated kinase 1/2; GAPDH, glyceraldehyde 3-phosphate dehydrogenase; H1R, histamine receptor 1; WT, wild type

Received 2 October 2013; revised 3 February 2014; accepted 6 February 2014; accepted article preview online 27 February 2014

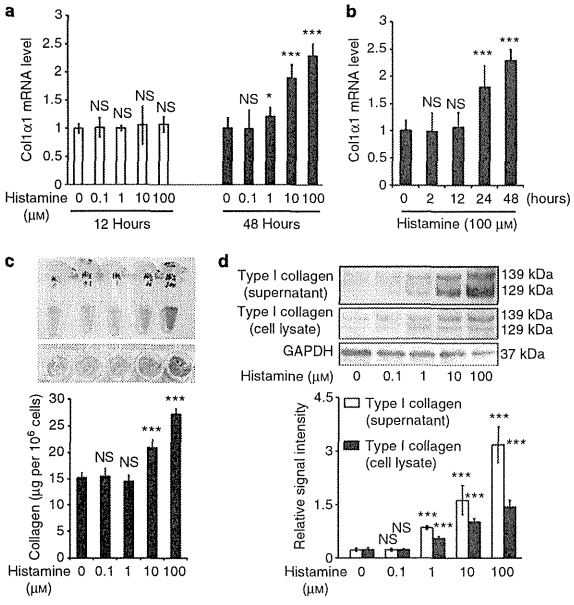

Figure 1. Collagen production is induced by histamine stimulation in cultured wild-type (WT) fibroblasts. (**a**) Effect of histamine on collagen type-I alpha 1 (Col1α1) mRNA expression was assessed by quantitative real-time reverse transcriptase–PCR (qRT-PCR) at 12 hours (white bar) and 48 hours (black bar) after the addition of histamine at the indicated concentration. (**b**) Effect of histamine on Col1α1 mRNA expression after the stimulation with histamine (100 μM) for the indicated time periods. (**c**) Soluble collagen content in the supernatants of WT fibroblasts that had been stimulated with histamine for 48 hours. (**d**) Representative western blotting and quantitative analyses of signal density on blots from three independent experiments analyzing collagen protein expression in response to 48 hours of histamine stimulation (using glyceraldehyde 3-phosphate dehydrogenase (GAPDH) as an internal control). Values were derived from three independent experiments using WT fibroblast cultures. Values represent the mean ± SD for the three independent experiments in each condition. *$P<0.05$; ***$P<0.001$; NS, no significance, compared with control (0 μM histamine) by one-way analysis of variance (ANOVA) followed by Dunnett's test.

RESULTS

Collagen production is induced by histamine stimulation

To investigate whether histamine influences collagen synthesis, primary cultured murine dermal fibroblasts were stimulated with histamine at concentrations ranging from 0 to 100 μM, as described in our previous report (Murota *et al.*, 2008; Murota and Katayama, 2009).

Histamine-induced type I collagen production was observed with concentrations of histamine from 1 to 100 μM (Figure 1). Compared with nontreated controls, collagen synthesis was significantly increased after histamine treatment in a dose-dependent manner (Figure 1a, c and d). No significant increase was observed at 2 and 12 hours, whereas collagen was markedly induced by histamine 24 and 48 hours after addition (Figure 1a and b). In our previous study (Yang *et al.*, 2012), the mRNA expression of type I collagen was found to be significantly increased in cultured mouse dermal fibroblasts after a 2-hour stimulation with recombinant periostin alone. Therefore, these late responses in the present study may be a result of *de novo* synthesis of certain second messengers.

Periostin is upregulated upon histamine stimulation in dermal fibroblasts

Next, to investigate whether histamine affects the expression level of periostin, we stimulated wild-type (WT) primary dermal fibroblasts with histamine at the indicated concentrations (Figure 2). As expected, two hours of incubation with histamine produced a significant dose-dependent increase of periostin mRNA expression in dermal fibroblasts, as assessed by reverse transcriptase–PCR and quantitative real-time reverse transcriptase–PCR (Figure 2a and b). After 24 hours of incubation with histamine, the periostin protein levels increased in the culture supernatant and cell lysates (Figure 2 c). These results suggest that histamine may directly upregulate the transcription and synthesis of periostin.

Histamine upregulates periostin expression via histamine receptor 1 (H1R)

To identify the histamine receptor subtype responsible for the histamine-induced periostin expression, antagonists for H1R, H2R, and H4R were tested *in vitro*. The effects of histamine on periostin mRNA and protein levels were evaluated at 2 hours or 24 hours, respectively, in dermal fibroblasts after histamine stimulation following preincubation with or without these histamine receptor antagonists (Figure 3a and b). Histamine-induced periostin expression was blocked by H1R antagonist

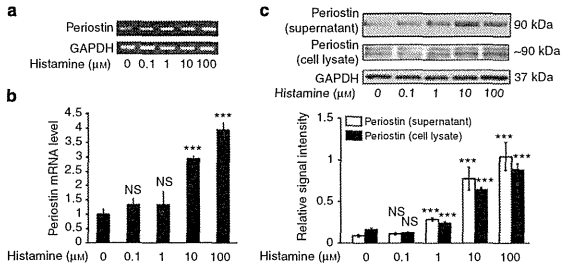

Figure 2. Periostin is upregulated upon histamine stimulation in cultured wild-type (WT) fibroblasts. WT fibroblasts were stimulated with histamine at the indicated concentrations for 2 hours (**a**, **b**) or 24 hours (**c**). Periostin mRNA expression was determined by reverse transcriptase–PCR (RT-PCR) analysis (**a**) and real-time PCR analysis (**b**). Periostin protein expression was evaluated by western blotting analysis (**c**). Three independent experiments were performed, and representative blots and quantitative analysis of signal density on blots from three independent experiments are shown (using glyceraldehyde 3-phosphate dehydrogenase (GAPDH) as an internal control). Values in **b** and **c** are shown as mean ± SD for three independent experiments. ***$P<0.001$; NS, no significance, compared with control (0 μM histamine) by one-way analysis of variance (ANOVA) followed by Dunnett's test.

but not by either H2R or H4R antagonists (Figure 3a and b), suggesting that histamine upregulates periostin expression through H1R activation *in vitro*.

Next, we determined whether periostin was induced by histamine via H1R *in vivo*. Histamine release was triggered through mast cell degranulation using the compound 48/80 in WT and H1R-deficient ($H1R^{-/-}$) mice. After treatment with compound 48/80 for three consecutive days, skin at the injected site was sampled. Periostin expression in WT and $H1R^{-/-}$ mouse skin was compared by western blotting analyses (Figure 3c). In WT mice, periostin expression markedly increased after compound 48/80 treatment, although no such increase was observed in $H1R^{-/-}$ mice (Figure 3c). These results suggest that H1R mediates histamine-induced periostin upregulation.

H1R activation upregulates periostin expression via the ERK1/2 pathway

Next, to investigate the signal transduction pathway involved after H1R activation by histamine in dermal fibroblasts, we used a commercial human phosphorylated kinase array kit to profile the phosphorylated kinases in normal human dermal fibroblasts (Figure 4a). Subsequently, phosphorylation of analogous kinases was confirmed in murine dermal fibroblasts by western blot analysis (Figure 4b). Compared with nontreated dermal fibroblasts, enhanced phosphorylation of extracellular signal-regulated kinase 1/2 (ERK1/2) and the downstream factor cAMP response element-binding protein (CREB) was observed after 10 minutes and 30 minutes of histamine stimulation (Figure 4a and b).

Furthermore, we found that histamine-induced phosphorylation of ERK1/2 and CREB was blocked not only with U0126 (a selective ERK1/2 kinase inhibitor) but also with an H1R antagonist (Figure 4c and d).

These observations demonstrated that histamine activates the ERK1/2 signal transduction pathway via H1R in dermal fibroblasts.

In addition, to verify the involvement of ERK1/2 activation in histamine-induced upregulation of periostin, western blotting analysis was performed (Figure 4c and d). Both U0126 and H1R antagonists decreased the expression of periostin, as well as suppressed the phosphorylation of CREB (Figure 4c and d). These results indicated that H1R-mediated signaling upregulated periostin expression via the ERK1/2 pathway.

H1R-mediated upregulation of periostin is essential for histamine-induced collagen production

To investigate the involvement of periostin in histamine-induced collagen production, primary dermal fibroblasts from WT and periostin-deficient ($PN^{-/-}$) mice were stimulated with histamine (100 μM) for 48 hours. The induction of collagen was abolished in $PN^{-/-}$ fibroblasts at both the mRNA (Figure 5a) and protein (Figure 5b and c) levels. Histamine-treated $PN^{-/-}$ fibroblasts did not exhibit increases in mRNA or protein expression of type I collagen (Col1; Figure 5a–c).

As described above, periostin was induced by histamine via the H1R pathway. To further clarify whether H1R was associated with histamine-induced collagen production, H1R antagonist was added to WT fibroblasts before histamine stimulation. After 48 hours of histamine stimulation, collagen production was evaluated as determined by quantitative real-time reverse transcriptase–PCR, Sircol Collagen Assay, and western blotting analyses (Figure 6). As expected, histamine-induced collagen synthesis was blocked by an H1R antagonist (Figure 6a–c). Furthermore, this inhibitory effect was rescued by the addition of recombinant mouse periostin (rmPeriostin; Figure 6a–c).

In addition, this mechanism was confirmed in cultured primary human dermal fibroblasts derived from healthy donor skin biopsies (Supplementary Figure S1 online).

Finally, we addressed the question of how strong the effect of histamine on tissue remodeling was in AD. Compared with normal skin and AD nonlesioned skin, increased expression of periostin was observed in both acute AD lesioned skin and skin tissues with positive *Dermatophagoides farinae* (Derf1) scratch tests (Supplementary Figure S2 online). Our results suggest that histamine may contribute to the initiation of tissue remodeling during the acute phase of AD.

DISCUSSION

Here, we report that histamine increases the expression of periostin in dermal fibroblasts. Moreover, periostin increases *de novo* synthesis of Col1 via an ERK1/2-mediated pathway.

It is widely recognized that mast cells contribute to the healing of skin wounds (Hebda *et al.*, 1993; Artuc *et al.*, 1999; Trautmann *et al.*, 2000; Gailit *et al.*, 2001; Noli and Miolo, 2001). Impaired wound closure in mast cell–deficient mice indicates that mast cells have a crucial role in the wound repair process (Weller *et al.*, 2006). An increased number of mast cells in fibrotic tissues such as scleroderma, keloid, or healing wounds has been identified (Hawkins *et al.*, 1985; Atkins and Clark, 1987), although it is still unclear whether mast cells are fibrogenic. In many instances, chemical mediators, such as histamine, which is derived from degranulated mast cells or basophils, have been implicated as a cause of inflammation and tissue remodeling in AD (Davies and Greaves, 1980; Nishioka *et al.*, 1987; Wahlgren, 1999; Murota and Katayama, 2009). In support of these findings, H1R antagonist has been shown to inhibit the synthesis of Col1 by dermal fibroblasts (Murota *et al.*, 2008). Interestingly, histamine H1R antagonists but not H2R antagonists reduced wound closure in experimentally induced skin wounds in mice (Weller *et al.*, 2006). Therefore, histamine is believed to have an important role in the wound-healing process. Indeed, disruption of histamine in histidine decarboxylase knockout mice resulted in delayed cutaneous would healing, and this phenotype was rescued by exogenous histamine administration (Numata *et al.*, 2006). It remains unclear how histamine promotes wound healing. Some reports indicated that histamine induces fibroblast proliferation after a long period of coculturing (Russel *et al.*, 1977; Topol *et al.*, 1981). In our study, increased expression of Col1 mRNA was observed after 48 hours of co-incubation with histamine. Thus, histamine-mediated tissue remodeling may require the expression of periostin as a second messenger in order to elicit tissue remodeling.

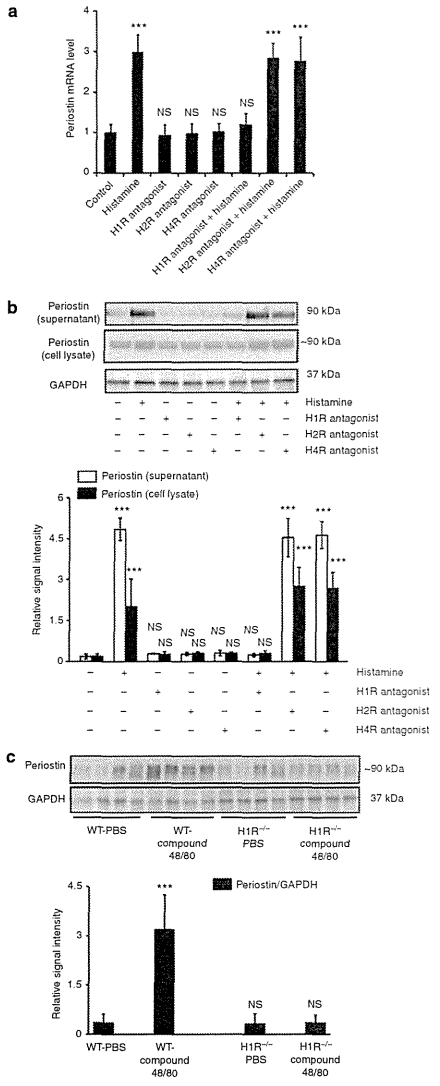

Figure 3. Histamine upregulates periostin expression via histamine receptor 1 (H1R) *in vitro* and *in vivo*. *In vitro*, wild-type (WT) fibroblasts were either treated with histamine antagonists (H1R, H2R, or H4R; 100 mM) or left untreated for 2 hours, and then cells were stimulated with histamine (100 μM) for an additional 2 hours (**a**) or 24 hours (**b**). Periostin expression was examined by quantitative real-time reverse transcriptase–PCR (qRT-PCR) (**a**) and western blotting analysis (**b**). *In vivo*, WT and $H1^{-/-}$ mice were treated with mast cell stimulator compound 48/80 for 3 days by subcutaneous injection, and periostin protein expression in the injected site skin was evaluated by western blotting analysis ($n = 4$ mice per group); representative blots and quantitative analysis of signal density on blots from four mice of each group are shown (using glyceraldehyde 3-phosphate dehydrogenase (GAPDH) as an internal control). (**c**) Values in **a** and **b** are shown as mean ± SD for three independent experiments. Values in **c** are shown as mean ± SD for blot signals from four mice. ***$P<0.001$; NS, no significance, compared with control (0 μM histamine in **a** and **b**; WT-phosphate-buffered saline in **c** by one-way analysis of variance (ANOVA) followed by Dunnett's test.

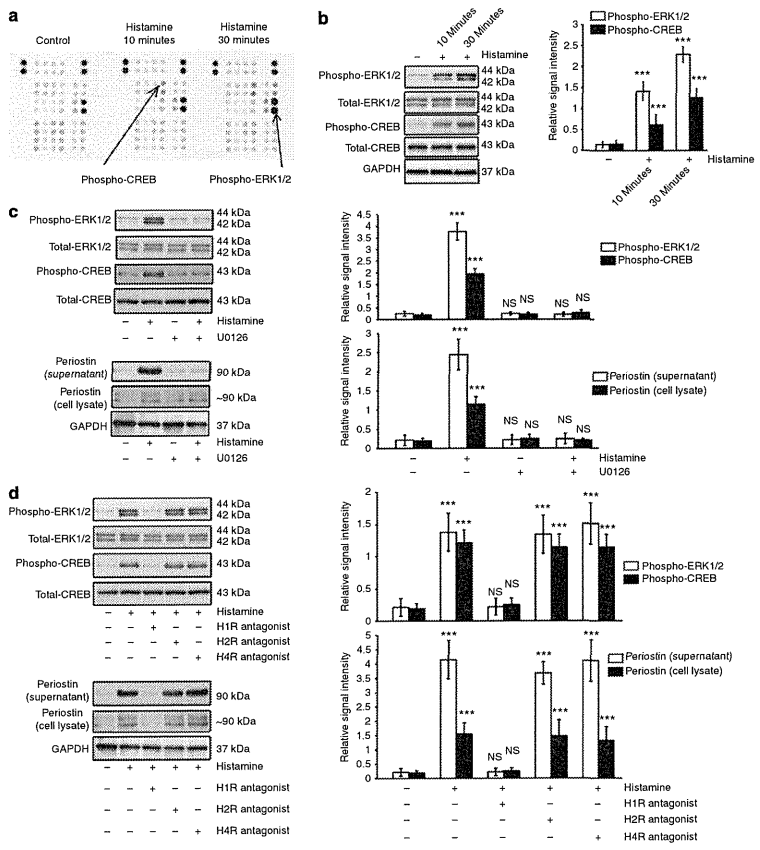

Figure 4. Histamine receptor 1 (H1R) activation upregulates periostin expression via the extracellular signal-regulated kinase 1/2 (ERK1/2) pathway. (**a**) The phosphorylation state was detected by R&D Systems Proteome Profiler Phospho-Kinase Array in normal human dermal fibroblasts, which were either untreated or treated with histamine for 10 minutes or 30 minutes. The activated kinases are indicated by arrows. (**b**) Phosphorylated ERK1/2 and phosphorylated cAMP response element-binding protein (CREB) were evaluated by western blotting analyses in murine wild-type (WT) fibroblasts following histamine stimulation for 10 minutes and 30 minutes. (**c**) WT fibroblasts with or without ERK1/2 inhibitor (U0126, 20 μM) preincubation were stimulated with histamine (30 minutes, upper panel; 24 hours, lower panel). Phosphorylated ERK1/2, phosphorylated CREB, and periostin protein expression was examined by western blotting analyses. (**d**) WT fibroblasts cultured in the presence or absence of preincubation with histamine receptor antagonists (H1R, H2R, or H4R; 100 mM) were stimulated with histamine (30 minutes, upper panel; 24 hours, lower panel). Phosphorylated ERK1/2, phosphorylated CREB, and periostin protein expression was examined by western blotting analyses. Three independent experiments were performed, and representative blots and quantitative analysis of signal density on blots from three independent experiments are shown (using glyceraldehyde 3-phosphate dehydrogenase (GAPDH) as an internal control). ***$P<0.001$; NS, no significance, compared with control (0 μM histamine) by one-way analysis of variance (ANOVA) followed by Dunnett's test.

Periostin, a recently characterized matricellular protein, has been reported to have crucial roles in tooth and periodontium development (Horiuchi *et al.*, 1999), cancer proliferation and invasion (Siriwardena *et al.*, 2006; Baril *et al.*, 2007; Kudo *et al.*, 2012), cardiac healing after acute myocardial infarction (Shimazaki *et al.*, 2008), idiopathic interstitial pneumonia (Okamoto *et al.*, 2011), and bone marrow fibrosis (Oku *et al.*, 2008). Furthermore, periostin is highly expressed in connective tissue and at the remodeling tissue site after injury or inflammation. This protein is secreted from fibroblasts via

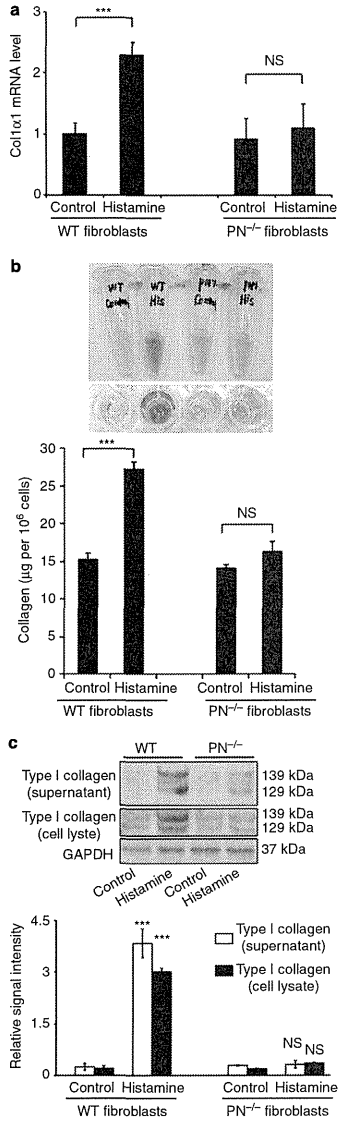

Figure 5. Periostin is essential in histamine-induced collagen production *in vitro*. Primary dermal fibroblasts from wild type (WT) and periostin-deficient ($PN^{-/-}$) mice were stimulated with histamine (100 μM) or phosphate-buffered saline (PBS) (control) for 48 hours. The collagen type-I alpha 1 (Col1α1) mRNA level was examined by quantitative real-time reverse transcriptase–PCR (qRT-PCR) (**a**), and collagen protein expression was evaluated by Sircol assay (**b**) and western blotting analysis; representative blots and quantitative analysis of signal density on blots from three independent experiments are shown (using glyceraldehyde 3-phosphate dehydrogenase (GAPDH) as an internal control) (**c**). Values are shown as mean ± SD for three independent experiments. ***$P<0.001$; NS, no significance, compared with paired control (WT fibroblasts control or $PN^{-/-}$-fibroblasts control) by Student's *t*-test.

transforming growth factor beta stimulation (Horiuchi *et al.*, 1999). Periostin was shown to accelerate cardiac healing after acute myocardial infarction (Dorn, 2007; Oka *et al.*, 2007; Shimazaki *et al.*, 2008) and during full-thickness cutaneous wound repair (Nishiyama *et al.*, 2011; Elliott *et al.*, 2012; Ontsuka *et al.*, 2012) by modulating fibroblast differentiation.

Periostin has also been reported to be induced by other factors, including bone morphogenetic proteins, vascular endothelial growth factor, connective tissue growth factor, vitamin K, IL-3, IL-4, IL-6, and IL-13 (Asano *et al.*, 2005; Takayama *et al.*, 2006; Iekushi *et al.*, 2007; Blanchard *et al.*, 2008; Coutu *et al.*, 2008; Banerjee *et al.*, 2009; Norris *et al.*, 2009). Recently, the increased expression of periostin was confirmed in various allergic diseases such as bronchial asthma (Takayama *et al.*, 2006), AD (Masuoka *et al.*, 2012), and eosinophilic chronic rhinosinusitis (Hur *et al.*, 2012). As an IL-4- and IL-13-inducible protein, periostin is associated with tissue remodeling in bronchial asthma (Takayama *et al.*, 2006), allergic eosinophilic esophagitis (Blanchard *et al.*, 2008), AD (Masuoka *et al.*, 2012), and allergic rhinitis (Hur *et al.*, 2012). In the present study, histamine was found to directly induce periostin expression, whereas the expression levels of transforming growth factor beta, IL-4, and IL-13 were not altered by histamine stimulation (data not shown). Thus, we postulate that periostin is involved in the initiation of tissue remodeling in chronic allergic diseases.

AD is known to develop tissue remodeling, which is characterized by epidermal thickening, hyperkeratosis and fibrosis of the papillary dermis, increased fibroblast proliferation, and collagen accumulation, and these features are caused by nonspecific stimuli, constant scratching, and rubbing (Lee *et al.*, 2009). Tissue remodeling and repair are thought to be the underlying causes of chronic allergic inflammation, such as in asthmatic diseases and AD (Leung, 1995). Recently, increased expressions of periostin and the inducers of periostin (IL-4, IL-13, and transforming growth factor beta) were identified in a screening of AD-associated genes in genome-wide association studies and quantitative mRNA expression analysis in lesion tissues (Hoffjan and Epplen, 2005; Wood *et al.*, 2009a, 2009b). Furthermore, in the present study, elevated expression of periostin was found in lesional skin of patients with AD. These results suggest that periostin may be involved in AD and in asthma.

In WT and $PN^{-/-}$ mice, a mite extract–induced AD model was established and analyzed. In contrast to WT mice, $PN^{-/-}$ mice showed amelioration of epidermal hyperplasia and inflammatory cell infiltration (Masuoka *et al.*, 2012). Moreover, periostin directly induces production of thymic stromal lymphoprotein in keratinocytes (Masuoka *et al.*, 2012). Thus, periostin was suggested to have a critical role in the amplification and chronicity of allergic skin inflammation.

The results of the present study demonstrate the role of periostin in histamine-mediated collagen production. We found that H1R-mediated phosphorylation of ERK1/2 had a crucial role in histamine-induced collagen production. These observations may open a new window of therapeutic opportunity against airway remodeling in asthma or dermal remodeling in AD, as histamine H1R anatagonists are expected to ameliorate tissue remodeling.

As refractory chronic allergic symptoms are known to impair the quality of life, work productivity, and overall activity (Meltzer *et al.*, 1999; Thompson *et al.*, 2000; Kawashima *et al.*, 2002; Baiardini *et al.*, 2003; Spector *et al.*, 2007), we believe that these studies will provide a basis for exploring the fibrotic components of allergic diseases in skin and other tissues.

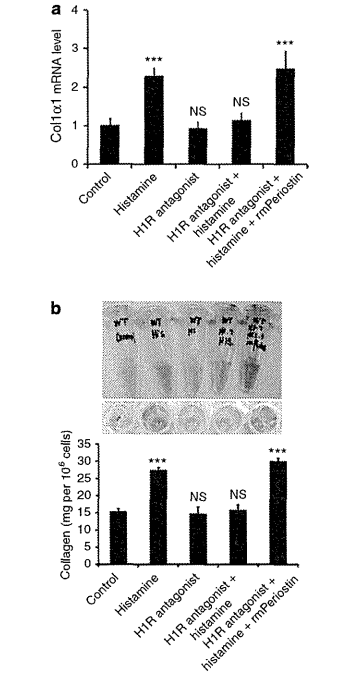

Figure 6. Histamine receptor 1 (H1R)-mediated upregulation of periostin is essential in histamine-induced collagen production. Wild-type (WT) fibroblasts cultured with or without H1R antagonist preincubations were stimulated with histamine (100 μM) alone or in the presence of recombinant mouse periostin (rmPeriostin, 100 ng ml^{-1}). The collagen type-I alpha 1 (Col1α1) mRNA level was examined by quantitative real-time reverse transcriptase–PCR (qRT-PCR) (**a**), and collagen protein expression was evaluated by Sircol assay (**b**) and western blotting analysis; representative blots and quantitative analysis of signal density on blots from three independent experiments are shown (using glyceraldehyde 3-phosphate dehydrogenase (GAPDH) as an internal control) (**c**). Values are shown as mean ± SD for three independent experiments. ***$P<0.001$; NS, no significance compared with control (0 μM histamine) according to one-way analysis of variance (ANOVA) followed by Dunnett's test.

MATERIALS AND METHODS

Mice

WT mice (C57BL/6 strain) were purchased from CLEA Japan (Osaka, Japan). Periostin gene knockout ($PN^{-/-}$) mice (C57BL/6 strain) were generated as previously described.(Shimazaki and Kudo, 2008) Histamine receptor 1 gene knockout ($H1R^{-/-}$) mice (C57BL/6 strain) were purchased from Oriental Bio Service (Kyoto, Japan). Mice were maintained in our pathogen-free animal facility. Animal care and experimentation were performed in accordance with the institutional guidelines of the National Institute of Biomedical Innovation, Osaka, Japan and Osaka University, Osaka, Japan. Six-week-old male mice were used in all experiments. All experiments used four mice per group.

Compound 48/80 treatment

Compound 48/80 (Sigma, St Louis, MO) was dissolved in phosphate-buffered saline at a concentration of 1 mg ml^{-1} and sterilized by filtration. With the use of a 27-gauge needle, 100 μl of compound 48/80 or phosphate-buffered saline was subcutaneously injected into the back side of mice each day for 3 days. One day after the final injection, the skin at the injected site was removed and solubilized at 4 °C in lysis buffer (0.5% sodium deoxycholate, 1% Nonidet P40, 0.1% sodium dodecyl sulfate, 100 μg ml^{-1} phenylmethylsulfonyl fluoride, 1 mM sodium orthovanadate, and protease inhibitor cocktail) for western blotting analysis.

Cell culture

Murine primary dermal fibroblasts from the skin of four newborn WT and four newborn $PN^{-/-}$ mice were isolated and cultured as previously described (Terao *et al.*, 2010). Human primary dermal fibroblasts were purchased from DS Pharma Biomedical (Osaka, Japan). After 24 hours of serum starvation, dermal fibroblasts at confluence were treated with 0.1 to 100 μM histamine (Sigma–Aldrich, Tokyo, Japan) or 100 ng ml^{-1} recombinant mouse periostin (rmPeriostin, R&D Systems, Minneapolis, MN) for the indicated periods of time before extraction of RNA and protein. Cells were used at passage three. In each experiment, the obtained fibroblasts were examined at the same time point and under the same culture conditions (e.g., cell density, passage, and days after plating). For inhibition experiments, fibroblasts were preincubated for 2 hours with specific histamine receptor antagonists (Pyrilamine maleate, Cimetidine, JNJ7777120, 100 mM, Sigma–Aldrich) or ERK1/2 inhibitor (U0126, 20 μM, Cell Signaling Technology, Beverly, MA) before the addition of histamine. We performed serial dilutions of each agent to identify the most effective concentrations to be used in the experiments, as determined by MTT assays and western blotting analyses.

Quantitative real-time and direct reverse transcriptase–PCR analysis of mRNA

Total RNA was isolated from fibroblasts using the RNeasy Mini Kit (QIAGEN, Tokyo, Japan) according to the manufacturer's protocol. First, 100 ng of RNA was reverse-transcribed using the QuantiTect Reverse Transcription Kit (QIAGEN). For quantitative real-time reverse transcriptase–PCR analysis, standard curves for periostin, collagen, and glyceraldehyde 3-phosphate dehydrogenase (GAPDH) were generated from serial dilutions of positively expressing cDNA. Relative quantification of the PCR products was carried out using the ABI prism 7000 (Applied Biosystems, Darmstadt, Germany) and the comparative threshold cycle (C_T) method. The "fold-induction" was calculated as the ratio to values of cells that were not incubated with histamine or periostin. The primers used for real-time PCR were as follows: periostin, sense 5′-GAACGAATCATTACAGGTCC-3′, antisense 5′-GGAGACCTCTTTTTGCAAGA-3′; collagen type-I alpha 1 (Col1-α1), sense 5′-GAGCCCTCGCTTCCGTACTC-3′, antisense 5′-TGTTCCCTACTCAGCCGTCTGT-3′; and GAPDH, sense 5′-TGTC ATCATACTTGGCAGGTTTCT-3′, antisense 5′-CATGGCCTTCCGTG TTCCTA-3′. Each reaction was performed in triplicate. Variation within samples was less than 10%. Statistical analysis was performed with the Student's paired *t*-test.

Western blotting analyses

For preparation of protein samples, cell pellets and skin samples were extracted as described above, and 5 μg of extracted protein was used for western blotting analysis, as described previously (Terao *et al.*, 2010). The primary antibodies were used at the following dilutions: anti-type I collagen (Calbiochem, San Diego, CA) at 1:500, anti-periostin (R&D Systems, Minneapolis, MN) at 1:500, anti-phospho-ERK1/2 (Cell Signaling Technology) at 1:1,000, anti-total ERK1/2 (Cell Signaling Technology) at 1:1,000, anti-phospho-CREB (Cell Signaling Technology) at 1:1,000, anti-total CREB (Cell Signaling Technology) at 1:1,000, and anti-GAPDH (Santa Cruz Biotechnology, Santa Cruz, CA) at 1:500. Staining with the anti-GAPDH antibody was used as a loading control. Signal intensity of bands was quantified using the ImageJ densitometry software (http://rsb.info.nih.gov/ij/index.html) and normalized to GAPDH signal intensity.

Sircol collagen assay

The soluble collagen levels in culture supernatants were measured using a Sircol Collagen Assay (Biocolor, Belfast, UK). This assay measured total secreted collagen from cultured cells. Briefly, cells were cultured for 48 hours with or without treatment, and then supernatants were collected. One milliliter of Sirius red, an anionic dye that specifically reacts with the basic side chain groups of collagens, was added to 200 μl of the supernatant and incubated with gentle rotation for 30 minutes at room temperature. After centrifugation, the collagen-bound dye was resolubilized in 1 ml of 0.5 M NaOH, and the absorbance at 540 nm was measured.

Phosphorylated kinase array

Phosphorylated kinase was profiled with the Proteome Profiler Human Phospho-Kinase Array Kit (R&D Systems). The procedures were performed according to the manufacturer's protocol using 300 μg of protein lysate per array.

Statistical analysis

All experiments reported in this paper were repeated at least three times, yielding similar results, and data are presented as mean ± SD. The Student's two-tailed *t*-test (Microsoft Excel software, Redmond, WA) was used for comparison between two groups. When analysis included more than two groups, one-way analysis of variance (ANOVA) followed by Dunnett's test was used. *P*-values less than 0.05 were considered statistically significant.

CONFLICT OF INTEREST

The authors state no conflict of interest.

ACKNOWLEDGMENTS

We thank Kenju Nishida for excellent technical support. This study was partly supported by a research grant from the Ministry of Health, Labour and Welfare, Japan.

SUPPLEMENTARY MATERIAL

Supplementary material is linked to the online version of the paper at http://www.nature.com/jid

REFERENCES

Artuc M, Hermes B, Steckelings UM *et al.* (1999) Mast cells and their mediators in cutaneous wound healing–active participants or innocent bystanders? *Exp Dermatol* 8:1–16

Asano M, Kubota S, Nakanishi T *et al.* (2005) Effect of connective tissue growth factor (CCN2/CTGF) on proliferation and differentiation of mouse periodontal ligament-derived cells. *Cell Commun Signal* 3:11

Atkins FM, Clark RA (1987) Mast cells and fibrosis. *Arch Dermatol* 123:191–3

Baiardini I, Giardini A, Pasquali M *et al.* (2003) Quality of life and patients' satisfaction in chronic urticaria and respiratory allergy. *Allergy* 58:621–3

Banerjee I, Fuseler JW, Intwala AR *et al.* (2009) IL-6 loss causes ventricular dysfunction, fibrosis, reduced capillary density, and dramatically alters the cell populations of the developing and adult heart. *Am J Physiol Heart Circ Physiol* 296:H1694–704

Baril P, Gangeswaran R, Mahon PC *et al.* (2007) Periostin promotes invasiveness and resistance of pancreatic cancer cells to hypoxia-induced cell death: role of the beta4 integrin and the PI3k pathway. *Oncogene* 26:2082–94

Blanchard C, Mingler MK, McBride M *et al.* (2008) Periostin facilitates eosinophil tissue infiltration in allergic lung and esophageal responses. *Mucosal Immunol* 1:289–96

Cohen IK, Beaven MA, Horáková Z *et al.* (1972) Histamine and collagen synthesis in keloid and hypertrophic scar. *Surg Forum* 23:509–10

Coutu DL, Wu JH, Monette A *et al.* (2008) Periostin, a member of a novel family of vitamin K-dependent proteins, is expressed by mesenchymal stromal cells. *J Biol Chem* 283:17991–8001

Davies MG, Greaves MW (1980) Sensory responses of human skin to synthetic histamine analogues and histamine. *Br J Clin Pharmacol* 9:461–5

Dorn GW (2007) Periostin and myocardial repair, regeneration, and recovery. *N Engl J Med* 357:1552–4

Elliott CG, Wang J, Guo X *et al.* (2012) Periostin modulates myofibroblast differentiation during full-thickness cutaneous wound repair. *J Cell Sci* 125:121–32

Gailit J, Marchese MJ, Kew RR *et al.* (2001) The differentiation and function of myofibroblasts is regulated by mast cell mediators. *J Invest Dermatol* 117:1113–9

Hawkins RA, Claman HN, Clark RA *et al.* (1985) Increased dermal mast cell populations in progressive systemic sclerosis: a link in chronic fibrosis? *Ann Intern Med* 102:182–6

Hebda PA, Collins MA, Tharp MD (1993) Mast cell and myofibroblast in wound healing. *Dermatol Clin* 11:685–96

Hoffjan S, Epplen JT (2005) The genetics of atopic dermatitis: recent findings and future options. *J Mol Med (Berl)* 83:682–92

Horiuchi K, Amizuka N, Takeshita S *et al.* (1999) Identification and characterization of a novel protein, periostin, with restricted expression to periosteum and periodontal ligament and increased expression by transforming growth factor beta. *J Bone Miner Res* 14:1239–49

Hur DG, Khalmuratova R, Ahn SK *et al.* (2012) Roles of periostin in symptom manifestation and airway remodeling in a murine model of allergic rhinitis. *Allergy Asthma Immunol Res* 4:222–30

Iekushi K, Taniyama Y, Azuma J *et al.* (2007) Novel mechanisms of valsartan on the treatment of acute myocardial infarction through inhibition of the antiadhesion molecule periostin. *Hypertension* 49:1409–14

Kawashima M, Harada S, Tango T (2002) Review of fexofenadine in the treatment of chronic idiopathic urticaria. *Int J Dermatol* 41:701–6

Kudo Y, Iizuka S, Yoshida M *et al.* (2012) Periostin directly and indirectly promotes tumor lymphangiogenesis of head and neck cancer. *PLoS One* 7:e44488

Lee JH, Chen SY, Yu CH *et al.* (2009) Noninvasive *in vitro* and *in vivo* assessment of epidermal hyperkeratosis and dermal fibrosis in atopic dermatitis. *J Biomed Opt* 14:014008

Leung DY (1995) Atopic dermatitis: the skin as a window into the pathogenesis of chronic allergic diseases. *J Allergy Clin Immunol* 96:302–18

Masuoka M, Shiraishi H, Ohta S *et al.* (2012) Periostin promotes chronic allergic inflammation in response to Th2 cytokines. *J Clin Invest* 122:2590–600

Meltzer EO, Casale TB, Nathan RA *et al.* (1999) Once-daily fexofenadine HCl improves quality of life and reduces work and activity impairment in patients with seasonal allergic rhinitis. *Ann Allergy Asthma Immunol* 83:311–7

Murakami T, Yoshioka M, Yumoto R *et al.* (1998) Topical delivery of keloid therapeutic drug, tranilast, by combined use of oleic acid and propylene glycol as a penetration enhancer: evaluation by skin microdialysis in rats. *J Pharm Pharmacol* 50:49–54

Murota H, Bae S, Hamasaki Y *et al.* (2008) Emedastine difumarate inhibits histamine-induced collagen synthesis in dermal fibroblasts. *J Invest Allergol Clin Immunol* 18:245–52

Murota H, Katayama I (2009) Emedastine difumarate: a review of its potential ameliorating effect for tissue remodeling in allergic diseases. *Expert Opin Pharmacother* 10:1859–67

Nishioka K, Katayama I, Doi T (1987) Histamine release by scratching inflamed skin. *J Dermatol* 14:284–5

Nishiyama T, Kii I, Kashima TG *et al.* (2011) Delayed re-epithelialization in periostin-deficient mice during cutaneous wound healing. *PLoS One* 6:e18410

Noli C, Miolo A (2001) The mast cell in wound healing. *Vet Dermatol* 12:303–13

Norris RA, Moreno-Rodriguez R, Hoffman S *et al.* (2009) The many facets of the matricellular protein periostin during cardiac development, remodeling, and pathophysiology. *J Cell Commun Signal* 3:275–86

Numata Y, Terui T, Okuyama R *et al.* (2006) The accelerating effect of histamine on the cutaneous wound-healing process through the action of basic fibroblast growth factor. *J Invest Dermatol* 126:1403–9

Oka T, Xu J, Kaiser RA *et al.* (2007) Genetic manipulation of periostin expression reveals a role in cardiac hypertrophy and ventricular remodeling. *Circ Res* 101:313–21

Okamoto M, Hoshino T, Kitasato Y *et al.* (2011) Periostin, a matrix protein, is a novel biomarker for idiopathic interstitial pneumonias. *Eur Respir J* 37:1119–27

Oku E, Kanaji T, Takata Y *et al.* (2008) Periostin and bone marrow fibrosis. *Int J Hematol* 88:57–63

Ontsuka K, Kotobuki Y, Shiraishi H *et al.* (2012) Periostin, a matricellular protein, accelerates cutaneous wound repair by activating dermal fibroblasts. *Exp Dermatol* 21:331–6

Russel JD, Russell SB, Trupin KM (1977) The effect of histamine on the growth of cultured fibroblasts isolated from normal and keloid tissue. *J Cell Physiol* 93:389–93

Sandberg N (1962) Accelerated collagen formation and histamine. *Nature* 194:183

Sandberg N (1964) Enhanced rate of healing in rats with an increased rate of histamine formation. *Acta Chir Scand* 127:9–21

Shimazaki M, Kudo A (2008) Impaired capsule formation of tumors in periostin-null mice. *Biochem Biophys Res Commun* 367:736–42

Shimazaki M, Nakamura K, Kii I *et al.* (2008) Periostin is essential for cardiac healing after acute myocardial infarction. *J Exp Med* 205:295–303

Siriwardena BS, Kudo Y, Ogawa I *et al.* (2006) Periostin is frequently overexpressed and enhances invasion and angiogenesis in oral cancer. *Br J Cancer* 95:1396–403

Spector SL, Shikiar R, Harding G *et al.* (2007) The effect of fexofenadine hydrochloride on productivity and quality of life in patients with chronic idiopathic urticaria. *Cutis* 79:157–62

Takayama G, Arima K, Kanaji T *et al.* (2006) Periostin: a novel component of subepithelial fibrosis of bronchial asthma downstream of IL-4 and IL-13 signals. *J Allergy Clin Immunol* 118:98–104

Terao M, Murota H, Kitaba S *et al.* (2010) Tumor necrosis factor-alpha processing inhibitor-1 inhibits skin fibrosis in a bleomycin-induced murine model of scleroderma. *Exp Dermatol* 19:38–43

Thompson AK, Finn AF, Schoenwetter WF (2000) Effect of 60 mg twice-daily fexofenadine HCl on quality of life, work and classroom productivity, and regular activity in patients with chronic idiopathic urticaria. *J Am Acad Dermatol* 43:24–30

Topol BM, Lewis VL, Benveniste K (1981) The use of antihistamine to retard the growth of fibroblasts derived from human skin, scar, and keloid. *Plast Reconstr Surg* 68:227–32

Trautmann A, Toksoy A, Engelhardt E *et al.* (2000) Mast cell involvement in normal human skin wound healing: expression of monocyte chemoattractant protein-1 is correlated with recruitment of mast cells which synthesize interleukin-4 *in vivo*. *J Pathol* 190:100–6

Wahlgren CF (1999) Itch and atopic dermatitis: an overview. *J Dermatol* 26:770–9

Weller K, Foitzik K, Paus R *et al.* (2006) Mast cells are required for normal healing of skin wounds in mice. *FASEB J* 20:2366–8

Wood SH, Clements DN, Ollier WE *et al.* (2009a) Gene expression in canine atopic dermatitis and correlation with clinical severity scores. *J Dermatol Sci* 55:27–33

Wood SH, Ke X, Nuttall T *et al.* (2009b) Genome-wide association analysis of canine atopic dermatitis and identification of disease related SNPs. *Immunogenetics* 61:765–72

Yang L, Serada S, Fujimoto M *et al.* (2012) Periostin facilitates skin sclerosis via PI3K/Akt dependent mechanism in a mouse model of scleroderma. *PLoS One* 7:e41994

UICC global cancer control

IJC
International Journal of Cancer

Annexin A4-conferred platinum resistance is mediated by the copper transporter ATP7A

Shinya Matsuzaki[1,2], Takayuki Enomoto[3], Satoshi Serada[2], Kiyoshi Yoshino[1], Shushi Nagamori[4], Akiko Morimoto[1], Takuhei Yokoyama[1,2], Ayako Kim[2], Toshihiro Kimura[1], Yutaka Ueda[1], Masami Fujita[1], Minoru Fujimoto[2], Yoshikatsu Kanai[4], Tadashi Kimura[1] and Tetsuji Naka[2]

[1] Department of Obstetrics and Gynecology, Osaka University Graduate School of Medicine, Osaka, Japan
[2] Laboratory for Immune Signal, National Institute of Biomedical Innovation, Osaka, Japan
[3] Department of Obstetrics and Gynecology, Niigata University Graduate School of Medicine, Niigata, Japan
[4] Department of Pharmacology, Osaka University Graduate School of Medicine, Osaka, Japan

Although platinum drugs are often used for the chemotherapy of human cancers, platinum resistance is a major issue and may preclude their use in some cases. We recently reported that enhanced expression of Annexin A4 (Anx A4) increases chemoresistance to carboplatin through increased extracellular efflux of the drug. However, the precise mechanisms underlying that chemoresistance and the relationship of Anx A4 to platinum resistance *in vivo* remain unclear. In this report, the *in vitro* mechanism of platinum resistance induced by Anx A4 was investigated in endometrial carcinoma cells (HEC1 cells) with low expression of Anx A4. Forced expression of Anx A4 in HEC1 cells resulted in chemoresistance to platinum drugs. In addition, HEC1 control cells were compared with Anx A4-overexpressing HEC1 cells in xenografted mice. Significantly greater chemoresistance to cisplatin was observed *in vivo* in Anx A4-overexpressing xenografted mice. Immunofluorescence analysis revealed that exposure to platinum drugs induced relocation of Anx A4 from the cytoplasm to the cellular membrane, where it became colocalized with ATP7A, a copper transporter also well known as a mechanism of platinum efflux. ATP7A expression suppressed by small interfering RNA had no effect on HEC1 control cells in terms of chemosensitivity to platinum drugs. However, suppression of ATP7A in Anx A4-overexpressing platinum-resistant cells improved chemosensitivity to platinum drugs (but not to 5-fluorouracil) to a level comparable to that of control cells. These results indicate that enhanced expression of Anx A4 confers platinum resistance by promoting efflux of platinum drugs *via* ATP7A.

Platinum drugs, widely used for treating gynecological cancers, can improve survival rates dramatically, particularly in patients with ovarian and endometrial carcinomas.[1–6] Compared with platinum-sensitive tumors, prognosis is poorer for tumors that are (or become) platinum-resistant; for these tumors, other chemotherapeutic drugs also tend to be less effective. For example, an efficacy of 81% has been demonstrated for chemotherapy regimens that include platinum drugs for treatment of ovarian serous adenocarcinoma (SAC), the most common subtype of ovarian carcinoma; however, the efficacy of these regimens is only 18% for ovarian clear cell carcinomas (CCC), which are frequently resistant to multiple drugs.[7] Compared with advanced SAC, the clinical prognosis of patients with similarly advanced CCC is markedly worse largely because of the considerably higher rate of recurrence after CCC treatment.[7–11] Therefore, determining the mechanism underlying platinum resistance may aid in identification of therapeutic targets for platinum-resistant tumors such as CCC. Studies using proteomic screening approaches have previously demonstrated overexpression of Annexin A4 (Anx A4) protein in ovarian CCC, which is frequently a highly platinum-resistant tumor compared with SAC.[12] Similar findings have been reported in a study comparing SAC and CCC using a genomic screening approach.[13] Anx A4, a previously understudied member of the Annexin protein family, binds to phospholipids in a Ca^{2+}-dependent manner, self-associates on phospholipid

Key words: Annexin A4, ATP7A, platinum resistance, platinum transporter, copper transporter
Abbreviations: 5-FU: 5-fluorouracil; Anx A4: Annexin A4; CCC: clear cell carcinoma; D-MEM: Dulbecco's modified Eagle's medium; FBS: fetal bovine serum; PBS: phosphate-buffered saline; SAC: serous adenocarcinoma; siRNA: small interfering RNA
Additional Supporting Information may be found in the online version of this article.
Grant sponsor: Japanese Ministry of Education, Science, Culture and Sports; **Grant number:** 22791560; **Grant sponsors:** Program for Promotion of Fundamental Studies in Health Sciences of the National Institute of Biomedical Innovation, Ministry of Health, Labour and Welfare of Japan
DOI: 10.1002/ijc.28526
History: Received 4 Dec 2012; Accepted 26 Sep 2013; Online 8 Oct 2013
Correspondence to: Dr. Tetsuji Naka, Laboratory for Immune Signal, National Institute of Biomedical Innovation, 7-6-8 Saito-asagi, Ibaraki, Osaka 567-0085, Japan, Tel.: +81-72-641-9843, Fax: +81-72-641-9837, E-mail: tnaka@nibio.go.jp

What's new?

Although platinum-based drugs are often used in chemotherapy, resistance to these drugs is frequently a problem. The protein Annexin A4 (Anx A4) is known to be involved in platinum efflux in ovarian tumours; however, its precise mechanism of action has been unclear. In this study, the authors demonstrated that the strong platinum-resistance in Anx A4-overexpressing cells involves the transporter protein ATP7A, both in vitro and in vivo. This suggests that Anx A4 may be a highly useful therapeutic target in Anx A4-expressing carcinomas.

membrane surfaces and causes membrane aggregation.[12,14–17] Enhanced expression of Anx A4 has recently shown to increase tumor chemoresistance to carboplatin (a key drug for treating gynecological cancers) *via* increased extracellular efflux of the drug.[12] Another study showed that Anx A4 suppresses NF-κB transcriptional activity, which is significantly upregulated early after etoposide treatment. Anx A4 translocates to the nucleus together with p50 and imparts greater resistance to apoptotic stimulation by etoposide treatment.[18] Anx A4 may also be associated with drug resistance in other types of tumors; enhanced expression of Anx A4 has been reported in colon, renal, lung and pancreatic cancers.[19–23] However, the details of Anx A4-mediated extracellular efflux of platinum drugs remain unclear.

HEC1 is an endometrial carcinoma cell line with low Anx A4 expression levels. In our study, Anx A4-overexpressing derivative HEC1 cell lines were established and their chemosensitivity toward platinum drugs was analyzed both *in vitro* and *in vivo*. Anx A4-conferred platinum chemoresistance was shown to be mediated by the copper transporter ATP7A.[24–28]

Material and Methods

Cell lines

The human endometrial carcinoma cell lines HEC1, HEC1A, HEC6, HEC88nu, HEC108, HEC116 and HEC251; SNGII and SNGM cells, the human ovarian SAC cell line OVSAHO and the ovarian CCC cell lines OVISE and OVTOKO were obtained from the Japanese Collection of Research Bioresources (Osaka, Japan); A2780 cells from the human ovarian SAC cell line were obtained from the European Collection of Animal Cell Culture (Salisbury, Scotland). The identity of each cell line was confirmed by DNA fingerprinting *via* short tandem repeat profiling, as described previously.[29] HEC1, HEC1A, HEC6, HEC88nu, HEC108, HEC116 and HEC251 cells were maintained in Dulbecco's modified Eagle's medium (D-MEM) (Wako Pure Chemical Industries, Osaka, Japan) supplemented with 10% fetal bovine serum (FBS) (HyClone Laboratories, Logan, UT) and 1% penicillin–streptomycin (Nacalai Tesque, Kyoto, Japan) at 37°C under a humidified atmosphere of 5% CO_2. SNGII and SNGM cells were maintained in Ham's F12 medium (Invitrogen, Carlsbad, CA) supplemented with 10% FBS and 1% penicillin–streptomycin. OVSAHO, A2780, OVISE and OVTOKO cells were maintained in Roswell Park Memorial Institute 1640 medium (Wako Pure Chemical Industries) supplemented with 10% FBS and 1% penicillin–streptomycin.

Generation of Anx A4 stably transfected cell lines

To generate cell lines that stably expressed Anx A4, HEC1 cells were transfected with the pcDNA3.1–Anx A4 expression plasmid, as described previously.[12] Transfected cells were selected with 600 μg/ml of Geneticin (Invitrogen). Clones were maintained in 250 μg/ml of Geneticin for stability of expression. Four stable Anx A4-expressing cell lines were established and designated HEC1-A25, HEC1-A43, HEC1-A63 and HEC1-A77. A control cell line of HEC1 was also established and stably transfected with an empty vector. This cell line was designated as HEC1-CV.

Western blotting

Cells were lysed in radioimmunoprecipitation assay buffer [10 mM Tris-HCl, pH 7.5, 150 mM NaCl, 1% Nonidet P-40, 0.5% sodium deoxycholate, 0.1% sodium dodecyl sulfate, 1% protease-inhibitor cocktail (Nacalai Tesque) and 1% phosphatase-inhibitor cocktail (Nacalai Tesque)]. After centrifugation (13,200 rpm, 4°C, 15 min), soluble proteins in the supernatant were separated using sodium dodecyl sulfate-polyacrylamide gel electrophoresis, as described previously.[12] Additional information can be found in Supporting Information Material and Methods.

Measurement of IC_{50} values after treatment with cisplatin or carboplatin

Cells were suspended in D-MEM medium supplemented with 10% FBS and were seeded in 96-well plates (2,000 cells per well) (Costar; Corning, Corning, NY) for 24 hr. They were then exposed to various concentrations of carboplatin (0–500 μM), cisplatin (0–100 μM) or 5-fluorouracil (5-FU) (0–50 μM) for 72 hr. Cell proliferation was evaluated using the WST-8 assay (Cell Counting Kit-SF; Nacalai Tesque) after treatment at the time points indicated by the manufacturer. The absorption of WST-8 was measured at a wavelength of 450 nm (reference wavelength: 630 nm) using a Model 680 microplate reader (Bio-Rad Laboratories, Hercules, CA). Absorbance values for treated cells indicative of proliferation rates were expressed as percentages relative to results for untreated controls, and the drug concentrations resulting in a 50% inhibition of cell growth (IC_{50} values) were calculated.

Small interfering RNA transfection

Two commercial small interfering RNAs (siRNAs) against ATP7A and a nonspecific control siRNA were obtained from Qiagen (Venlo, The Netherlands) and designated ATP7A siRNA4 and ATP7A siRNA6, respectively. For gene silencing, a specific sense strand 5′-GCAGCUUGUAGUAUUGAA ATT-3′ was used for ATP7A siRNA4, and an antisense strand 5′-UUUCAAUACUACAAGCUGCTA-3′ was also used. For ATP7A siRNA6, a specific sense strand 5′-GCGUA GCUCCAGAGGUUUATT-3′ was used, and an antisense strand 5′-UAAACCUCUGGAGCUACGCAG-3′ was also used. Cells were transfected with siRNA using Lipofectamine 2000 reagent (Invitrogen) according to the manufacturer's instructions. Selective silencing of ATP7A was confirmed by Western blot analysis.

In vivo model of cisplatin resistance

All animal experiments were conducted in accordance with the Institutional Ethical Guidelines for Animal Experimentation of our National Institute of Biomedical Innovation (Osaka, Japan). Four-week-old, female Institute of Cancer Research (ICR) nu/nu mice were obtained from Charles River Japan (Yokohama, Japan). For subcutaneous xenograft experiments, 2.5×10^6 HEC1, HEC1-CV, HEC1-A63 and HEC1-A77 cells were suspended in 100 μl of 1/1 (v/v) phosphate-buffered saline (PBS)/Matrigel (Becton Dickinson, Bedford, MA) and injected subcutaneously into the flanks of the ICR nu/nu mice ($n = 5$ per group). One week after xenograft establishment, tumors measured ~100 mm^3. Mice were then randomly divided into two groups and administered cisplatin (3 mg/kg) or PBS i.p. twice weekly for 4 weeks. Tumor volumes were determined twice weekly by measuring length (L), width (W) and depth (D). Tumor volume was calculated using the formula: tumor volume (mm^3) = $W \times L \times D$. At 56 days after tumor implantation, tumors were removed and weighed.

Quantification of intracellular platinum accumulation

Cisplatin accumulation in cells was analyzed according to a previously established method, with certain minor modifications. In brief, 6×10^6 cells (HEC1, HEC1-CV, HEC1-A25, HEC1-A43, HEC1-A63 and HEC1-A77 cells) were seeded into two 150-mm tissue culture dishes and incubated for 24 hr. The cells were then exposed to 1 mM cisplatin for 60 min at 37°C and then washed twice with PBS. After 3 hr of incubation in cisplatin-free D-MEM medium (supplemented with 10% FBS), whole extracts were prepared and the concentration of intracellular platinum was determined using an Agilent 7500ce inductively coupled plasma mass spectrometer (ICP-MS; Agilent, Santa Clara, CA). The absolute concentration of platinum in each sample was determined from a calibration curve prepared with a platinum standard solution.

Preparation of crude membrane fractions

To investigate the localization of Anx A4, crude membrane fractions (CMFs) of cells treated in various ways were prepared. Cells were divided into three groups: those that received no treatment, those pretreated with 10 μM cisplatin for 4 hr and those pretreated with 50 μM carboplatin for 4 hr. CMF were prepared as described elsewhere,[30] with modifications. Prepared proteins were investigated using Western blot analysis. Additional information can be found in Supporting Information Material and Methods.

Biotinylation of HEC1 cell membrane surface proteins after *cisplatin or carboplatin exposure*

To investigate the localization of ATP7A after exposure to platinum drugs, treated or mock-treated HEC1 cells were surface-biotinylated and the presence of ATP7A was investigated by Western blot analysis. Additional information can be found in Supporting Information Material and Methods.

Immunofluorescence for ATP7A and Anx A4

Immunofluorescence staining was performed 2 days after cells had been seeded on cover slips. Before staining, cells in the treatment groups were pretreated with 10 μM cisplatin or 50 μM carboplatin for 4 hr. Cells were then analyzed for localization of Anx A4 and ATP7A. Additional information can be found in Supporting Information Material and Methods.

Statistical analysis

Statistical analyses were performed using one-way analysis of variance (ANOVA) followed by Dunnett's analysis to evaluate the significance of differences. In all analyses, $p < 0.05$ was considered to be statistically significant.

Results

Expression of Anx A4 in endometrial carcinoma cell lines

To investigate Anx A4 expression in nine common endometrial carcinoma cell lines, Western blot analyses were performed. Expression of Anx A4 was strongest in SNGM cells compared with the other eight cell lines (Fig. 1*a*). Thus, enhanced expression of Anx A4 was confirmed in this endometrial carcinoma cell line.

Anx A4 and platinum resistance in HEC1 cell lines

From control HEC1 cells (low Anx A4 expression levels), four stable lines of Anx A4-overexpressing cells (HEC1-A25, HEC1-A43, HEC1-A63 and HEC1-A77 cells) and one line of empty vector transfected cells (HEC1-CV cells) were established. Overexpression of Anx A4 was confirmed using Western blot analysis and was compared with CCC cell lines (OVTOKO and OVISE) used as positive controls (Fig. 1*b*). Significantly higher IC_{50} values for cisplatin were observed in HEC1-A25 (32.1 μM, $p < 0.01$), HEC1-A43 (23.8 μM, $p < 0.01$), HEC1-A63 (34.9 μM, $p < 0.01$) and HEC1-A77 cells (17.3 μM, $p < 0.01$) compared with HEC1 (9.8 μM) and HEC1-CV cells (8.4 μM) (Fig. 1*c*). Similarly, IC_{50} values for carboplatin were significantly increased in HEC1-A25 (194.6 μM, $p < 0.01$), HEC1-A43 (153.3 μM, $p < 0.01$), HEC1-A63 (371.5 μM, $p < 0.01$) and HEC1-A77 cells (158.1 μM, $p < 0.01$) compared with HEC1 (59.1 μM) and HEC1-CV cells (60.9 μM) (Fig. 1*c*). Thus, Anx A4 overexpression conferred platinum resistance in HEC1 cell lines.

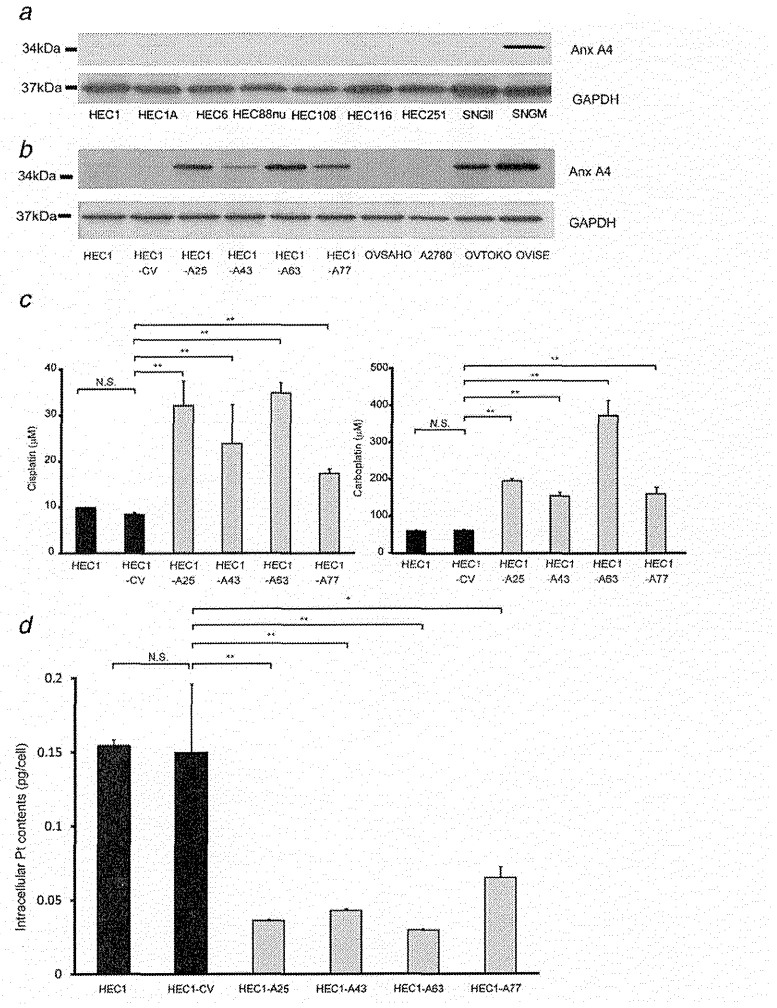

Figure 1. Enforced expression of Anx A4 in HEC1 cells confers platinum resistance *in vitro*. (*a*) Western blot analysis of nine endometrial carcinoma cell lines. Anx A4 was expressed in one cell line. (*b*) Establishment of an Anx A4-stably-expressing HEC1 cell line by transfection with the pcDNA3.1-Anx A4 expression plasmid into a HEC1 cell line with low Anx A4 expression levels. Enforced expression of Anx A4 was confirmed by Western blot analysis. (*c*) The IC_{50} sensitivity to cisplatin or carboplatin was investigated in HEC1, HEC1-CV, HEC1-A25, HEC1-A43, HEC1-A63 and HEC1-A77 cells. (*d*) Intracellular platinum accumulation was investigated after treatment with 1 mM cisplatin for 60 min and further incubation with cisplatin-free medium for 180 min and was determined by ICP-MS analysis.

Intracellular platinum accumulation in Anx A4-overexpressing cells

To elucidate the mechanism underlying platinum resistance induced by Anx A4, intracellular platinum accumulation of HEC1, HEC1-CV, HEC1-A25, HEC1-A43, HEC1-A63 and HEC1-A77 cells after cisplatin exposure was analyzed. Significantly less platinum had accumulated in HEC1-A25, HEC1-A43, HEC1-A63 and HEC1-A77 cells compared with HEC1 and HEC1-CV cells (0.036 pg/cell, $p < 0.01$; 0.04 pg/cell, $p < 0.01$; 0.03 pg/cell, $p < 0.01$; 0.065 pg/cell, $p < 0.05$ and 0.154 and 0.150 pg/cell, respectively) (Fig. 1*d*). Thus, intracellular platinum accumulation was decreased in Anx A4-overexpressing cells.

Anx A4-overexpressing cells and cisplatin in xenograft models

To determine the involvement of Anx A4 in platinum resistance *in vivo*, HEC1, HEC1-CV, HEC1-A63 and HEC1-A77 cells were subcutaneously injected into nude mice. After the tumor xenograft had been established, cisplatin or PBS was given twice a week for 1 month. On Day 56, average tumor volumes were 11,496 ± 950 mm^3 in PBS-treated HEC1-CV control mice and 3,554 ± 872 mm^3 in cisplatin-treated HEC1-CV controls. A significant antitumor effect of cisplatin was therefore observed in HEC1-CV-xenografted mice compared with the PBS-treated group. The parent HEC1 and HEC1-CV xenografts responded similarly to cisplatin (Fig. 2*a*; $p < 0.01$).

In HEC1-A63-xenografted mice, the average tumor volume on Day 56 was 8,245 ± 160 mm^3 in the PBS-treated group and only slightly less (7,078 ± 257 mm^3) in the cisplatin-treated group (Fig. 2*a*; $p = 0.42$). A similar response to cisplatin was observed in the HEC1-A63 and HEC1-A77 xenografts. On Day 56, no significant differences in tumor weight were found in HEC1-A63-xenografted mice between the PBS treatment (4.66 ± 0.42 g) and the cisplatin treatment groups (4.43 ± 0.16 g) (Fig. 2*b*). Similar results were observed in HEC1-A77 xenograft models. In contrast, a significant decrease in tumor weight was observed in HEC1-CV-xenografted mice between the PBS mock treatment (5.95 ± 1.16 g) and the cisplatin treatment groups (3.20 ± 0.76 g; $p < 0.05$) (Fig. 2*b*). Similar results were observed for the HEC1 and HEC1-CV xenografts. No significant differences in tumor weight in the PBS treatment group were observed among HEC1-CV-xenografted (5.95 ± 1.16 g), HEC1-xenografted (7.48 ± 0.34 g), HEC1-A63-xenografted (4.66 ± 0.42 g) and HEC1-A77-xenografted mice (4.82 ± 1.08 g) (Fig. 2*b*). These results indicated that overexpression of Anx A4 in HEC1 endometrial carcinoma cell lines conferred significant platinum resistance to the cells as tumors growing *in vivo*.

Translocation of Anx A4 and ATP7A after platinum exposure

In our study, platinum transporters were the focus of an investigation of the molecular mechanisms of chemoresistance induced by Anx A4. In previous research, intracellular platinum levels were decreased after enhanced expression of Anx A4, and ATP7A and ATP7B are well known as efflux transporters of platinum drugs.[27,28,31] However, the relationship of Anx A4 with ATP7A and ATP7B has not been previously examined. The results of our study demonstrated no change in expression of ATP7A at the protein levels owing to enforced overexpression of Anx A4 (Fig. 3*a*) and no ATP7B expression in HEC1 cells (data not shown). Therefore, the effects of Anx A4 expression on ATP7B in these cells were not investigated.

Because Anx A4 is normally localized to the cytoplasm, we theorized that exposure to platinum drugs may induce translocation of Anx A4 to the cellular membrane, resulting in an increase in chemoresistance owing to the influence of ATP7A. To investigate the possibility of induced translocation of Anx A4 and ATP7A by platinum drugs, CMFs were prepared. By Western blot analysis, Anx A4 expression in CMF of HEC1 and HEC1-CV cells before and after treatment with cisplatin or carboplatin was barely detectable because of its low endogenous expression in these cells (Fig. 3*b*). In contrast, Anx A4 expression was increased in CMF of HEC1-A63 cells and HEC1-A77 cells treated with cisplatin and carboplatin compared with untreated cells (Fig. 3*b*). Biotinylation-based cell surface membrane protein enrichment revealed a marked increase in biotinylation of ATP7A after exposure to cisplatin or carboplatin in HEC1, HEC1-CV, HEC1-A63 and HEC1-A77 cells (Fig. 3*c*). In the biotinylated samples, no Anx A4 expression was detected on the cell surface, although it had been previously detected in the cell CMF (data not shown). These results suggested that exposure to cisplatin or carboplatin induced massive translocation of Anx A4 to CMF, including the inner surface of the cell membrane (inaccessible to biotinylation). Before exposure of the cell to cisplatin or carboplatin, ATP7A was not expressed in biotinylated samples but after exposure, strong ATP7A expression was detected. These results suggested that exposure to cisplatin or carboplatin induced massive translocation of ATP7A to the outer surface of the cell (accessible to biotinylation).

Anx A4 and ATP7A localization

By immunofluorescence analysis, Anx A4 was localized in the perinuclear and cytoplasmic regions of untreated cells, whereas ATP7A was localized mainly in the perinuclear and cytoplasmic regions and slightly less in the cellular membrane in HEC1, HEC1-CV, HEC1-A63 and HEC1-A77 cells (Figs. 4*a*–4*d*). After 4-hr exposure to cisplatin or carboplatin, Anx A4 and ATP7A were found to be colocalized to the cellular membrane in HEC1-A63 cells (Fig. 4*c*). Similar findings were observed in HEC1-A77 cells (Fig. 4*d*). Because of the low expression of Anx A4 in HEC1 and HEC1-CV cells, no Anx A4 was detected in the cellular membranes in these cells (Figs. 4*a* and 4*b*). Thus, the results of the immunofluorescence analysis were in accordance with those of both Western blot analysis of CMF preparations and biotinylation

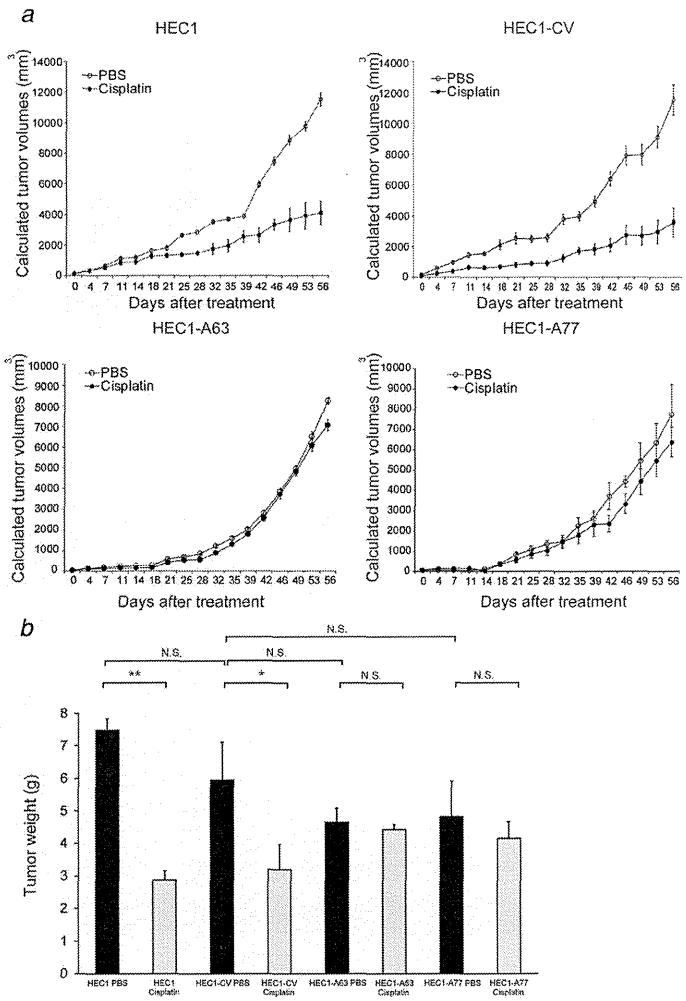

Figure 2. Enforced expression of Anx A4 in HEC1 cells confers platinum resistance *in vivo*. Analysis of Anx A4 as a platinum-resistant protein *in vivo*. (*a*) To determine the resistance of Anx A4-stably-expressing HEC1 cells to platinum *in vivo*, parent HEC1, HEC1-CV, HEC1-A63 and HEC1-A77 cells were subcutaneously injected into nude mice ($n = 5$ per group). After tumor xenografts were established, cisplatin (3 mg/kg) or PBS was administered i.p. twice weekly for 1 month. Figure shows the average (points) for five animals ± SD (bars). (*b*) Fifty-six days after implantation, tumors were removed and weighed. Values shown are the means (±SD) of five mice. NS: not significant (*$p < 0.05$; **$p < 0.01$; one-way ANOVA, followed by Dunnett's analysis).

Cancer Cell Biology

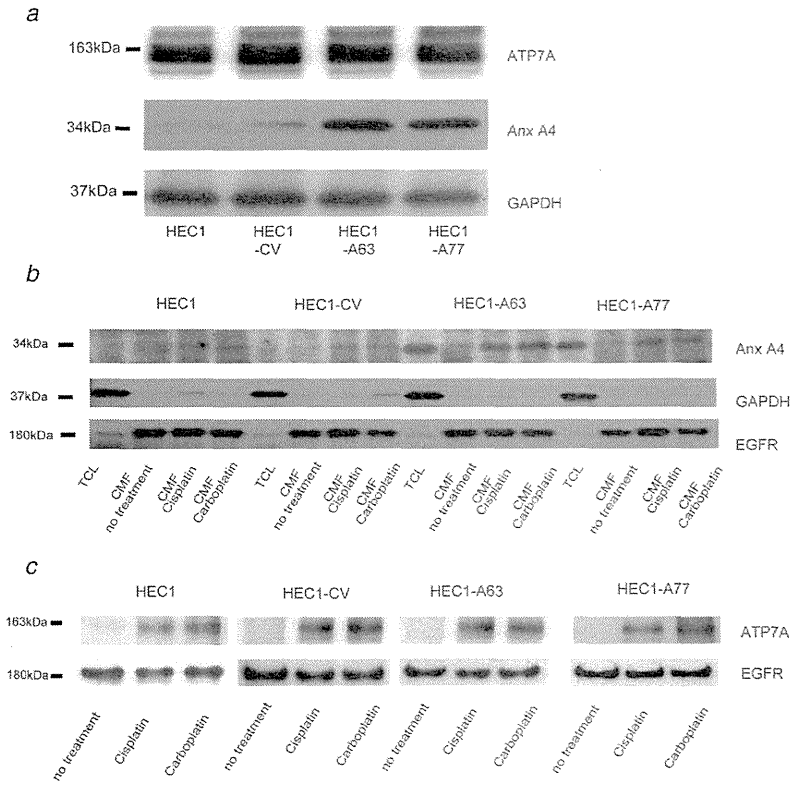

Figure 3. Localization of Anx A4 and ATP7A was investigated using Western blot analysis. The localization of Anx A4 and ATP7A was investigated using two techniques: orthogonal crude membrane fractions and biotinylation of cell surface proteins. (*a*) No significant change in expression levels of ATP7A was observed in HEC1, HEC1-CV, HEC1-A63 or HEC1-A77 cells. (*b*) In both HEC1-A63 and HEC1-A77 cells (but not in HEC1 and HEC1-CV cells), the drug-induced translocation of Anx A4 into the crude membrane fraction was shown by Western blot analysis after exposure to 10 μM cisplatin or 50 μM carboplatin for 4 hr. TCL: total cell lysate. Epidermal growth factor receptor was used as the control for cell surface protein labeling. (*c*) In HEC1, HEC1-CV, HEC1-A63 and HEC1-A77 cells, translocation of ATP7A to the cell surface was shown by Western blot analysis. Cells were treated with 25 μM cisplatin or 150 μM carboplatin for 4 hr, and cell surface proteins were biotinylated with 500 μM sulfo-NHS-SS-biotin. Biotinylated surface proteins were enriched with UltraLink Immobilized Neutroavidin (Thermo Fisher Scientific, Waltham, MA) and analyzed by Western blot analysis using anti-ATP7A. Levels of epidermal growth factor receptor, a surface protein, are shown as loading controls.

assays (Figs. 3*b* and 3*c*). Anx A4 and ATP7A were localized in the cytoplasm before cisplatin or carboplatin exposure; Anx A4 and ATP7A were then translocated to the cellular membrane after cisplatin or carboplatin exposure. Thus, Anx A4 and ATP7A are colocalized to the cellular membrane in platinum-treated HEC1-A63 and HEC1-A77 cells but not in HEC1 and HEC1-CV cells.

Effect of ATP7A expression on resistance to platinum drugs

The mechanism of platinum resistance conferred by Anx A4 overexpression was explored further by suppression of ATP7A expression using siRNA. The suppression of ATP7A was confirmed using Western blot analysis (Fig. 5*a*). Anx A4 expression was unchanged by silencing ATP7A (Fig. 5*a*). The

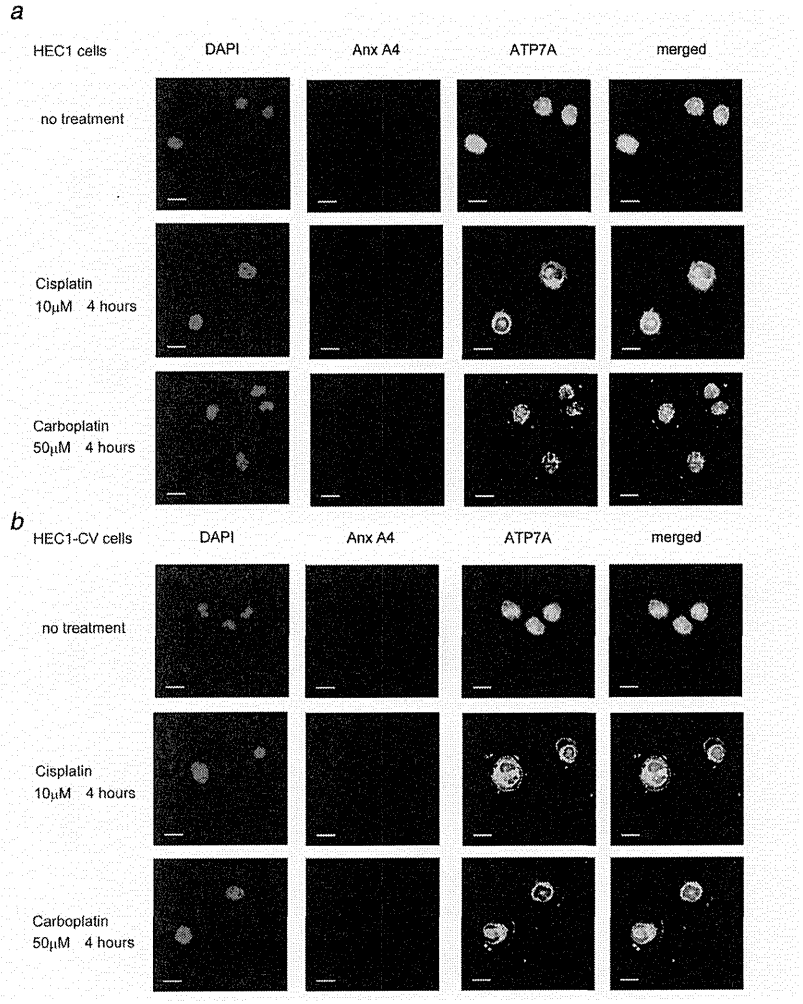

Figure 4. Immunofluorescence staining for ATP7A and Anx A4. HEC1, HEC1-CV, HEC1-A63 and HEC1-A77 cells were divided into three groups: the no treatment, cisplatin exposure and carboplatin exposure groups. (*a*) HEC1 cells, (*b*) HEC1-CV cells, (*c*) HEC1-A63 cells and (*d*) HEC1-A77 cells. Cells were incubated with anti-Anx A4 antibody (red) or anti-ATP7A antibody (green). Nuclei were stained with DAPI (blue). In the no treatment group for each cell, Anx A4 was localized in perinuclear and cytoplasmic regions and ATP7A was strongly localized in perinuclear regions. In HEC1 and HEC1-CV cells, after exposure to cisplatin or carboplatin, ATP7A was relocalized in the cellular membrane, although some ATP7A remained in the cytoplasm; however, no change in location of Anx A4 was observed. In HEC1-A63 and HEC1-A77 cells, Anx A4 and ATP7A were newly colocalized in the cellular membrane as well as remaining in the cytoplasm. In a comparison of HEC1 and HEC1-CV cells with HEC1-A63 and HEC1-A77 cells, expression of Anx A4 in HEC1-A63 and HEC1-A77 cells was stronger in the cytoplasm and cellular membrane. Scale bar = 30 μm.

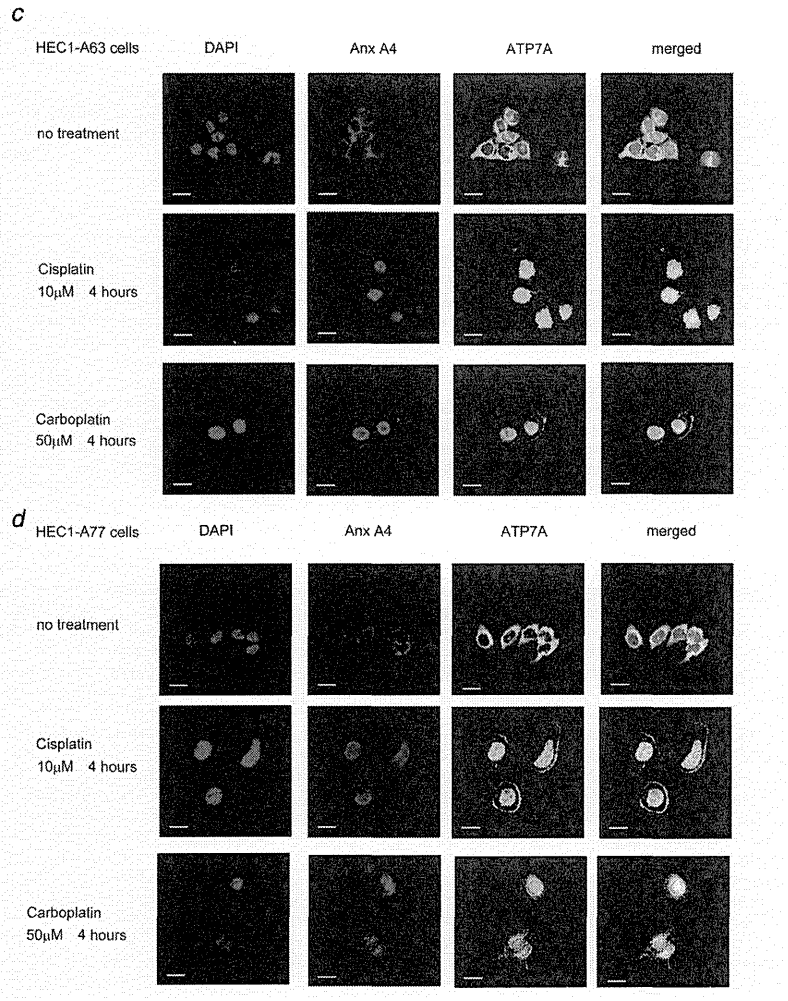

Figure 4. (Continued)

control and commercial siRNAs against ATP7A were transfected and the IC_{50} values of cisplatin and carboplatin were determined for each cell line. The IC_{50} value for cisplatin was significantly lower for the two kinds of ATP7A-silenced HEC1-A63 cells (ATP7A siRNA4, $IC_{50} = 11.0$ μM, $p < 0.01$; ATP7A siRNA6, $IC_{50} = 11.2$ μM, $p < 0.01$) compared with

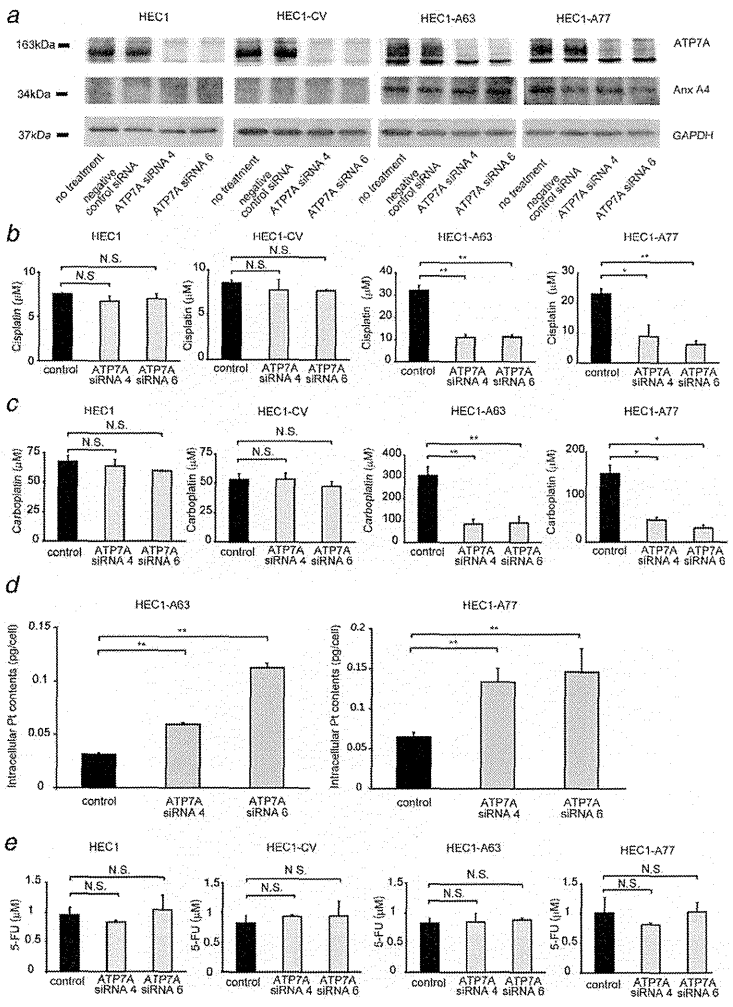

Figure 5. Knockdown of ATP7A expression improves platinum chemosensitivity in Anx A4-overexpressing cells. (*a*) Knockdown expression of ATP7A by siRNA in HEC1, HEC1-CV, HEC1-A63 and HEC1-A77 cells by Western blot analysis. (*b*) IC_{50} values are shown for cisplatin in HEC1, HEC1-CV, HEC1-A63 and HEC1-A77 cells transfected with negative control siRNA and two types of siRNA targeting ATP7A. A significant decrease in IC_{50} value for cisplatin was observed for the two types of ATP7A-silenced HEC1-A63 and HEC1-A77 cells but not for the HEC1 and HEC1-CV cells. (*c*) IC_{50} values are shown for carboplatin in HEC1, HEC1-CV, HEC1-A63 and HEC1-A77 cells transfected with negative control siRNA and two kinds of siRNA targeting ATP7A. A significant decrease in IC_{50} value for carboplatin was observed for the two types of ATP7A-silenced HEC1-A63 and HEC1-A77 cells but not for the HEC1 and HEC1-CV cells. (*d*) Intracellular platinum content after treatment with 1 mM cisplatin for 60 min and further incubation with cisplatin-free medium for 180 min in D-MEM medium in HEC1-A63 cells and HEC1-A77 cells transfected with negative control siRNA and ATP7A-targeting siRNA, as determined by ICP-MS analysis. Significantly higher intracellular platinum accumulation was observed in HEC1-A63 cells and HEC1-A77 ATP7A-silencing cells than in control siRNA-transfected HEC1-A63 cells and HEC1-A77 cells. (*e*) No significant differences in IC_{50} values for 5-FU were noted between HEC1, HEC1-CV, HEC1-A63 and HEC1-A77 cells. Similar results were observed in ATP7A-silenced cell lines for HEC1, HEC1-CV, HEC1-A63 and HEC1-A77 cells (*$p < 0.05$; **$p < 0.01$; one-way ANOVA followed by Dunnett's analysis).

the HEC1-A63 control siRNA-transfected cells (IC_{50} = 32.2 μM) (Fig. 5*b*).

In addition to cisplatin, improved chemosensitivity associated with ATP7A silencing was observed with carboplatin. Significantly lower IC_{50} values for carboplatin were observed in both types of ATP7A-silenced HEC1-A63 cells (siRNA4, IC_{50} = 85.9 μM, $p < 0.01$; siRNA6, IC_{50} = 92.8 μM, $p < 0.01$) compared with the HEC1-A63 control siRNA-transfected cells (IC_{50} = 300.7 μM) (Fig. 5*c*). Similar results were found for HEC1-A77 ATP7A-silenced cells, where a significantly lower IC_{50} value for cisplatin was observed (siRNA4, IC_{50} = 8.9 μM, $p < 0.05$; siRNA6, IC_{50} = 6.2 μM, $p < 0.01$) compared with that for HEC1-A77 control siRNA-transfected cells (IC_{50} = 23.3 μM). IC_{50} values for carboplatin were also significantly lower for the two kinds of ATP7A-silenced HEC1-A77 cells (siRNA4, IC_{50} = 49.8 μM, $p < 0.05$; siRNA6, IC_{50} = 31.9 μM, $p < 0.05$) compared with the HEC1-A77 control siRNA-transfected cells (IC_{50} = 152.1 μM, $p < 0.01$) (Fig. 5*c*). In contrast, siRNA treatments targeting ATP7A were ineffective in HEC1 and HEC1-CV cells treated with cisplatin or carboplatin (Figs. 5*b* and 5*c*). Intracellular platinum accumulation after cisplatin exposure was significantly increased in HEC1-A63 cells treated with ATP7A siRNA (0.060 pg/cell, $p < 0.01$ to 0.113 pg/cell, $p < 0.01$) compared with control siRNA-transfected cells (0.030 pg/cell) (Fig. 5*d*). Similarly, a significant increase in intracellular platinum accumulation was observed in HEC1-A77 cells treated with ATP7A siRNA (0.133 pg/cell, $p < 0.01$ to 0.146 pg/cell, $p < 0.01$) compared with control siRNA-transfected cells (0.065 pg/cell) (Fig. 5*d*).

To investigate the relationship between resistance to drugs other than platinum drugs and Anx A4 or ATP7A expression, IC_{50} values for 5-FU were determined for each cell line. No significant change in IC_{50} values for 5-FU was observed in HEC1 (IC_{50} = 0.96 μM), HEC1-CV (IC_{50} = 1.00 μM), HEC1-A63 (IC_{50} = 0.83 μM) or HEC1-A77 cells (IC50 = 1.01 μM) (Fig. 5*e*). Similar results were observed in the ATP7A-silenced cell lines for HEC1, HEC1-CV, HEC1-A63 and HEC1-A77 cells as well as in ATP7A-silenced cell lines (Fig. 5*e*). These results suggested that platinum resistance induced by enforced expression of Anx A4 was mainly dependent on the platinum transporter ATP7A and that expression of Anx A4 and ATP7A was unrelated to resistance to 5-FU.

Discussion

In our study, overexpression of Anx A4 in HEC1 cells decreased cell sensitivity to platinum drugs *in vitro*. Increased drug efflux was the mechanism underlying this change. In addition, an association between Anx A4 and platinum resistance was demonstrated for the first time *in vivo*. The mechanism of Anx A4-induced drug efflux may prove to be a promising therapeutic target because blockage of that mechanism may improve the prognosis of patients with Anx A4-associated platinum-resistant tumors.

Anx A4 itself is not a drug transporter, but it does bind to phospholipids in a Ca^{2+}-dependent manner and self-associates onto phospholipid membrane surfaces, causing membrane aggregation.[12,14–17] Thus, we assumed an indirect mediating effect of Anx A4 on drug efflux through an association between an unidentified drug transporter and Anx A4. Recently, MRP2 (an ABC ATPase-like multidrug-resistant protein) and ATP7A and ATP7B (two P-type Cu-transporting ATPases) were identified as platinum efflux transporters strongly associated with platinum resistance.[32,33] In an analysis of clinical gynecological samples, expression of MRP2 failed to predict tumor response to chemotherapy and did not correlate with overall survival.[34–36] In contrast, poor survival rates were associated with overexpression of ATP7A in patients with ovarian cancer.[37] Similarly, a correlation was found between ATP7B overexpression in endometrial carcinomas and an unfavorable clinical outcome in patients treated with cisplatin-based chemotherapy.[37] Therefore, we focused on the platinum transporters ATP7A and ATP7B and investigated their relationships with expression of Anx A4. In normal, unchallenged cells, ATP7A and ATP7B are localized in the Golgi apparatus and are involved in copper homeostasis, using ATP hydrolysis to transport copper ions across cellular membranes. They function in both the export of excess copper and its delivery to copper-dependent enzymes. ATP7A and ATP7B are also known to be efflux transporters of platinum drugs.[8,27,28,31,38,39] In one study, only a slight increase in expression of transfected ATP7A was seen in a human ovarian cancer cell line; however, that small increase was sufficient to confer significant resistance to cisplatin or carboplatin.[40] In a similar study in another human cisplatin-resistant ovarian cancer cell line, silencing of ATP7B by siRNA transfection resulted in a 2.5-fold decrease in cisplatin IC_{50} levels and a significant increase in DNA-platinum adduct formation.[41] Preparing CMF of treated cells facilitated the localization of Anx A4 expression in cells before and after exposure to platinum drugs. The abundance of AnxA4 in the membrane fraction along with the translocation to the membrane was increased. Using the orthogonal method of cell surface protein labeling to monitor proteins appearing on the cell surface, biotinylated ATP7A was increased after cisplatin or carboplatin exposure both in HEC1 and HEC1-CV cells (cells expressing low levels of Anx A4) and HEC1-A63 and HEC1-A77 cells (cells overexpressing Anx A4). Taken together, these results suggest that platinum drug exposure causes relocalization of Anx A4 expression to the membrane fraction and relocalization of ATP7A transporters (to a minimum) to the external surface of the cellular membrane. Unfortunately, no similar analysis of ATP7B was possible because it is not expressed in HEC1 cells (data not shown). However, in cells that express both ATP7A and ATP7B proteins, other immunofluorescence studies have shown similar changes in localization of both proteins after cisplatin exposure.[42] After cisplatin or carboplatin exposure in HEC1-A63 and HEC1-A77 Anx

A4-overexpressing cells, immunofluorescence showed that Anx A4 expression was relocated from the perinuclear and cytoplasmic Golgi regions to the cellular membrane. This relocalization was not observed in HEC1 and HEC1-CV cells, in which overexpression of Anx A4 does not occur.

ATP7A also relocates from the perinuclear and cytoplasmic regions to the cellular membrane after cisplatin or carboplatin exposure. However, this occurs both in HEC1 and HEC1-CV cells (cells expressing low levels of Anx A4) and HEC1-A63 and HEC1-A77 cells (cells overexpressing Anx A4). Although no direct interaction between ATP7A and Anx A4 was detected by coimmunoprecipitation analysis (data not shown), immunofluorescence analysis showed colocalization of ATP7A and Anx A4 at least within the cellular membrane in Anx A4-overexpressing cells. These results suggested that Anx A4 is not required for ATP7A translocation and that ATP7A translocation is unrelated to expression of Anx A4.

Translocation of Anx A4 to plasma membranes is reportedly mediated by an increase in intracellular free Ca^{2+}, which is increased by exposure to platinum drugs.[43,44] In addition to the translocation of ATP7A and Anx A4 to the plasma membrane, our results also showed translocation of ATP7A to the nucleus in HEC1 and HEC1-CV cells. Translocation to the nucleus and colocalization of both ATP7A and Anx A4 were also observed in HEC1-A63 and HEC1-A77 cells after exposure to cisplatin or carboplatin in the immunofluorescence staining analysis in our study (Fig. 4). Anx A4 translocates to the nucleus after etoposide treatment and suppresses NF-κB transcriptional activity, which induces expression of Bax, a proapoptotic Bcl-2 family protein.[18] In addition, a correlation has been reported between nuclear staining of Anx A4 and poor survival in patients with ovarian cancer.[45] However, the role of ATP7A in the nucleus and its relationship with NF-κB transcriptional activity has not been investigated. Further investigation is needed to elucidate the role of nuclear colocalization of Anx A4 and ATP7A in platinum resistance.

In our study, translational silencing of ATP7A in HEC1 and HEC1-CV (Anx A4-nonexpressing cells) and HEC1-A63 and HEC1-A77 cells (Anx A4-overexpressing cells) was performed. Western blot analysis demonstrated no detectable changes in protein expression of Anx A4 when ATP7A was silenced in any of these four cell lines.

In HEC1 and control HEC1-CV cells (low Anx A4 expression levels), IC_{50} values for cisplatin or carboplatin cells after the knockdown of ATP7A expression caused no improvement in the sensitivity of these cells to cisplatin or carboplatin. Similar results were observed in a previous study in which no improvement in sensitivity to cisplatin resulted from silencing of ATP7A in platinum-resistant or -sensitive ovarian cancer cell lines.[41] However, Mangala *et al.* reported improved sensitivity to cisplatin in both platinum-resistant ovarian cancer cells and parental cells expressing ATP7B as a result of silencing of ATP7B expression.[41] An important discovery related to ATP7A was communicated in our study: in cells overexpressing both Anx A4 and ATP7A, silencing of ATP7A significantly improved sensitivity to cisplatin and carboplatin, thus restoring them to sensitivity levels comparable to those of HEC1 and HEC1-CV cells. These results were supported by a quantitative analysis of the accumulation of intracellular platinum, demonstrating that siRNA silencing of ATP7A in Anx A4-overexpressing HEC1-A63 and HEC1-A77 cells resulted in greater intracellular platinum accumulation than HEC1-A63 and HEC1-A77 cells transfected with a control siRNA. On the other hand, the analysis of IC_{50} values for 5-FU showed no relationship between overexpression of Anx A4 and resistance to 5-FU. In addition, no improvement in sensitivity to 5-FU was observed as a result of ATP7A silencing. These results suggested a specific relationship of Anx A4 with ATP7A and resistance to platinum drugs but with to nonplatinum drugs such as 5-FU. Differences in efficacy and improvement in drug sensitivity of ATP7A silencing were observed between cell lines (HEC1, HEC1-CV, HEC1-A63 and HEC1-A77 cells). These variations may be related to the colocalization of Anx A4 and ATP7A in the cellular membrane after cisplatin or carboplatin exposure. Colocalization of Anx A4 and ATP7A after exposure to platinum drugs was specific to changes in Anx A4-overexpressing cells, which are probably related to drug efflux. These results suggest that in conjunction with higher Anx A4 expression levels, ATP7A had a positive effect on efflux of platinum drugs, resulting in significantly increased platinum resistance. Because overexpression of Anx A4 had no effect on ATP7A expression and because no direct interaction between ATP7A and Anx A4 was detected in the coimmunoprecipitation analysis, Anx A4 seems to promote ATP7A activity in a manner which is currently unexplained.

In addition to the effects of Anx A4 on drug resistance in ovarian cancer, similar findings have been reported for other overexpressed members of the Annexin family such as Annexin A3 (Anx A3).[46,47] Intracellular platinum concentrations of cisplatin and levels of platinum DNA binding in that study were significantly lower in Anx A3-overexpressing cells than in control cells, suggesting a more general involvement of the Annexin family in platinum resistance.[46] From the results of these related reports and those of our study, we conclude that the Annexin family may potentially enhance the activity of numerous drug transporters. Identifying these enhancement mechanisms may be extremely useful for developing additional therapeutic targets for drug-resistant tumors.

In summary, our study demonstrated that enhanced expression of Anx A4 induces chemoresistance by promoting platinum drug efflux *via* ATP7A. These findings suggested that Anx A4 is a potential therapeutic target for chemosensitization, particularly in tumors with higher expression of both Anx A4 and ATP7A. Thus, our study provides a clear example of applied genotoxicology. However, platinum resistance induced by overexpression of Anx A4 may occur as a result of multiple processes, including regulation of apoptosis and efflux of platinum drugs. Thus, other unknown chemoresistant mechanisms may be induced by overexpression of Anx A4. Because overexpression of Anx A4 has been reported in several other types of clinically important cancers, such as rectal, renal, lung and pancreatic cancer,[19–23] targeting Anx A4 may lead to the development of an effective therapy for overcoming chemoresistance in more types of cancer.

Acknowledgements

The authors thank Y. Kanazawa and S. Sugiyama for their secretarial assistance, M. Urase for technical assistance and Dr. G.S. Buzard for helpful editing.

References

1. Omura G, Blessing JA, Ehrlich CE, et al. A randomized trial of cyclophosphamide and doxorubicin with or without cisplatin in advanced ovarian carcinoma. *A Gynecologic Oncology Group Study. Cancer* 1986;57:1725–30.
2. Thigpen T, Vance R, Puneky L, et al. Chemotherapy in advanced ovarian carcinoma: current standards of care based on randomized trials. *Gynecol Oncol* 1994;55:S97–S107.
3. Vaughan S, Coward JI, Bast RC, Jr, et al. Rethinking ovarian cancer: recommendations for improving outcomes. *Nat Rev Cancer* 2011;11:719–25.
4. Fleming GF, Brunetto VL, Cella D, et al. Phase III trial of doxorubicin plus cisplatin with or *without paclitaxel plus filgrastim in advanced* endometrial carcinoma: a Gynecologic Oncology Group Study. *J Clin Oncol* 2004;22:2159–66.
5. Hoskins PJ, Swenerton KD, Pike JA, et al. Paclitaxel and carboplatin, alone or with irradiation, in advanced or recurrent endometrial cancer: a phase II study. *J Clin Oncol* 2001;19:4048–53.
6. Obel JC, Friberg G, Fleming GF. Chemotherapy in endometrial cancer. *Clin Adv Hematol Oncol* 2006;4:459–68.
7. Enomoto T, Kuragaki C, Yamasaki M, et al. Is clear cell carcinoma and mucinous carcinoma of the ovary sensitive to combination chemotherapy with paclitaxel and carboplatin? *Proc Am Soc Clin Oncol* 2003;22:(abstr 1797).
8. Nakayama K, Kanzaki A, Terada K, et al. Prognostic value of the Cu-transporting ATPase in ovarian carcinoma patients receiving cisplatin-based chemotherapy. *Clin Cancer Res* 2004;10:2804–11.
9. Pectasides D, Fountzilas G, Aravantinos G, et al. Advanced stage clear-cell epithelial ovarian cancer: the Hellenic Cooperative Oncology Group experience. *Gynecol Oncol* 2006;102:285–91.
10. Goff BA, Sainz de la Cuesta R, Muntz HG, et al. Clear cell carcinoma of the ovary: a distinct histologic type with poor prognosis and resistance to platinum-based chemotherapy in stage III disease. *Gynecol Oncol* 1996;60:412–17.
11. Sugiyama T, Kamura T, Kigawa J, et al. Clinical characteristics of clear cell carcinoma of the ovary: a distinct histologic type with poor prognosis and resistance to platinum-based chemotherapy. *Cancer* 2000;88:2584–9.
12. Kim A, Enomoto T, Serada S, et al. Enhanced expression of Annexin A4 in clear cell carcinoma of the ovary and its association with chemoresistance to carboplatin. *Int J Cancer* 2009;125:2316–22.
13. Miao Y, Cai B, Liu L, et al. Annexin IV is differentially expressed in clear cell carcinoma of the ovary. *Int J Gynecol Cancer* 2009;19:1545–9.
14. Gerke V, Moss SE. Annexins: from structure to function. *Physiol Rev* 2002;82:331–71.
15. Kaetzel MA, Hazarika P, Dedman JR. Differential tissue expression of three 35-kDa annexin calcium-dependent phospholipid-binding proteins. *J Biol Chem* 1989;264:14463–70.
16. Kaetzel MA, Mo YD, Mealy TR, et al. Phosphorylation mutants elucidate the mechanism of annexin IV-mediated membrane aggregation. *Biochemistry* 2001;40:4192–9.
17. Kim A, Serada S, Enomoto T, et al. Targeting annexin A4 to counteract chemoresistance in clear cell carcinoma of the ovary. *Expert Opin Ther Targets* 2010;14:963–71.
18. Jeon YJ, Kim DH, Jung H, et al. Annexin A4 interacts with the NF-kappaB p50 subunit and modulates NF-kappaB transcriptional activity in a *Ca2+-dependent manner. Cell Mol Life Sci* 2010;67:2271–81.
19. Alfonso P, Canamero M, Fernandez-Carbonie F, et al. Proteome analysis of membrane fractions in colorectal carcinomas by using 2D-DIGE saturation labeling. *J Proteome Res* 2008;7:4247–55.
20. Duncan R, Carpenter B, Main LC, et al. Characterisation and protein expression profiling of annexins in colorectal cancer. *Br J Cancer* 2008;98:426–33.
21. Sitek B, Luttges J, Marcus K, et al. Application of fluorescence difference gel electrophoresis saturation labelling for the analysis of microdissected precursor lesions of pancreatic ductal adenocarcinoma. *Proteomics* 2005;5:2665–79.
22. Zimmermann U, Balabanov S, Giebel J, et al. Increased expression and altered location of annexin IV in renal clear cell carcinoma: a possible role in tumour dissemination. *Cancer Lett* 2004;209:111–18.
23. Wei R, Zhang Y, Shen L, et al. Comparative proteomic and radiobiological analyses in human lung adenocarcinoma cells. *Mol Cell Biochem* 2012;359:151–9.
24. Furukawa T, Komatsu M, Ikeda R, et al. Copper transport systems are involved in multidrug resistance and drug transport. *Curr Med Chem* 2008;15:3268–78.
25. Gourdon P, Liu XY, Skjorringe T, et al. Crystal structure of a copper-transporting PIB-type ATPase. *Nature* 2011;475:59–64.
26. Owatari S, Akune S, Komatsu M, et al. Copper-transporting P-type ATPase, ATP7A, confers multidrug resistance and its expression is related to resistance to SN-38 in clinical colon cancer. *Cancer Res* 2007;67:1860–8.
27. Samimi G, Varki NM, Wilczynski S, et al. Increase in expression of the copper transporter ATP7A during platinum drug-based treatment is associated with poor survival in ovarian cancer patients. *Clin Cancer Res* 2003;9:5853–9.
28. Safaei R, Holzer AK, Katano K, et al. The role of copper transporters in the development of resistance to Pt drugs. *J Inorg Biochem* 2004;98:1607–13.
29. Iwahori K, Serada S, Fujimoto M, et al. SOCS-1 gene delivery cooperates with cisplatin plus pemetrexed to exhibit preclinical antitumor activity against malignant pleural mesothelioma. *Int J Cancer* 2013;132:459–71.
30. Khunweeraphong N, Nagamori S, Wiriyasermkul P, et al. Establishment of stable cell lines with high expression of heterodimers of human 4F2hc and human amino acid transporter LAT1 or LAT2 and delineation of their differential interaction with (alpha)-alkyl moieties. *J Pharmacol Sci* 2012;119:368–80.
31. Rabik CA, Maryon EB, Kasza K, et al. Role of copper transporters in resistance to platinating agents. *Cancer Chemother Pharmacol* 2009;64:133–42.
32. Galluzzi L, Senovilla L, Vitale I, et al. Molecular mechanisms of cisplatin resistance. *Oncogene* 2012;31:1869–83.
33. Kelland L. The resurgence of platinum-based cancer chemotherapy. *Nat Rev Cancer* 2007;7:573–84.
34. Arts HJ, Katsaros D, de Vries EG, et al. Drug resistance-associated markers P-glycoprotein, *multidrug resistance-associated protein 1, multidrug* resistance-associated protein 2, and lung resistance protein as prognostic factors in ovarian carcinoma. *Clin Cancer Res* 1999;5:2798–805.
35. Guminski AD, Balleine RL, Chiew YE, et al. MRP2 (ABCC2) and cisplatin sensitivity in hepatocytes and human ovarian carcinoma. *Gynecol Oncol* 2006;100:239–46.
36. Materna V, Pleger J, Hoffmann U, et al. RNA expression of MDR1/P-glycoprotein, DNA-topoisomerase I, and MRP2 in ovarian carcinoma patients: correlation with chemotherapeutic response. *Gynecol Oncol* 2004;94:152–60.
37. Aida T, Takehayashi Y, Shimizu T, et al. Expression of copper-transporting P-type adenosine triphosphatase (ATP7B) as a prognostic factor in human endometrial carcinoma. *Gynecol Oncol* 2005;97:41–5.
38. Katano K, Kondo A, Safaei R, et al. Acquisition of resistance to cisplatin is accompanied by changes in the cellular pharmacology of copper. *Cancer Res* 2002;62:6559–65.
39. Kuo MT, Chen HH, Song IS, et al. The roles of copper transporters in cisplatin resistance. *Cancer Metastasis Rev* 2007;26:71–83.
40. Samimi G, Safaei R, Katano K, et al. Increased expression of the copper efflux transporter ATP7A mediates resistance to cisplatin, carboplatin, and oxaliplatin in ovarian cancer cells. *Clin Cancer Res* 2004;10:4661–9.
41. Mangala LS, Zuzel V, Schmandt R, et al. Therapeutic targeting of ATP7B in ovarian carcinoma. *Clin Cancer Res* 2009;15:3770–80.
42. Kalayda GV, Wagner CH, Buss I, et al. Altered localisation of the copper efflux transporters ATP7A and ATP7B associated with cisplatin

resistance in human ovarian carcinoma cells. *BMC Cancer* 2008;8:175.
43. Al-Bahlani S, Fraser M, Wong AY, et al. P73 regulates cisplatin-induced apoptosis in ovarian cancer cells via a calcium/calpain-dependent mechanism. *Oncogene* 2011;30:4219–30.
44. Splettstoesser F, Florea AM, Busselberg D. IP(3) receptor antagonist, 2-APB, attenuates cisplatin induced $Ca2+$-influx in HeLa-S3 cells and prevents activation of calpain and induction of apoptosis. *Br J Pharmacol* 2007;151:1176–86.
45. Choi CH, Sung CO, Kim HJ, et al. Overexpression of annexin A4 is associated with chemoresistance in papillary serous adenocarcinoma of the ovary. *Hum Pathol* 2013;44:1017–23.
46. Yan X, Yin J, Yao H, et al. Increased expression of annexin A3 is a mechanism of platinum resistance in ovarian cancer. *Cancer Res* 2010;70:1616–24.
47. Yin J, Yan X, Yao X, et al. Secretion of annexin A3 from ovarian cancer cells and its association with platinum resistance in ovarian cancer patients. *J Cell Mol Med* 2012;16:337–48.

Journal of Virology

Varicella-Zoster Virus ORF49 Functions in the Efficient Production of Progeny Virus through Its Interaction with Essential Tegument Protein ORF44

Tomohiko Sadaoka, Satoshi Serada, Junko Kato, Mayuko Hayashi, Yasuyuki Gomi, Tetsuji Naka, Koichi Yamanishi and Yasuko Mori

J. Virol. **2014, 88(1):188. DOI: 10.1128/JVI.02245-13. Published Ahead of Print 23 October 2013.**

JVI
Journals.ASM.org

Varicella-Zoster Virus ORF49 Functions in the Efficient Production of Progeny Virus through Its Interaction with Essential Tegument Protein ORF44

Tomohiko Sadaoka,[a,b] Satoshi Serada,[c] Junko Kato,[a] Mayuko Hayashi,[a,b] Yasuyuki Gomi,[d] Tetsuji Naka,[c] Koichi Yamanishi,[e] Yasuko Mori[a,b]

Division of Clinical Virology, Center for Infectious Diseases, Kobe University Graduate School of Medicine, Kusunoki-cho, Chuo-ku, Kobe, Japan[a]; Laboratory of Virology and Vaccinology, Division of Biomedical Research, National Institute of Biomedical Innovation, Saito-Asagi, Ibaraki, Osaka, Japan[b]; Laboratory of Immune Signal, Division of Biomedical Research, National Institute of Biomedical Innovation, Saito-Asagi, Ibaraki, Osaka, Japan[c]; Kanonji Institute, The Research Foundation for Microbial Diseases of Osaka University, Kanonji, Kagawa, Japan[d]; National Institute of Biomedical Innovation, Saito-Asagi, Ibaraki, Osaka, Japan[e]

The ORF49 tegument protein of varicella-zoster virus (VZV) is one of the core gene products that is conserved among herpesvirus family members. Although ORF49 is known to be a cell-tropic factor, its detailed functions remain elusive. ORF44 is another core gene product reported to be essential, although its characterization and detailed functional analysis have not been reported. These two core gene products form a complex in other herpesviruses beyond the host species and herpesvirus subfamilies. Here, we show that complex formation between ORF44 and ORF49 is conserved in VZV. We serendipitously found that binding is eliminated by an amino acid substitution at position 129 (phenylalanine 129), and four amino acids in the carboxyl-terminal half of the acidic cluster in ORF49 (i.e., aspartate-phenylalanine-aspartate-glutamate from positions 41 to 44 [41DFDE44]) were identified as its binding motif. Alanine substitutions in each domain rendered the ORF44F129A mutation lethal for VZV, similar to deletion of the entire ORF44. The phenotype of the ORF49-41AAAA44 mutation was comparable to that of the ORF49-defective virus, including small-plaque formation, impaired growth, and low infectious virus production. These results suggest that the interaction between ORF44 and ORF49 is essential for their role in VZV infection and that ORF49 is required for the efficient production of infectious progeny virus mediated by the conserved interaction between the two proteins.

Varicella-zoster virus (VZV) is a member of the human alphaherpesvirus subfamily and the etiologic agent of two diseases: varicella is the result of primary infection with VZV, and herpes-zoster is caused by reactivation of the virus from the latent state (1). VZV shares many features, especially a tropism for epithelial and neural tissues, with other human alphaherpesvirus members, including herpes simplex viruses 1 and 2 (HSV-1 and -2, respectively), and with the nonhuman alphaherpesviruses. However, VZV spreads only via cell-to-cell infection in culture and is more akin to the betaherpesviruses (i.e., human herpesviruses 6 and 7) in its apparent T-cell-tropism (1).

The VZV genome is approximately 125 kb and contains at least 70 unique open reading frames (ORFs), and it is the smallest genome in terms of length and gene set among human herpesviruses (1–3). Of the 70 identified ORFs, 44 are core genes that are conserved among all human herpesvirus subfamilies (4). Recent genome-wide mutagenesis analysis showed that 34 ORFs among the core genes are essential for virus reconstitution in cell culture, whereas deletion of seven ORFs results in viral growth defects, and three ORFs are dispensable in cell culture or skin organ culture (5). Eight core genes encode tegument proteins, which are the structural components of the virion and are located between the nucleocapsid and the envelope.

VZV ORF49 encodes a nonessential tegument protein that functions as a cell-tropic factor in cell culture via an unknown mechanism (6). VZV ORF49 is the homolog of HSV-1 UL11 and human cytomegalovirus (HCMV) UL99, which are among the most extensively studied tegument protein-encoding genes. The UL11 and UL99 gene products, pUL11 and pp28, function in secondary envelopment (7–9), but they have different roles in the viral life cycle. HSV-1 UL11 is not essential for the viral life cycle; however, the UL11 deletion mutant forms small plaques, and the final titers are reduced to 80 to 95% of wild-type levels (10). In contrast, HCMV UL99 is an essential gene, and pp28-deficient mutants show extremely impaired growth in normal fibroblasts and produce no detectable infectious progeny (9). However, this mutant spreads from cell to cell via an unknown mechanism (11).

Several recent reports, beginning with one on HSV-1 UL16, which is a core gene within the intron of a conserved herpesvirus spliced gene, (12), showed that interactions between pUL11 and pUL16 homologs were conserved beyond the host species and herpesvirus subfamilies (13–15). HSV pUL16 localizes to the nucleus and the cytoplasm of infected cells and functions in virus entry and in nuclear and cytoplasmic egress (16–19); pUL16 homologs may function in secondary envelopment, as reviewed in reference 20. As described for UL11 homologs, whether UL16 homologs are required for the viral life cycle differs among viruses (13, 15, 21–25). In a genome-wide mutagenesis analysis, deletion of the entire gene region from the viral genome of VZV ORF44, the UL16 homolog, showed that it is an essential gene by loss-of-function analysis in the MeWo cell line (5), although this was not confirmed by a revertant virus generated for gain-of-function analysis.

Received 11 August 2013 Accepted 10 October 2013
Published ahead of print 23 October 2013
Address correspondence to Yasuko Mori, ymori@med.kobe-u.ac.jp.

doi:10.1128/JVI.02245-13

The LI motif and the conserved acidic cluster of pUL11 are essential for its interaction with pUL16 of HSV-1, whereas the critical sequences in pUL16 have not been determined because it is highly sensitive to deletions. Its short N-terminal 75-amino-acid (aa) fragment was recently shown to include the pUL11 binding site, and its C-terminal region functions as the binding regulatory domain (26), although this has not been confirmed in the context of HSV-1 infection. HCMV pUL94 directs pp28 to the assembly compartment, where it plays a role in secondary envelopment. Amino acids 37 to 39, near the acidic cluster of pp28, and one of the conserved cysteine residues of pUL94 are involved in binding in the context of infection (24, 27). In VZV, potential ORF49 protein (ORF49p)-binding proteins, including the pUL16 homolog ORF44 protein (ORF44p), were identified by global screening using the yeast two-hybrid system (28, 29), although these interactions have not been confirmed, even by coexpression experiments in mammalian cells.

In our previous study on VZV ORF49 (6), ORF49p was identified as one of the cell-tropic factors for VZV lytic infection in cell culture. However, the precise function of ORF49 in cells in which the ORF49-defective virus showed impaired growth was not elucidated. To address this issue, we established a complete *trans*-complementation system for ORF49 and identified ORF44p as its binding partner in the context of infection. In the present study, we aimed to reveal the precise role of ORF49p by using this system and by analyzing the conserved mechanism of interaction between these proteins and its role in VZV infection.

MATERIALS AND METHODS

Cells and viruses. The melanoma cell line MeWo was propagated in Dulbecco's modified Eagle's medium (DMEM) (Nissui Pharmaceutical, Ueno, Tokyo) supplemented with 8% fetal bovine serum (FBS) (Sigma-Aldrich, St. Louis, MO), 0.6 mg/ml L-sodium glutamate, and 0.02 mg/ml gentamicin sulfate (Nacalai Tesque, Kyoto, Japan) (DMEM complete). MeWo cells stably expressing Cre recombinase, designated MeWo-Cre cells, were maintained in DMEM complete supplemented with 500 μg/ml G418 (Nacalai Tesque) (30). MeWoORF49 cells stably expressing ORF49 were generated as follows: MeWo cells were transfected with CAG/ORF49 (described below) using Lipofectamine 2000 (Invitrogen, Carlsbad, CA) according to the manufacturer's instructions, selected, and propagated in DMEM complete supplemented with 1.5 μg/ml puromycin (Invitrogen). Recombinant viruses derived from the parental VZV strain Oka (pOka), rpOka, rpOkaΔ44Rev, rpOkaORF44F129ARev, rpOkaORF44T128A, rpOkaORF44K130A, rpOkaORF49M1L, rpOkaORF49M1LRev, rpOka-*ORF49-41AAAA44*, and *rpOkaORF49-41AAAA44Rev* were maintained in DMEM complete supplemented with 3% FBS.

Cell-free virus was prepared as described previously with slight modifications (6). At 48 h postinfection (hpi) by cell-to-cell spread, cells were harvested with a cell scraper (Iwaki, Tokyo, Japan), spun at 800 × *g* for 5 min at 4°C, and suspended in SGP buffer (phosphate-buffered saline [PBS] containing 0.1% L-sodium glutamate and 7% sucrose). The suspended cells were treated with an ultrasonic disruptor (UD-201; Tomy Seiko, Tokyo, Japan) at 1.5° for 30 s on ice and spun at 800 × *g* for 5 min at 4°C, and the supernatant was stored at −80°C until use. The purified viral particles were prepared as described in reference 6. Briefly, the cell-free virus solutions were subjected to Histodenz (Sigma-Aldrich) gradient purification (5 to 50% in PBS) by ultracentrifugation at 50,200 × *g* for 2 h at 4°C in a P40ST rotor (CP80WX; Hitachi Koki, Hitachinaka, Japan). Aliquots of the peak particle-containing fractions were subjected to ultracentrifugation at 52,600 × *g* for 2 h at 4°C in a P28S rotor (CP80WX; Hitachi Koki), and the pellets were stored at −80°C for further analyses.

Plasmids. The pGEX/ORF44, pGEX/ORF44A, and pGEX/ORF44P plasmids were generated to express the full length (corresponding to aa 2 to 363), anterior half (aa 2 to 200), and posterior half (aa 181 to 363) of the ORF44 protein in *Escherichia coli*. The primer pairs ORF44ecoF4 (5′-ACCGAATTCGAATTACAACGCATATTTCCG-3′) and ORF44salR (5′-ACCGTCGACCTAGGTGGTTGTAGG-3′) for ORF44, ORF44ecoF4 and ORF44salR600 (5′-ACCGTCGACTAAATTAGGTTCCATAGCC-3′) for ORF44A, and ORF44ecoF541 (5′-ACCGAATTCGGAGTGTGGTGGTCAGACG-3′) and ORF44salR for ORF44P were used to amplify each indicated region of the ORF44 gene from the rpOka cDNA. The PCR products were inserted in frame into the pGEX6P-1 bacterial expression vector (GE Healthcare Bio-Sciences, Piscataway, NJ) via the EcoRI and SalI sites (underlined). The same procedure was used to construct pGEX/ORF61. The DNA fragment (positions 406 to 744) of ORF61 was cloned into pGEX6P-1 via the BamHI and SalI sites (underlined). The primer pair was ORF61bamF406 (5′-ACCGGATCCGGGCCCCTTCAATCGTCGG-3′) and ORF61salR744stop (5′-ACCGTCGACCTAGAATCTCGCGTTTCCCTC-3′). The eukaryotic ORF44 expression plasmid CAG/ORF44 or CAG/FLAGORF44, which was N-terminally tagged with FLAG (DYKDD DDK), was generated as follows: the entire ORF44 gene was amplified by PCR with the primers ORF44-25kpnF (5′-ACCGGTACCAATCCGCTAGACTG-3′) or ORF44FLAGkpnF4 (5′-ACCGGTACCGCCACCATGgacta caaagacgatgacgacaagGAATTACAACGCATATTTCCG-3′) and ORF44salR, and the PCR fragment was cut by KpnI and SalI (underlined) and cloned into pCAGGS-MCS-neo via the KpnI and XhoI sites. The FLAG tag coding sequence within the primer for ORF44FLAGkpnF4 is shown in lowercase letters. The ORF49 expression plasmid CAG/ORF49 was generated as follows: the entire ORF49 gene was amplified by PCR with the primers ORF49-24ecoF (5′-ACCGAATTCTTACATCAGCATTGCG−3′) and ORF49bamR (5′-ACCGGATCCTTAACATTTTGCGCATTTGG-3′), and the PCR fragment was cut by EcoRI and BamHI (underlined) and cloned into pCAGGS-MCS-puro via the EcoRI and BglII sites. The pCAGGS plasmid was kindly provided by Jun-ichi Miyazaki (Osaka University, Japan) (31). A Cre recombinase-expressing plasmid, pCX-Cre-neo, was previously generated (30) from pCX-Cre, which was a generous gift from Masaru Okabe (Osaka University, Japan).

Construction of mutant ORF44 and ORF49 expression plasmids. The ORF44 mutant plasmids pGEX/ORF44F129A, CAG/ORF44T128A, CAG/ORF44F129A, CAG/ORF44K130A, CAG/FLAGORF44I121stop, CAG/FLAGORF44P136stop, and CAG/FLAGORF44F129AP136stop and the ORF49 mutant plasmid CAG/ORF49-41AAAA44 were generated with a QuikChange Lightning multisite-directed mutagenesis kit (Agilent Technologies, La Jolla, CA) according to the manufacturer's recommendations, using the primers listed in Table 1 based on pGEX/ORF44, CAG/ORF44, CAG/FLAGORF44, and CAG/ORF49, respectively. The ORF49 C-terminal deletion mutant plasmids CAG/ORF49N40, CAG/ORF49N44, and CAG/ORF49N48 were generated using the following primer pairs: ORF49-24ecoF (5′-ACCGAATTCTTACATCAGCATTGCG-3′) as the forward primer for all the deletion mutants and ORF49mycxhoR120 (5′-ACCCTCGAGcagatcctcttctgagatgagtttttgttcAAAGTCTTCAAAGAACTCTG-3′), ORF49mycxhoR132 (5′-ACCCTCGAGcagatcctcttctgagatgagtttttgttcCTCATCAAAGTCAAAGTCTT-3′), or ORF49mycxhoR144 (5′-ACCCTCGAGcagatcctcttctgagatgag ttttgttcCTCTGTTACATTCTCATCAAAGTC-3′) as the reverse primer for CAG/ORF49N40, CAG/ORF49N44, or CAG/ORF49N48. All of the reverse primers contained a c-myc tag, indicated by lowercase letters, and the PCR products were cloned into pCAGGS-MCS-puro via the EcoRI and XhoI sites (underlined).

Antibodies. To produce a mouse monoclonal antibody (MAb) against ORF44, a glutathione *S*-transferase (GST)-ORF44A recombinant protein was expressed in *E. coli* BL21 transformed with pGEX/ORF44A, purified, and used to immunize mice; hybridoma clones producing the anti-ORF44 MAb were established as described previously (32). To produce polyclonal anti-ORF61 Abs, a GST-ORF61 fusion protein was purified from *E. coli* BL21 transformed with pGEX-ORF61 and used to immunize a rabbit

TABLE 1 Primers used for ORF44 or ORF49 mutations

Primer	Sequence[a]	Amino acid substitution(s)
ORF44 361at-ta	5′-TAT CCG GTT GAA AAC TAA GAC CAT GTT TTT GGA-3′	Ile 121 to stop (TAA)
ORF44 382a-g	5′-CAT GTT TTT GGA GCA GCG TTT AAG AAC CC-3′	Thr 128 to Ala
ORF44 385tt-gc	5′-TT TTT GGA GCA ACG GCT AAG AAC CCG ATC G-3′	Phe 129 to Ala
ORF44 388aa-gc	5′-TTT GGA GCA ACG TTT GCG AAC CCG ATC GCG-3′	Lys 130 to Ala
ORF44 406ccc-taa	5′-AAC CCG ATC GCG TAC TAA CTT CCA ACA TCT ATT-3′	Pro 136 to stop (TAA)
ORF49 M1L	5′-ATT GCG GTC ATT GCG TTG GGA CAA TCT TCA-3′	Met 1 to Leu
ORF49 41AAAA44	5′-TTT GAA GAC TTT GCC GCT GCG AAT GTA ACA GAG-3′	Asp-Phe-Asp-Glu (41–44) to Ala-Ala-Ala-Ala

[a] Nucleotides that differ from those of the wild type are underlined.

(Sigma Genosys, Hokkaido, Japan). The anti-ORF61 Ab was purified with GST-conjugated normal human serum (NHS)-activated Sepharose and GST-ORF61-conjugated NHS-activated Sepharose. Rabbit polyclonal anti-ORF49 and anti-gB-C Abs were described previously (6). The mouse anti-glycoprotein E (anti-gE) (clone 9) Ab was described in reference 33. Mouse anti-glycoprotein H (gH) (VgIII-3) was obtained as described previously (33). Sheep anti-*trans*-Golgi network (anti-TGN46) Ab (AHP500G; AbD Serotec, Oxford, United Kingdom), anti-α-tubulin Ab (B-5-1-2; Sigma-Aldrich), and goat anti-GST Ab (GE Healthcare Bio-Sciences) were commercially available. Alexa Fluor 488-labeled donkey anti-mouse immunoglobulin G (IgG), Alexa Fluor 594-labeled donkey anti-rabbit IgG, and Alexa Fluor 647-labeled donkey anti-sheep IgG (Invitrogen) were used as secondary Abs, and Hoechst 33342 (Sigma-Aldrich) was used for nuclear staining in confocal microscopic analyses. ECL enhanced chemiluminescence anti-mouse or anti-rabbit IgG horseradish peroxidase-linked whole antibodies from donkey (GE Healthcare Bio-Sciences) were used as secondary Abs in immunoblotting.

Mutagenesis of viral genomes in *E. coli*. The mutant bacterial artificial chromosomes (BACs) pOka-BACORF49M1L, containing a methionine-to-leucine substitution at residue Met-1, and pOka-BACORF49-41AAAA44, containing a tetra-alanine substitution at residues 41-Asp-Phe-Asp-Glu-44, were generated by *recA*-mediated allelic replacement in pOka-BAC-harboring DH10B transformed with pST76A-SR/pOkaORF49M1L and pST76A-SR/pOkaORF49-41AAAA44, respectively, which were derived from pST76A-SR/pOkaORF50 (including nucleotide positions 84361 to 89970 of pOka) (30), using the primers listed in Table 1 and a QuikChange Lightning multisite-directed mutagenesis kit. The revertant BACs pOka-BACORF49M1LRev and pOkaBACORF49-41AAAA44Rev were generated by recA-mediated allelic replacement using pST76A-SRORF50 transformed into DH10B cells harboring pOka-BACORF49M1L and pOka-BACORF49-41AAAA44, respectively.

To generate pOka-BACΔ44, in which the nucleotides (nt) 1 to 800 of the ORF44 gene were replaced with an FRT (*flp* recombinase recognition target) sequence, a linear fragment was amplified by PCR using the primer pair ORF44FRTfKMF0 (5′-TTAAACCCACAAGTACC CGGGCGGCAATCCGCTAGACTGTTTTTCTGCTCGAAGTTCCTA TTCTCTAGAAAGTATAGGAACTTCAGCAAGCGAACCGGAAT TGC-3′) and ORF44FRTrKMR800 (5′-TCCCGCTGACCGGCCTTT CTCCACATACACGGAGCCCAACACACACAACCGAAGTTCCTAT ACTTTCTAGAGAATAGGAACTTCCTTTTTTCAATTCAGAAGA ACTC-3′) (FRT is underlined) using pCR2.1-TOPO as the template (Invitrogen). The amplified fragment was then transformed into DH10B harboring pOka-BAC (34) with pGETrec (a kind gift from Panayiotis A. Ioannou, The Murdoch Institute for Research into Birth Defects, Royal Children's Hospital, Melbourne, Australia) (35); *recE/T* recombination for pOka-BACΔ44KMr and excision of the kanamycin resistance gene from pOka-BACΔ44KMr by the *flp*/FRT system using pCP20 (a kind gift from Wilfried Wackernagel, Universität Oldenburg, Germany) (36), resulting in pOka-BACΔ44, were carried out as described previously (6).

To construct pOka-BACΔ44Rev, the revertant BAC genome against pOka-BACΔ44, *recA*-mediated mutagenesis was performed as described previously (30), using the shuttle plasmid pST76A-SR/pOkaORF44. For pST76A-SR/pOkaORF44, a 3.2-kbp fragment of viral DNA corresponding to nt 79230 to 82453 of pOka was amplified from the pOka-BAC genome using the primer pair ORF43F1201 (5′-ACCGCTGCGTGTATA AATGCCCGGGTTGAC-3′) and ORF42/45F (5′-ACCATGTCATTGAT AATGTTTGG-3′), cloned into pCR2.1-TOPO, sequenced, cut with EcoRI, blunted, and cloned into the plasmid pST76A-SR (kindly provided by Ulrich H. Koszinowski, Max von Pettenkofer Institut, Ludwig-Maximilians-Universität München, Munich, Germany) (37), which was cut with KpnI and blunted.

The shuttle plasmids for the ORF44 point mutant BACs, pST76A-SRORF44T128A (with an alanine substitution for threonine at residue Thr-128), pST76A-SR/pOkaORF44F129A (with an alanine substitution for phenylalanine at residue Phe-129), and pST76A-SR/pOkaORF44K130A (with an alanine substitution for lysine at residue Lys-130), were generated from pST76A-SR/pOkaORF44 with a QuikChange Lightning multisite-directed mutagenesis kit using the primers listed in Table 1. Each mutated shuttle plasmid was transformed into DH10B harboring pOka-BACΔ44KMr, and *recA*-mediated allelic replacement was performed as described elsewhere (30) to generate pOka-BACORF44T128A, pOka-BACORF44F129A, and pOka-BACORF44K130A. The revertant BAC for the ORF44F129A mutant BAC, pOka-BACORF44F129ARev, was generated by *recA*-mediated allelic replacement using pST76A-SRORF44 transformed into pOka-BACORF44F129A-harboring DH10B.

All of the purified BACs were digested with BamHI or EcoRI to ensure that the expected DNA fragments were present, and the whole region for allelic replacement was sequenced to ensure that unexpected deletions or substitutions were not present.

Reconstitution of recombinant viruses and excision of the BAC cassette. MeWo cells or MeWoORF49 cells for rpOkaORF49M1L and rpOkaORF49-41AAAA44 seeded in one well of a 12-well plate were transfected with 3 μg of BAC DNA using Lipofectamine 2000 or X-treamGene HP (Roche Applied Science, Basel, Switzerland). After typical cytopathic effects (CPE) were seen in cells expressing green fluorescent protein (GFP), cell-free virus was prepared as described above and used to infect MeWo-Cre cells or pCX-Cre-neo-transfected MeWoORF49 cells for rpOkaORF49M1L and rpOkaORF49-41AAAA44 to excise the BAC cassette.

Immunoblotting, immunoprecipitation, and immunofluorescence. Immunoblotting, immunoprecipitation, and immunofluorescence were performed as described previously (30, 32) with slight modifications. The proteins in immunoblots were visualized by Chemi-Lumi One Super (Nacalai Tesque) in combination with LAS4000mini (GE Healthcare Bio-Sciences). Radioimmunoprecipitation assay (RIPA) lysis buffer (0.01 M Tris-HCl [pH 7.4], 0.15 M NaCl, 1% sodium deoxycholate, 1% Nonidet P-40, 0.1% SDS, 1 mM EDTA) supplemented with protease inhibitor cocktail (Sigma-Aldrich) was used for cell lysis, and the supernatants obtained by ultracentrifugation at 216,900 × *g* for 1 h at 4°C in a P50A3 rotor (CP80WX; Hitachi Koki) and precleared with protein G Sepharose 4 Fast Flow (GE Healthcare Bio-Sciences) were used for immunoblotting and immunoprecipitation. Immunofluorescence images were captured and analyzed by an FV1000D confocal microscope (Olympus, Tokyo, Japan).

***In vitro* binding assay.** To analyze the interaction of GST-ORF44 with ORF49, GST-ORF44, GST-ORF44F129A, or GST-ORF44P recombinant protein was expressed in and purified using BugBuster master mix (Merck Millipore, Darmstadt, Germany) from *E. coli* BL21 transformed with pGEX/ORF44, pGEX/ORF44F129A, or pGEX/ORF44P as described above. ORF49p was expressed in MeWo cells by transfection of CAG/ORF49 using Lipofectamine 2000 and solubilized as described above. GST-ORF44 recombinant protein was bound to glutathione Sepharose 4B (GE Healthcare Bio-Sciences) overnight at 4°C, washed with PBS three times, pelleted, and reacted with soluble ORF49p overnight at 4°C. The bead–GST-ORF44 recombinant protein–ORF49p complex was washed with RIPA lysis buffer three times, pelleted, suspended in SDS-PAGE sample buffer, boiled, and subjected to SDS-PAGE and immunoblotting as described above.

Protein identification by MS. MeWo cells were infected with pOka by cell-to-cell infection and lysed with RIPA lysis buffer as described above. The cell lysates from pOka- or mock-infected MeWo cells were precleared with protein G Sepharose and subjected to immunoprecipitation with anti-ORF49 Ab cross-linked protein G Sepharose. The immunoprecipitates were separated by SDS-PAGE and stained with a SilverQuest silver staining kit (Invitrogen). Protein bands were excised from the gel and digested with trypsin (sequencing grade; Promega, Madison, WI) according to published procedures (38). Nano-liquid chromatography-tandem mass spectrometry (nano-LC-MS/MS) analyses were performed on an LTQ-Orbitrap XL mass spectrometer (Thermo Fisher Scientific, Waltham, MA) equipped with a nano-electrospray ionization (nano-ESI) source (AMR, Tokyo, Japan) and coupled to a Paradigm MG4 pump (Michrom Bioresources, Auburn, CA) and autosampler (HTC PAL; CTC Analytics, Zwingen, Switzerland). A spray voltage of 1,800 V was applied. The peptide mixture was separated on a Magic C_{18} AQ column (100 μm by 150 mm, 3.0-μm particle size, 300 Å; Michrom Bioresources) with a flow rate of 500 nl/min. The linear gradient was as follows: 5% to 45% B in 30 min, 45% to 95% B in 0.1 min, 95% B for 2 min, and finally 5% B (solvent A = 0.1% formic acid in 2% acetonitrile, and B = 0.1% formic acid in 90% acetonitrile). Intact peptides were detected in the Orbitrap at a resolution of 60,000. For the LC-MS/MS analysis, six precursor ions were selected for subsequent MS/MS scans in a data-dependent acquisition mode following each full scan (*m/z*, 350 to 1,500). A lock mass function was used for the LTQ-Orbitrap to obtain constant mass accuracy during the gradient analysis. Peptides and proteins were identified by automated database searches using Proteome Discoverer v.1.1 (Thermo Fisher Scientific, Waltham, MA) against human entries or all entries of the Swiss-Prot protein database (version 3.26) with a precursor mass tolerance of 10 parts per million (ppm), a fragment ion mass tolerance of 0.8 Da, and strict trypsin specificity, allowing for up to two missed cleavages. Cysteine carbamidomethylation was set as a fixed modification, and methionine oxidation was allowed as a variable modification.

Plaque size and infectious-center assays for growth kinetics. To analyze the growth kinetics of the recombinant viruses, infectious-center assays were performed as described previously (6) with slight modifications. Briefly, 5×10^5 MeWo or MeWoORF49 cells were seeded on one well of a 12-well plate and inoculated with 50 PFU of cell-free virus per well. For the plaque size measurement, the infected cells were cultured for 7 days. For the infectious-center assay, infected cells were harvested at 24-h intervals and then titrated on newly prepared cells. The cells were fixed in 30% methanol and 70% acetone and stained with an anti-gE MAb (clone 9) and secondary ECL anti-mouse IgG horseradish peroxidase-linked whole antibody (GE Healthcare Bio-Sciences). The stain was developed with 3,3′,5,5′-tetramethylbenzidine-H (TMB-H) peroxidase substrate (Moss, Inc., Pasadena, MD). Images of the plaques were captured and traced, and the number of plaques was counted, or the plaque area was measured using ImageJ (http://rsbweb.nih.gov/ij/).

RESULTS

ORF49 functions in the efficient production of infectious progeny virus. To examine the mechanism of action of ORF49, we performed loss-of-function and gain-of-function analyses by generating an ORF49-defective virus, rpOkaORF49M1L, and its revertant virus, rpOkaORF49M1LRev, from the pOka-BACORF49M1L and pOka-BACORF49M1LRev genomes, respectively (Fig. 1A and C). In addition, the MeWoORF49 cell line was established to express ORF49 constitutively in MeWo cells in which the previous ORF49-defective virus, rpOkaΔ49, specifically showed an impaired growth phenotype (6), and gain-of-function analysis was performed by ORF49 *trans*-complementation assay.

None of the assayed viral proteins, including glycoprotein H (gH), ORF61 protein (ORF61p), ORF44p, and ORF49p, were detected in MeWo cells (Fig. 2A, lane 1). In MeWoORF49 cells, ORF49p was the only protein detected among the tested viral proteins (Fig. 2A, lane 2), and its expression level was comparable to that of ORF49p in rpOka-infected MeWo cells (Fig. 2A, lane 3). In rpOkaORF49M1L-infected cells, ORF49p was not detected in the infected MeWo cells (Fig. 2A, lane 4) or in the viral particles (Fig. 2C, lane 2), although gH and ORF61p were clearly expressed in infected cells (Fig. 2A, lane 4), as was gH in the viral particles (Fig. 2C, lane 2). The rpOkaORF49M1LRev line expressed all of the viral proteins tested (Fig. 2A, lane 5), similar to rpOka-infected MeWo cells (Fig. 2A, lane 3).

To confirm the ORF49-defective phenotype and perform gain-of function analysis, plaque formation was analyzed on MeWo and MeWoORF49 cells (Fig. 3A). Plaque sizes were similar between rpOka-infected MeWo and MeWoORF49 cells (Fig. 3A, lanes 1 and 2), indicating that the exogenous expression of ORF49 had neither positive nor negative effects on normal VZV infection. Similar to our previous results using rpOkaΔ49, rpOkaORF49M1L formed significantly smaller plaques on MeWo cells (Fig. 3A, lane 3) than on MeWoORF49 cells, and this reduction was recovered in the revertant virus infection in MeWo cells (Fig. 3A, lane 5) and completely rescued by the exogenous expression of ORF49 in MeWoORF49 cells (Fig. 3A, lane 4). Consistent with the plaque formation assay results, rpOkaORF49M1L propagated on MeWo cells showed slower growth than rpOka or rpOkaORF49M1LRev on MeWo or MeWoORF49 cells in an infectious-center assay, and the growth impairment of rpOkaORF49M1L was completely rescued by exogenous ORF49p in MeWoORF49 cells (Fig. 3B).

During the preparation of cell-free viruses, another strikingly different phenotype of the ORF49 defect was observed. As summarized in Table 2, the titer of cell-free virus or plaque size formed by the cell-free virus infection of rpOka was almost the same whether the virus was propagated on MeWo or MeWoORF49 cells or titrated on MeWo or MeWoORF49 cells, again indicating that the exogenous ORF49p had no effect on normal VZV infection. When rpOkaORF49M1L was propagated on MeWo cells, the titer of cell-free virus was 3 to 5% of that observed with propagation of MeWoORF49 cells, and the plaque size depended on the kind of cells used for titration but not on the kind used for propagation. In addition, the rpOkaORF49M1L particles isolated from MeWoORF49 cells contained abundant ORF49p (Fig. 2C, lane 3) and produced almost the same titer of cell-free virus as the parental virus but formed significantly smaller plaques on MeWo cells (Table 2). This gain-of-function analysis performed using the ORF49 *trans*-complementation system suggested that the incom-

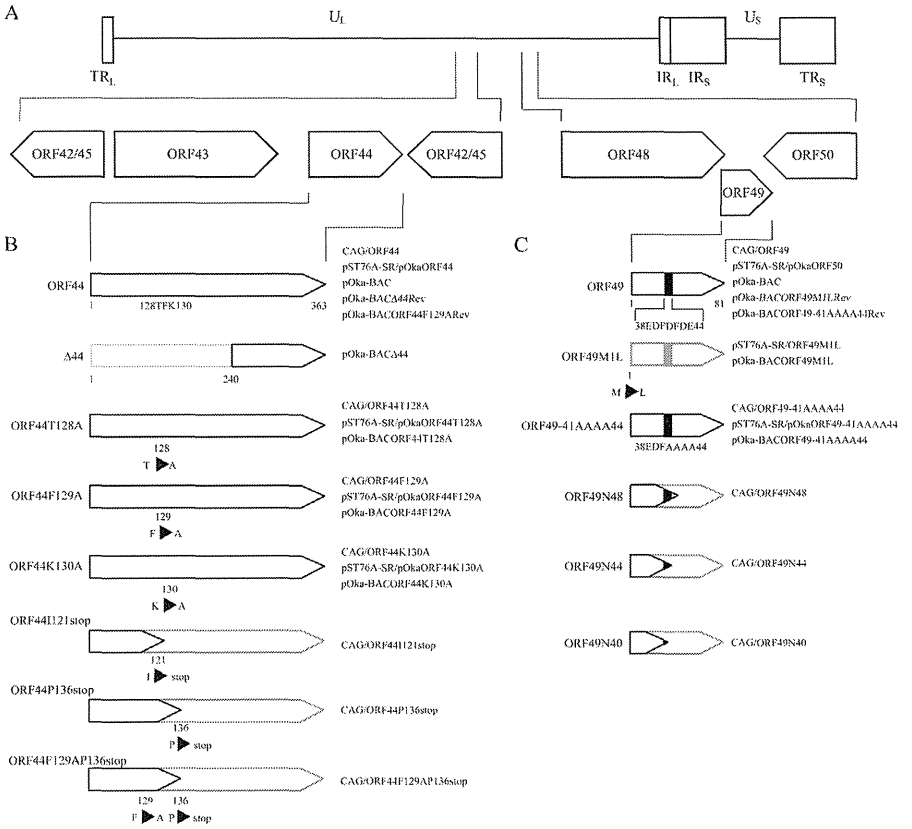

FIG 1 Schematics showing the plasmids and recombinant BAC genomes for ORF44 and ORF49. (A) Location of the ORF44 and ORF49 genes in the unique long region (U_L) segment of the genome of VZV strain pOka; terminal repeats (TR), unique short region (U_S), and internal repeats (IR) are indicated. (B) The wild type, deleted Δ44 region, and amino acid substitutions in ORF44p are shown. (C) The wild type, amino acid substitutions at the first methionine or the carboxyl-terminal half of the acidic cluster from amino acid positions 41 to 44, and the carboxyl-terminal truncations within ORF49p are shown. The acidic cluster is indicated as a black box. (B and C) Unexpressed regions of the mutant proteins are shown in gray outlined shapes. The names of relevant BACs, shuttle plasmids, and mammalian expression plasmids containing mutations are shown on the right.

ing ORF49p from the viral particles into the cells was not functional in any step and revealed that *de novo* ORF49p functioned in the production of infectious progeny viruses required for efficient propagation.

Furthermore, to examine the role of ORF49 in the production of infectious progeny viruses in detail, we redesigned our study on ORF49 to investigate its function by analyzing its binding partners.

Identification of the ORF44 protein as the binding partner for ORF49. ORF49p was immunoprecipitated from pOka- or mock-infected MeWo cells using an anti-ORF49 antibody (Ab), and the coimmunoprecipitating proteins were separated in a denaturing gel and visualized by silver staining (Fig. 4A). An approximately 36-kDa band was coimmunoprecipitated with the 13-kDa band corresponding to the ORF49p in pOka-infected MeWo cell lysates (Fig. 4A, lane 1). This 36-kDa band was identified as the ORF44 protein (ORF44p) of VZV by LC-MS/MS analysis (24.3% coverage of 363 amino acids).

ORF44p was specifically detected as a 36-kDa band in all recombinant VZV-infected MeWo cells, including rpOkaORF49M1L, by

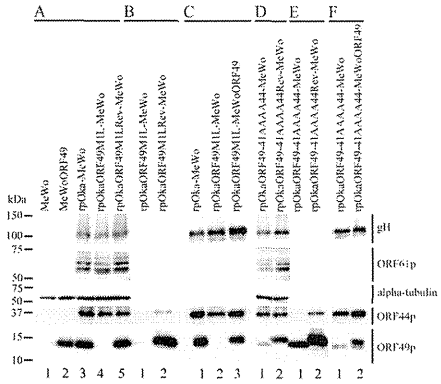

FIG 2 Expression and interaction of viral proteins during ORF49 mutant virus infection. (A) Proteins expressed in mock-infected MeWo cells (lane 1), mock-infected MeWoORF49 cells (lane 2), rpOka-infected MeWo cells (lane 3), rpOkaORF49M1L-infected MeWo cells (lane 4), and rpOkaORF49M1LRev-infected MeWo cells (lane 5) were visualized with Abs against gH, ORF61p, α-tubulin, ORF44p, and ORF49p. (B) The interaction between ORF44p and ORF49p was analyzed in rpOkaORF49M1L-infected cells (lane 1) and rpOkaORF49M1LRev-infected cells (lane 2). Immunoprecipitates obtained with an anti-ORF49 Ab from each type of virus-infected cells were electrophoretically separated and visualized using anti-ORF44 and anti-ORF49 Abs. (C) The viral proteins incorporated into virions from rpOka-infected MeWo cells (lane 1), rpOkaORF49M1L-infected MeWo cells (lane 2), and rpOkaORF49M1L-infected MeWoORF49 cells (lane 3) were visualized using Abs against gH, ORF61p, ORF44p, and ORF49p. (D) Proteins expressed in rpOkaORF49-41AAAA44-infected MeWo cells (lane 1) and rpOkaORF49-41AAAA44Rev-infected MeWo cells (lane 2) were visualized using Abs against gH, ORF61p, α-tubulin, ORF44p, and ORF49p. (E) The interaction between ORF44p and ORF49p was analyzed in rpOkaORF49-41AAAA44-infected cells (lane 1) and rpOkaORF49-41AAAA44Rev-infected cells (lane 2). Immunoprecipitates obtained using an anti-ORF49 Ab from each type of virus-infected cells were electrophoretically separated and visualized with anti-ORF44 and anti-ORF49 Abs. (F) The viral proteins incorporated into virions from rpOkaORF49-41AAAA44-infected MeWo cells (lane 1), and rpOka-ORF49-41AAAA44-infected MeWoORF49 cells (lane 2) were visualized with Abs against gH, ORF61p, ORF44p, and ORF49p.

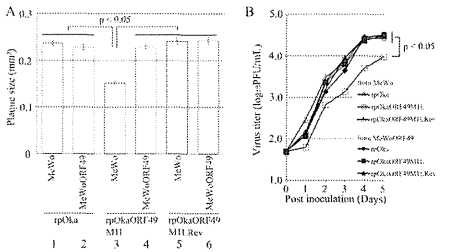

FIG 3 Growth properties of the ORF49M1L mutant virus in MeWo and MeWoORF49 cells. (A) Comparison of plaque sizes among recombinant viruses. MeWo cells or MeWoORF49 cells were infected with rpOka, rpOkaORF49M1L, or rpOkaORF49M1LRev (50 PFU/well) and cultured for 7 days. The infected cells were then stained with an anti-gE Ab, and the plaques were traced and measured by ImageJ software. Plaque size is shown with the standard error of the mean. Statistical significance was determined by Student's *t* test. (B) Growth kinetics of recombinant viruses in MeWo and MeWoORF49 cells. MeWo or MeWoORF49 cells were infected with rpOka, rpOkaORF49M1L, or rpOkaORF49M1LRev (50 PFU/well), harvested at the indicated times, serially diluted, added to newly prepared MeWo cells, and cultured for 5 days. The plaques were stained with an anti-gE Ab and counted. Each point represents the mean titer for two wells of one experiment. The experiments were performed twice independently. Statistical significance was determined by Student's *t* test.

immunoblotting with an anti-ORF44 Ab (Fig. 2A, lanes 3, 4, and 5). ORF44p was coimmunoprecipitated with ORF49p only in cells infected with the wild-type virus, rpOka, or rpOkaORF49M1LRev (data not shown) (Fig. 2B, lane 2) but not in the absence of ORF49p, as seen in rpOkaORF49M1L infection (Fig. 2B, lane 1). Thus, the interaction of ORF44p and ORF49p was specific and conserved in VZV.

ORF44 is essential for viral growth in cell culture. Because ORF49 is completely dispensable for viral reconstitution and propagation in MRC-5 cells, and the interaction between ORF44p and ORF49p was confirmed, we predicted that the ORF44 deletion mutant would be viable at least in MRC-5 cells, despite the fact that loss-of-function analysis showed that it is essential in MeWo cells (5). The ORF44 deletion mutant virus could not be reconstituted from pOka-BACΔ44 (Fig. 1B) in either MeWo cells or MRC-5 cells; however, the revertant virus of pOka-BACΔ44 reconstituted from the pOka-BACΔ44Rev genome (Fig. 1B) showed almost the same plaque size and growth as the parental virus, rpOka, in MeWo cells (data not shown). These findings confirmed that ORF44 is essential for VZV growth in cell culture even in MRC-5 cells.

ORF44p binds to and depends on ORF49p for its accumulation on the TGN in coexpressing cells and infection. When ORF44p was expressed alone by CAG/ORF44 transfection, it was dispersed throughout the cytoplasm and did not localize to the TGN (Fig. 5A). When ORF49p was expressed alone, it was predominantly localized to the juxtanuclear region with TGN46 (Fig. 5B), as reported previously (6). In cells coexpressing ORF44 and ORF49, ORF44p accumulated on the TGN with ORF49p (Fig. 5C), suggesting that the complex formation between ORF44p and ORF49p required no other viral factors and that it functioned in the accumulation of the ORF44p on the TGN. The expression of and interaction

TABLE 2 Comparison of cell-free virus titer and plaque formation

Virus	Cells for: Propagation	Titration	Titer (PFU/ml)[a]	Mean (SE) plaque size, mm²[b]
rpOka	MeWo	MeWo	2.3×10^5	0.232 (0.00891)
	MeWo	MeWoORF49	4.1×10^4	0.225 (0.00854)
	MeWoORF49	MeWo	4.0×10^4	0.232 (0.00911)
	MeWoORF49	MeWoORF49	1.3×10^5	0.206 (0.00828)
rpOkaORF49M1L	MeWo	MeWo	1.5×10^2	0.161 (0.00601)
	MeWo	MeWoORF49	1.7×10^2	0.235 (0.01319)
	MeWoORF49	MeWo	4.0×10^4	0.147 (0.00534)
	MeWoORF49	MeWoORF49	6.3×10^4	0.228 (0.01474)
rpOkaORF49-41AAAA44	MeWo	MeWo	1.2×10^2	0.141 (0.00726)
	MeWo	MeWoORF49	1.3×10^2	0.212 (0.00669)
	MeWoORF49	MeWo	2.1×10^4	0.149 (0.00796)
	MeWoORF49	MeWoORF49	4.7×10^4	0.227 (0.00740)

[a] Titers of cell free viruses are shown from one experiment performed in duplicate.
[b] Plaque sizes are shown as means (standard errors [SE]) from one experiment performed in duplicate.